

AD 672399

RESEARCH ON COMBUSTION OF SOLID PROPELLANTS

**FINAL REPORT
COVERING THE PERIOD
20 APRIL 1965 THROUGH 31 AUGUST 1968**

CONTRACT NO. DA-04-200-AMC-968 (X)

Prepared for
**U.S. ARMY BALLISTICS RESEARCH LABORATORIES
ABERDEEN PROVING GROUND, MARYLAND**

DDC
NOV 15 1968

This document has been approved for public release
and sale; its distribution is unlimited.

Reproduced by the
CLEARINGHOUSE
for Federal Scientific & Technical
Information Springfield Va 22151

DISCLAIMER NOTICE

THIS DOCUMENT IS BEST QUALITY PRACTICABLE. THE COPY FURNISHED TO DTIC CONTAINED A SIGNIFICANT NUMBER OF PAGES WHICH DO NOT REPRODUCE LEGIBLY.

UTC 2136-FR
September 1968

RESEARCH ON COMBUSTION OF SOLID PROPELLANTS


Research and Advanced Technology Department
UNITED TECHNOLOGY CENTER
Division of United Aircraft Corporation
Sunnyvale, California

FINAL REPORT
FOR THE PERIOD 20 APRIL 1965 THROUGH 31 AUGUST 1968

Prepared for


U. S. Army Ballistic Research Laboratories
Aberdeen Proving Ground, Maryland
Contract No. DA-04-200-AMC-968(x)

Prepared by:




R. J. Muzzey
Project Scientist

Submitted by:

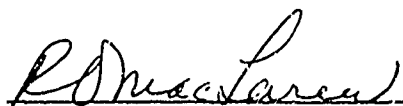


R. S. Brown
Project Manager

Approved by:



M. E. Steinle
Senior Research Chemist



R. O. MacLaren
Manager
Propulsion Research Branch

This document has been approved for public release
and sale; its distribution is unlimited.

ABSTRACT

A study has been made to relate theoretically predicted and experimentally observed pressure-coupled combustion instability behavior of solid propellants. Using a generalized theoretical model which incorporates both surface and gas phase combustion effects, the linear and nonlinear (higher pressure amplitude) region has been characterized by a group of combustion parameters. Concurrent experimental studies have been directed toward investigating (1) the effects of coating the solid oxidizer crystals, (2) the chemical and physical nature of the propellant binder, catalysts, and cross-linking agents on the acoustic admittance, (3) nonlinear response properties, and (4) propellant burning rate. The data show that small changes in propellant formulations can have a significant effect on the derived parameters characterizing the surface and, therefore, on relative contributions of these reactions to the acoustical response properties.

A comparison of the experimental data with theoretical predictions in the linear region (i.e., acoustic response functions) shows that propellants having 84% solids loading are more likely to show the surface gasification to be pressure dependent than those having lower loadings. The temperature dependence of the gasification process is extremely large—larger than can be explained by an Arrhenius rate expression with a reasonable activation energy. The rate of energy transfer into the solid phase was found to increase with increasing surface temperature. This suggests the influence of exothermic surface processes. The effect of pressure on the energy transfer was found to be consistent with the several proposed models for gas-phase combustion effects.

Higher order effects show that, depending on the magnitude of the constants, both positive and negative values for the shift in the time average burning rate with acoustic pressure can be obtained. Since Eisel has observed this effect to be negative, this defines the region of reasonable second order coefficients. Additional studies show that the acoustic response function decreases with increasing acoustic pressure for reasonable second and third order coefficients. Hence, the combustion process itself can limit the acoustic pressure amplitude in the T-burner. On the basis of these calculations, limiting amplitudes of 0.1 to 0.5 can be expected without consideration of acoustic losses.

The combined linear and nonlinear results indicate that a homogeneous non-reacting solid characterizes the transient behavior of the solid phase with sufficient accuracy. Comparison of the predicted response function-frequency curve with the experimental data shows agreement within reasonable experimental errors. The nonlinear behavior also shows that predicted results are consistent with observations. Although more complex and detailed descriptions can be proposed, this assumption represents an extremely useful and sufficiently accurate approximation for most practical purposes.

CONTENTS

<u>Section</u>		<u>Page</u>
1.0	INTRODUCTION	1
2.0	TECHNICAL DISCUSSION	2
2.1	Experimental Studies	3
2.1.1	Experimental Apparatus	4
2.1.2	Propellant Formulations	12
2.1.3	Reduction of Experimental Data	16
2.1.4	Experimental Results	17
2.2	Theoretical Studies	33
2.2.1	General Combustion Analysis	34
2.2.2	Linear Response	37
2.2.3	Second Order Behavior	39
2.2.4	Third Order Behavior	41
2.2.5	Utility of General Model	43
2.3	Comparison of Theory and Experiment	44
2.3.1	Method for Deriving Combustion Parameters	44
2.3.2	Statistical Significance of Q_1	47
2.3.3	Comparison of Data Reduction Method with Other Approaches	47
2.3.4	Approximate Method for Data Reduction	51
2.3.5	Analysis of Error Effects	54
2.3.6	Interpretation of Combustion Parameters	55
2.3.7	Nonlinear Behavior	62
2.3.8	Effect of Pressure	73
3.0	CONCLUSIONS	78
	REFERENCES	80
APPENDIX A.	Additional Experimental Studies	A-1
APPENDIX B.	Experimental Data	B-1
APPENDIX C.	Theoretical Analysis of Subsurface Reactions and Nonlinear Effects using Finite Difference Techniques	C-1
APPENDIX D.	Presentations and Publications	D-1

ILLUSTRATIONS

<u>Figure</u>		<u>Page</u>
1.	Diagram of T-Burner	5
2.	T-Burner	6
3.	T-Burner End Caps with and without Propellant Sample	8
4.	Schematic of T-Burner Electronics	10
5.	T-Burner Electronics	11
6.	Effect of Kel-F and Viton Coatings on Acoustical Response	18
7.	Effect of Cure Agents	19
8.	Effect of PBAN Binders	20
9.	Acoustic Response of CTPB and UTREZ Binders	21
10.	NOTS A-13 Propellant Data	22
11.	Effect of Pressure on Acoustic Response	23
12.	Effect of Pressure on Acoustic Response	24
13.	Effect of Ferric Oxide Catalysis	25
14.	Effect of Copper Chromite	26
15.	Effect of AP Particle Size	27
16.	Effect of Coating or Addition to Propellant Mix	28
17.	Effect of Kel-F Coatings	29
18.	Effect of Various Coatings	30
19.	Effect of Binders	31
20.	Frequency of Maximum Acoustic Response vs A_1	52
21.	Maximum Value of Acoustic Response Function	53

ILLUSTRATIONS (Continued)

<u>Figure</u>		<u>Page</u>
22.	Effect of Thermal Diffusivity on Shape of Response-Frequency Curve	56
23.	Effect of Steady-State Burning Rate Exponent and $Re(u/\bar{c})_{max}$ on Shape of Response-Frequency Curve	57
24.	Nonlinear Effect on Burning Rate Shift	64
25.	Effect of Gas Phase Pressure Exponent on Burning Rate Change	66
26.	Effect of Activation Energy A on Burning Rate Change	67
27.	Effect of Activation Energy A on Change in Acoustic Response	70
28.	Limit Amplitude of Combustion Zone	72
29.	Predicted Effect of Pressure on Response Function	74
30.	Effect of Pressure on Limit Amplitude	75

TABLES

<u>Table</u>		<u>Page</u>
I	Additives	13
II	Propellant Formulations	15
III	Linear Combustion Parameters at 200 psig	45
IV	Effect of Pressure on Combustion Parameters (UTX-8501)	45
V	Linear Combustion Parameters at 200 psig ($Q_1 = 0$)	48
VI	Effect of Pressure on Combustion Parameters (UTX-8501 with $Q_1 = 0$)	48
VII	Effect of n and $Re(u/\bar{c})_{max}$ on R_1	54

ABBREVIATIONS

AP	ammonium perchlorate
CEC	Consolidated Electrodynamics Corporation
C ₂ H ₅	ethyl group
CsNO ₃	cesium nitrate
CTPB	carboxy-terminated polybutadiene
ICRPG	Inter-Agency Chemical Rocket Propulsion Group
MAPO	(tris 1-(2 methyl) aziridine phosphine oxide)
NOTS	Naval Ordnance Test Station
NWC	Naval Weapons Center
PBAN	polybutadiene-acrylic acid-acrylonitrile
PEP	nitrate-plasticized imine-cured polyester binder
UTC	United Technology Center
UTREZ	polyisobutylene

Nomenclature

A_1	=	$[\partial H_n / \partial \theta]_o$
A_2	=	$[\partial^2 H_n / \partial \theta^2]_o$
A_3	=	$[\partial^3 H_n / \partial \theta^3]_o$
B_1	=	$[\partial F_n / \partial \epsilon]_o$
B_2	=	$[\partial^2 F_n / \partial \epsilon^2]_o$
B_3	=	$[\partial^3 F_n / \partial \epsilon^3]_o$
c	=	sonic velocity of the combustion gases
C_{11}	=	$[\partial^2 H_n / \partial \theta \partial c]_o$
C_{12}	=	$[\partial^3 H_n / \partial \theta^3]_o$
C_{21}	=	$[\partial^3 H_n / \partial \epsilon^3]_o$
D	=	defined by equation (C-7)
D_{11}	=	$[\partial^2 F_n / \partial \theta \partial c]_o$
D_{12}	=	$[\partial^3 F_n / \partial c \partial \theta^2]_o$
D_{21}	=	$[\partial^3 F_n / \partial \epsilon^2 \partial \theta]_o$
$E(\lambda)$	=	$\text{Re}(\mu_2 / c_1^2)$
E_2	=	activation energy of overall pyrolysis rate at surface
E_3	=	activation energy of solid phase combustion reactions
E_4	=	activation energy of exothermic surface reactions
E_f	=	activation energy of gas phase reactions
f_g, f_d	=	frequency of the acoustic pressure oscillations at the point where α_g and α_d measured
F	=	instantaneous heat flux into solid phase

F_n	=	F/F_0
F_0	=	steady-state heat flux into solid phase
$F(\lambda)$	=	$\text{Re}(\mu_3/c_1^3)$
G	=	gas temperature
H	=	rate of gasification at solid surface
H_n	=	\dot{r}/\dot{r}_0
$\text{Im}(\mu/c_1)$	=	imaginary part of acoustic response function
J	=	burning rate in the gas phase
k	=	thermal conductivity
K	=	energy transfer from gas phase to solid surface
L	=	length of combustion chamber
\dot{m}_g	=	mass burning rate in the gas phase
\dot{m}_s	=	mass flow rate from solid surface
m^1	=	order of gas phase reaction
n	=	steady-state burning rate exponent
n^1	=	pressure exponent on gas phase heat flux
P	=	instantaneous pressure
\tilde{P}	=	amplitude of acoustic pressure oscillations
P_0	=	steady-state pressure
Q_1	=	$[\partial H_n / \partial \epsilon]_0$
Q_2	=	$[\partial^2 H_n / \partial \epsilon^2]_0$
Q_3	=	$[\partial^3 H_n / \partial \epsilon^3]_0$
\dot{r}	=	instantaneous linear burning rate of propellant
\dot{r}_0	=	steady-state linear burning rate of propellant
\tilde{r}	=	amplitude of burning rate oscillations
R	=	universal gas constant

R_1	=	$[\partial F_n / \partial \theta]_o$
R_2	=	$[\partial^2 F_n / \partial \theta^2]_o$
R_3	=	$[\partial^3 F_n / \partial \theta^3]_o$
$\text{Re}(\mu/\epsilon)$	=	real part of acoustic response function
t	=	time
T	=	temperature
T_f	=	propellant flame temperature
T_s	=	steady state temperature at the solid surface
T_∞	=	initial temperature of the propellant
W_1	=	defined by equation (C-2)
x	=	distance into the solid from the surface
X_1	=	defined by equation (C-3)
Y_1	=	defined by equation (C-4)
Z_1	=	defined by equation (C-5)
Z_2	=	Arrhenius preexponential factor for overall pyrolysis rate at surface
Z_3	=	Arrhenius preexponential factor solid phase combustion reactions
Z_4	=	Arrhenius preexponential factor exothermic surface reactions

Greek Symbols

α	=	propellant thermal diffusivity
α_d	=	dP_c/dt during the decay of the acoustic pressure oscillations
α_g	=	dP_c/dt during the growth of the acoustic pressure oscillations
β	=	$\Delta H_v / C_p T_s^\circ$
Δ	=	perturbation parameter
Λ	=	E_4 / E_2
Γ	=	$P_o Z_4 \exp(-E_4 \Delta R T_s^\circ) / \dot{r}_o \rho C_p T_s^\circ$
ΔH_v	=	effective heat of gasification of propellant at the surface
ϵ	=	P / P_o
ϵ_1	=	amplitude of the first harmonic pressure oscillations
ϵ_1^i	=	instantaneous value of ϵ_1
ϵ_2	=	amplitude of the second harmonic pressure oscillations
ϵ_2^m	=	steady state shift resulting from second harmonic
ϵ_2^{sc}	=	component of ϵ_2 oscillating with second harmonic
ϵ_2^i	=	instantaneous value of ϵ_2
ϵ_3	=	amplitude of the third harmonic pressure oscillations
ϵ_3^i	=	instantaneous value of ϵ_3
ζ	=	$\frac{\dot{r}_o \times}{\alpha}$
η	=	$K_o / \dot{r}_o \rho C_p T_s^\circ$
θ	=	$(T - T_\infty) / (T_s - T_\infty)$
θ_1	=	component of temperature oscillating with first harmonic
θ_1^*	=	complementing function of θ_1

θ_1°	=	component of surface temperature oscillating with first harmonic
θ_1	=	amplitude of first harmonic surface temperature oscillation
θ_2	=	second order change in θ
θ_2°	=	component of surface temperature oscillating with second harmonic
θ_2^m	=	steady state shift resulting from second harmonic
θ_2^{sc}	=	component amplitude of θ_2 oscillating from second harmonic
θ_3	=	third order change in surface temperature
θ_3°	=	component of surface temperature oscillating with first harmonic
	=	$4 \rho_s / \dot{r}_o^2$
λ_1^r	=	$1 + i \frac{i}{(1+\lambda^2)^{1/4} \sin \nu} / 2$
λ_1^i	=	$- [1 + (1+\lambda^2)^{1/4} \cos \nu] / 2$
λ_2	=	defined by equation (C-7)
λ^i	=	$4 \rho_s / Z_2^2$
μ_1^i	=	first order change in burning rate
μ_1	=	first harmonic amplitude of μ
μ_2	=	second order change in burning rate
μ_2^m	=	steady state shift resulting from second harmonic
μ_2^{sc}	=	component of μ_2 oscillating with second harmonic
μ_3	=	third order change in burning rate
ρ	=	propellant density
τ	=	dimensionless time $\dot{r}_o^2 t / 4 \rho$
ϕ	=	T_∞ / T_s°
ψ_1	=	RT_s° / E_2

$$\begin{aligned}\omega &= 2\pi f_g \\ \omega^1 &= \text{complex frequency} = (\sigma_g + 2i\pi f_g) \\ \nu &= 0.5 \tan^{-1}(\lambda)\end{aligned}$$

1.0 INTRODUCTION

Unstable combustion of solid rocket propellants is of interest for two reasons: (1) it is one of several methods available for investigating the structure of the solid propellant combustion, and (2) unstable combustion has presented serious problems in the development of some operational solid propellant rocket motors. Under Contract No. DA-04-200-AMC-968(x), UTC has been investigating certain aspects of this problem, namely pressure-coupled combustion instability. The principal objective of these studies has been to examine the relationship between combustion instability, as observed by pressure oscillations in the gas phase, and exothermic reactions occurring on and within the solid phase surface.

Experimental studies have been directed toward investigating (1) the effects of coating the solid oxidizer crystals, the chemical and physical nature of the propellant binder, catalysts, and cross-linking agents on the acoustic admittance, (2) nonlinear response properties, and (3) propellant burning rate. Concurrent theoretical studies have been directed toward predicting the effects of these variables on the acoustic response function. Additional analytical studies were conducted to study the transition from linear to nonlinear acoustic response as the amplitude of the pressure oscillations increase. This report represents a summary of the work accomplished under Contract No. DA-04-200-AMC-968(x).

2.0 TECHNICAL DISCUSSION

Recent studies on the structure of the combustion zone of composite solid propellants indicate that there are exothermic processes which occur on and within the solid phase. (1 through 7)* The results of these studies indicate that the combustion process is controlled by two interdependent exothermic reaction zones near and on the surface of the propellant. One zone is in the gas phase at a finite distance from the solid propellant surface and is characterized by interdiffusion of gasified oxidizer and fuel species and combustion of particles of ejected matter from the surface. The second reaction zone occurs on and within the solid propellant surface. The primary heat release in this zone can occur as a result of exothermic decomposition processes and chemical reactions between the initial decomposition products of the various propellant constituents. Transient and steady-state combustion studies indicate that part of the pressure-dependent combustion process can be associated with these reactions.

The exothermic surface reactions can release sufficient heat to expel partially combusted products, pyrolysis products, and fuel and oxidizer fragments into the gas phase zone above the surface, where they intermix and burn completely. The maximum flame temperature is reached in the luminous zone, where the largest portion of the heat is released. However, because of the

* Parenthetical superscript numbers denote references appearing on page 80.

relatively large mass flow perpendicular to the surface, only a small amount of heat released in the luminous flame zone can normally reach the surface to supplement the heat generated by the surface and subsurface reactions.

Incorporation of the exothermic chemical processes at the solid surface represents an important addition to the analysis of propellant combustion phenomena. Until recently, theoretical treatments of steady-state combustion⁽⁸⁻¹¹⁾ as well as combustion instability⁽¹²⁻¹⁸⁾ have considered the effect of the exothermic combustion reactions to originate predominately in the gas phase. However, as Friedly⁽¹⁷⁾ and Marxman⁽¹⁵⁾ have shown theoretically, the principal time lags in the combustion zone are associated with energy transport within the solid phase for oscillations below 10,000 cps. By comparison, the time constants associated with the reaction and transport processes in the gas phase are small, and these processes can be considered to be in equilibrium at any instant. Because the reactions on and below the surface are exponentially dependent on the solid phase temperature, the energy released by these reactions should be an important consideration in the analysis of transient combustion phenomena. Furthermore, the reported data suggest that these reactions exhibit a significant dependence on pressure. Thus, the acoustic pressure oscillations will produce oscillations in reaction rates through both the pressure and temperature sensitivities of the reaction rates which can have a significant effect on the combustion stability behavior of solid propellants.

2.1 EXPERIMENTAL STUDIES

The experimental studies have been directed toward investigating the effects of propellant composition variables on the response of the combustion

process to acoustic pressure oscillations. The principal propellant property derived from these studies is the real part of the acoustic response function, $\text{Re}(\mu/\epsilon)$, which relates the amplitude of the burning rate oscillations to the amplitude of the incident acoustic pressure oscillations by the relationship

$$\text{Re}\left(\frac{\mu}{\epsilon}\right) = \frac{(\tilde{r}/\dot{r}_0)}{(\tilde{P}/P_0)} \quad (1)$$

where

\dot{r}_0 = steady-state burning rate

P_0 = mean combustion pressure

\tilde{r} = amplitude of the burning rate oscillations

\tilde{P} = amplitude of the acoustic pressure oscillation

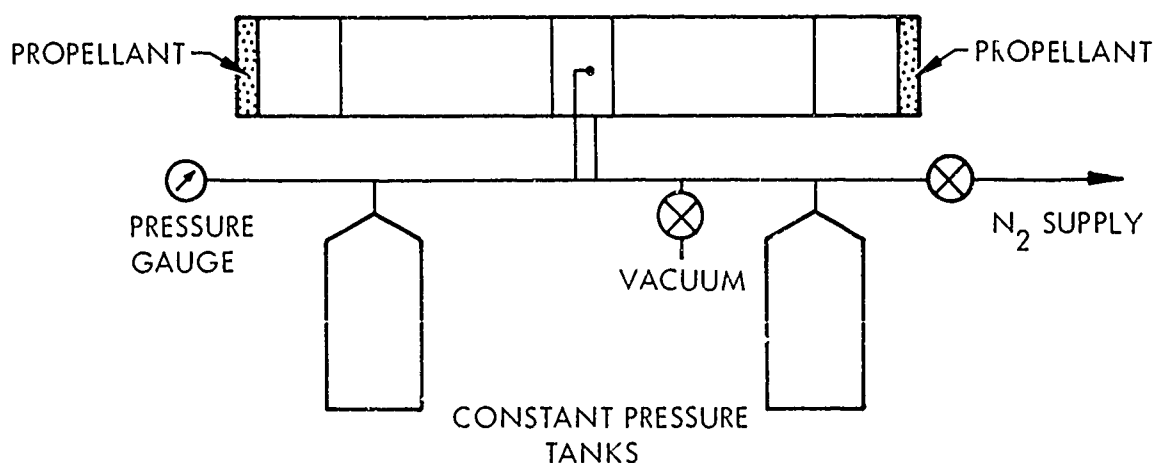
The approach taken in these studies has been to change the propellant composition in such a way that contributions from the possible exothermic surface reactions are varied and to observe the resultant effects on the acoustic response function.

An attempt was also made to examine the propellant combustion visually under oscillatory conditions. A series of preliminary experiments was conducted in which the combustion process was altered by phase shifting the pressure oscillations. These topics are discussed in appendix A.

2.1.1 Experimental Apparatus

Measurement of the acoustic response function can be obtained in a T-burner

apparatus. This type of equipment, which has become almost standard in the industry for acoustic measurements, consists of a cylindrical combustion bomb with end burning charges of propellant in either or both ends. By measuring the oscillating pressure at the ends of the burner, it is possible to derive the acoustic response function for the particular propellant under study. The apparatus used in these studies is based on the design concepts of Horton⁽¹⁹⁾ and Strittmater⁽²⁰⁾ and is shown schematically in figure 1. A photograph of the equipment appears in figure 2.



81309

Figure 1. Diagram of T-Burner

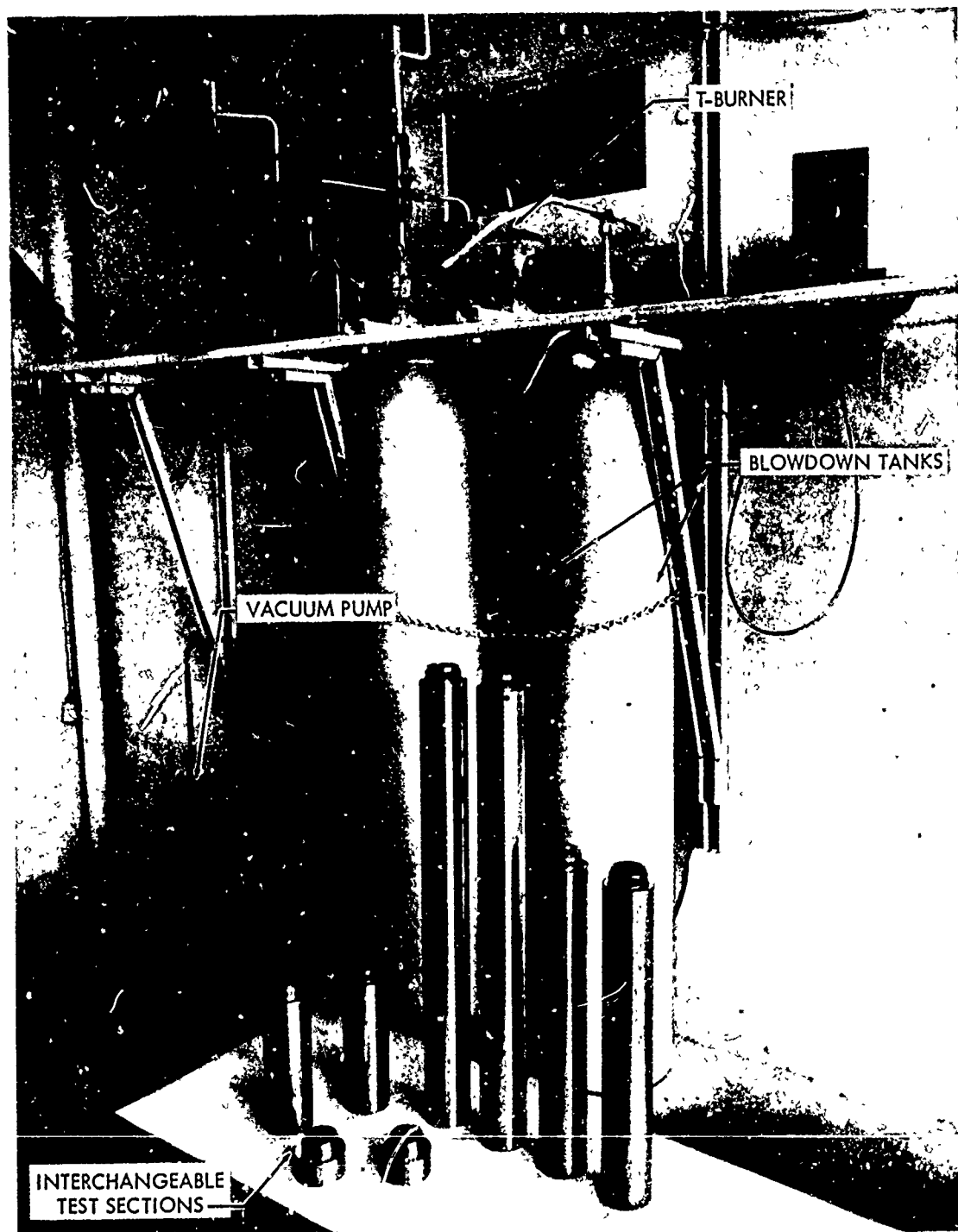


Figure 2. T-Burner

81310

The combustion chamber has an internal diameter of 1.5 in. over the entire length and can be operated as either a single- or double-ended T-burner. Propellant samples are located in the end caps, which also contain provision for the igniter leads and pressure transducers. Nichrome ignition wires are attached to two electrodes which, in turn, are located in a ceramic tube inside the cap and pressure sealed with a connax fitting. The nichrome wire is passed through the propellant sample and is secured to the surface with small staples. Powdered propellant is then placed over the wires. Ignition is obtained by electrically heating the nichrome wire secured to the propellant surfaces. The two end caps are shown with and without a propellant sample in figure 3. The end cap with the propellant sample also shows the ignition wires. Combustion products and pressurized gas are exhausted into two blowdown tanks through four orifices equally spaced around the circumference. The disturbances and resulting acoustic losses caused by this secondary flow are minimized by locating the orifices at the pressure node.

Both the combustion tube and blowdown tanks can be prepressurized with any inert gas to any pressure from 0 to 1,000 psig. A bleed valve is used to exhaust the system to atmospheric pressure, and the excess gases which remain in the system are evacuated with a vacuum pump. The frequency of the acoustic pressure oscillations can be varied by using interchangeable sections of different lengths, as shown in figure 2. Using the double-ended configuration, frequencies between 150 and 5,000 cps can be studied with the present design. This represents the region of interest since the response function curves appear to go through a maximum.

81311

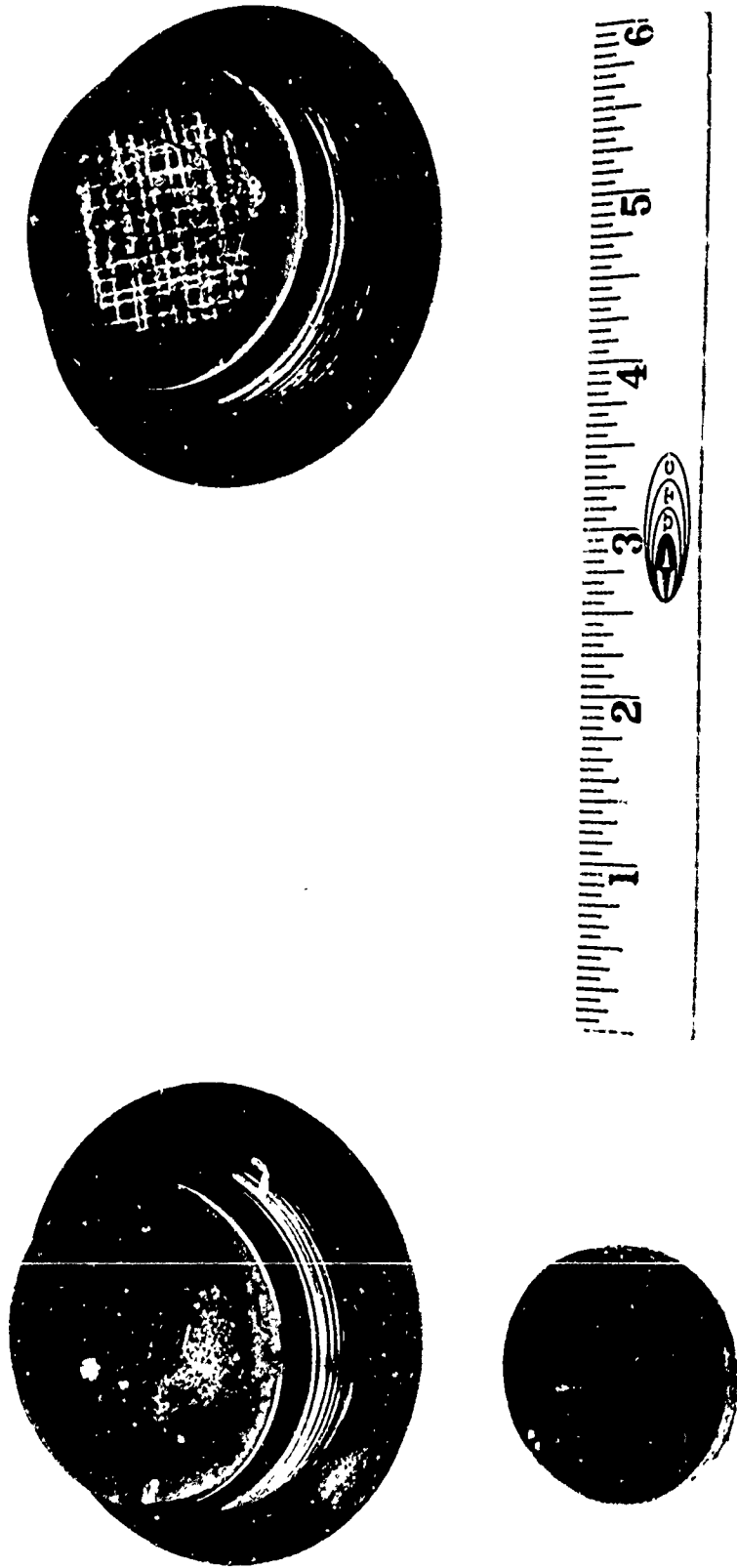
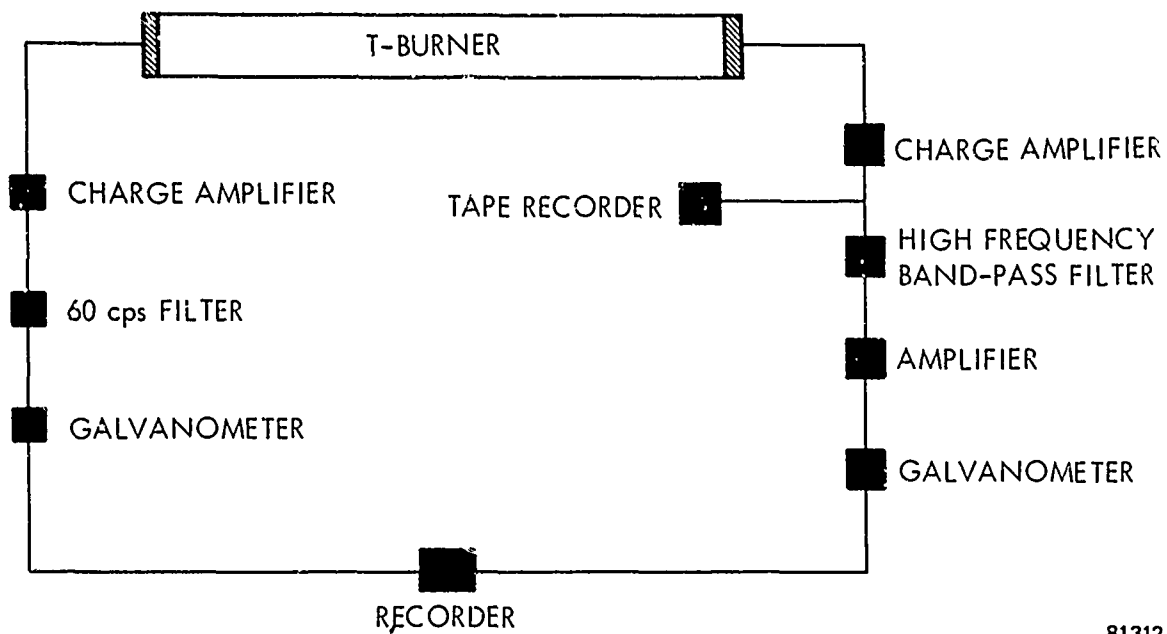


Figure 3. T-Burner End Caps with and without Propellant Sample

The steady-state and oscillating pressures were measured by Kistler model No. 601 pressure transducers in contact with the back surface of each propellant sample. The charge amplifiers were mounted in the test cell next to the transducers to reduce the line losses. Both the average chamber pressure and the oscillating component of pressure were recorded. To record the average chamber pressure, the transducer signal passed through a 60-cps filter and was recorded on a CEC recording oscillograph using a No. 7-346 galvanometer. The high-frequency signal from the transducers, which was used to determine pressure amplitude and wave forms, was recorded on an Ampex tape recorder. The tape output was then passed through a Spenser-Kennedy band-pass variable electronic filter and amplified with a McIntosh amplifier which provides the gain and power necessary to drive a CEC No. 7-361 high-frequency galvanometer. Zener diodes were used as voltage cutoff to protect the galvanometer. To eliminate any low-frequency signals (below 150 cps) from influencing the oscillatory pressure trace, a capacitor was installed between the McIntosh amplifier and the galvanometer. Thus, a low-frequency noise was removed from pressure traces, thereby improving the accuracy of the measurements.

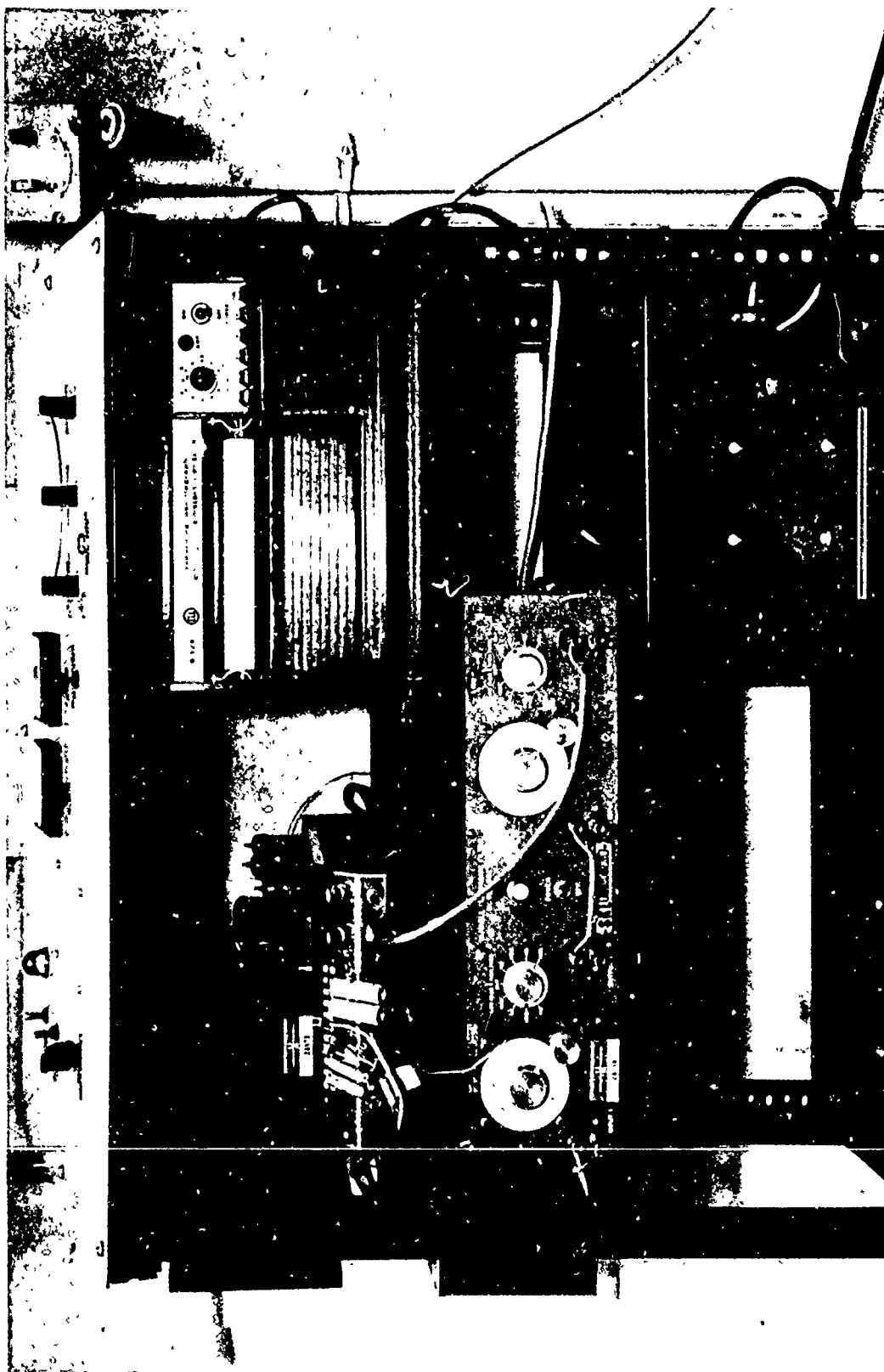
A schematic of the electronics is shown in figure 4, and a photograph of the main components appears in figure 5. The response of the instrumentation was investigated with an oscillator over the frequency range from 150 to 5,000 cps. The recorded wave forms and frequencies were not altered by the signal processing electronics.



81312

Figure 4. Schematic of T-Burner Electronics

At low frequencies the combustion chamber becomes long, and the quantity of room temperature gas required to pressurize the chamber becomes significant. After ignition, a significant period of time is required to achieve thermal equilibrium in the combustor. The acoustic pressure oscillations tend to grow during the period in which thermal equilibrium is being established. This contrasts with the situation in which the instability propagates from a steady-state condition, which usually occurs in actual motors and which is treated theoretically. To obtain more realistic measurements in the low-frequency range, four pieces of propellant $1/4$ in. wide by $3/4$ in. long by $1/16$ in. thick were mounted in the center of the tube near the four vent ports. Because these propellant pieces were located at a pressure node, the oscillations tended to



81313

Figure 5. T-Burner Electronics

be suppressed until these small samples burned out, allowing the propellant samples in the T-burner end caps to achieve steady state before the oscillations grew.

2.1.2 Propellant Formulations

There are several potential methods for controlling the contributions of surface reactions to the acoustical response. One method involves coating the oxidizer crystals to alter the reactivity of the crystal-binder interface. Also, changes in the chemical structure of the binder, in the agents used to crosslink the binder, in catalyst type and content, and in oxidizer particle size and loading were all postulated to influence the acoustic response function. Accordingly, propellants were prepared which permitted investigation of these variables.

The first phase of the experimental program examined the effect of coating the oxidizer with different polymeric materials. A composite propellant normally contains some fine-grind oxidizer; however, coating fine particles results in particle aggregation. With each polymer coating, the size of the aggregated particles vary, and the time involved to eliminate this problem from the program proved to be impracticable. The problem does not occur with larger particles; therefore, AP oxidizer, having average particle size of 190μ , was used.

The solvent-nonsolvent technique was used to apply the polymer coat to the oxidizer. The selected polymer was dissolved in a suitable solvent, and the required amount of AP was added to this solution in a mixer. The solvent was then evaporated from the mix until the gel state of the polymer was present. A second liquid that is nonsolvent for the polymer was then added to the polymer

solution at a low rate. This forced the polymer out of solution and around the particles of AP. Enough of the nonsolvent was added to harden the polymer. After stirring for a specified length of time, the liquid was decanted and the coated material dried. Table I identifies the polymers and additives used.

TABLE I
ADDITIVES

1. LiF - Lithium fluoride
2. Cab-O-Sil - Silicon dioxide
3. Kel-F-800 - Polychlorotrifluoroethylene
4. Hypalon-30 - Chlorosulfonated polyethylene
5. Ethyl cellulose - OH groups in cellulose partly or completely replaced by ethoxyl groups, $O-C_2H_5$

Samples were taken from each batch and tested for a coating by dispersing the oxidizer in a drop of water on a microscope slide. The slide was observed under a microscope, and as the AP dissolved, a coating was observed as an empty polymer shell.

A series of propellants was prepared using the coated oxidizer to study the effects of the coatings on admittance. The use of 190μ AP limited the propellant formulation to 78% oxidizer, and the binder system was a carboxy-terminated polybutadiene to give good flow properties to the mix. The mixer used for preparing the formulations was a 1-pint vertical Baker Perkins. After mixing, the propellant was cast into special molds for the T-burner, and strands

were made to acquire the burning rate of the formulation. The propellant was cured for 5 days at 160°F. The formulation containing the ethylcellulose-coated oxidizer did not wet properly during the mixing cycle, but the propellant cured in a normal manner after the propellant was placed in the molds.

Two formulations were prepared with the coating material added to the propellant mix. These propellants were used to check the effect of the location of the coating (e.g., in the propellant or as a coating on the oxidizer), to evaluate the possibility that the coating could be stripped from the oxidizer during mixing, and the effects of coating porosity.

The particular propellant formulations tested and the resultant burning rate data are shown in table II. Burning rate measurements were made in a standard strand burner at three pressure levels: 200, 500, and 1,000 psig. The data for each system were checked at the 200-psig level with the total burning time measurements in the T-burner, i.e., burn time of the 1/4-in.-thick samples. The difference between the two values was less than 10% in all cases. Because of the experimental scatter in the burning rate measurements, the strand data are valid to within $\pm 10\%$ of the reported values. In some cases, the reported burning rate pressure exponents are abnormally high at 200 psi, especially considering the large oxidizer particle size which was used. However, the data at higher pressures show that the exponents for many of these propellants are not constant over the entire range.

It should be noted that propellants No. 16 through No. 23 were tested for \dot{P} and L^* extinguishment behavior by Jensen.⁽²¹⁾ The catalysts had little effect

TABLE II
PROPELLANT FORMULATIONS

Propellant No.	Formulation No.	Composition Binder/Oxidizer	Oxidizer Particle Size	Oxidizer Coating Polymer, %	Oxidizer Coating Additive, %	Propellant Additive	Rate at 200 psi in./sec	Rate at 200 psi	Binder/Curative
1	UTX-8501	22/78	190.	0	0	0	0.113	0.49	CTPB/NAPO
2	UTX-8502	22/78	190.	1.5 Kel-F	0	0	0.116	0.55	CTPB/NAPO
3	UTX-8525	22/78	100.	0	0	0	0.129	0.58	CTPB/NAPO
4	UTX-8526	22/78	190.	1 Kel-F	1 Cab-O-Sil	0	0.170	0.61	CTPB/NAPO
5	UTX-8527	22/78	190.	1 Kel-F	2 LiF	0	0.063	0.78	CTPB/NAPO
6	UTX-8528	22/78	190.	1.5 Hypalon	0	0	0.128	0.52	CTPB/NAPO
7	UTX-8529	22/78	190.	1.5 Ethyl Cellulose	0	0	0.137	0.51	CTPB/NAPO
8	UTX-8531	22/76.5	190.	0	0	0.77 Kel-F 0.777 Cab-O-Sil	0.158	0.63	CTPB/NAPO
9	UTX-8532-1	22/76.8	190.	0	0	1.2 Kel-F	0.110	0.42	CTPB/NAPO
10	UTX-9164	22/78	190.	3.0 Kel-F	0	0	0.120	0.51	CTPB/NAPO
11	UTX-9165-1	22/78	190.	1.5 Viton A	0	0	0.108	0.45	CTPB/NAPO
12	UTX-9167	22/78	190.	0	0	0	0.145	0.50	PBAN/Epoxy
13	UTX-9168	22/78	190.	0	0	0	0.127	0.50	PBAN/NAPO
14	UTX-9173	22/78	190.	0	0	0	0.138	0.42	CTPB/Epoxy
15	UTX-9368	16/84	70% 190. 30% 8.	0	0	0	0.126	0.30	UTREZ/Cure 1
16	UTX-9379	16/84	65% 190.	0	0	0	0.130	0.37	UTREZ/Cure 2
17	UTX-9395	16/84	35% 8. 65% 190.	0	0	0	0.24	0.21	PEP
18	UTX-9715	16/84	35% 8. 65% 190.	0	0	0.25% Fe ₂ O ₃	0.156	0.36	UTREZ/Cure 2
19	UTX-9717	16/84	35% 8. 65% 190.	0	0	0.50% Fe ₂ O ₃	0.188	0.38	UTREZ/Cure 2
20	UTX-9718	16/84	35% 8. 65% 190.	0	0	0.25% Copper Chromite	0.179	0.49	UTREZ/Cure 2
21	UTX-9719	16/84	35% 8. 65% 190.	0	0	0.50% Copper Chromite	0.182	0.51	UTREZ/Cure 2
22	UTX-9720	16/84	35% 8. 65% 190.	0	0	0.13% Copper Chromite	0.173	0.47	UTREZ/Cure 2
23	UTX 9754	16/84	35% 400. 35% 8.	0	0	0	0.10	0.18	UTREZ/Cure 2

on the L^* extinguishment characteristics. The iron oxide also had no influence on the \dot{P} behavior, while the copper chromite increased the \dot{P} requirement by approximately 30% for the 0.5% catalyzed propellant. In addition, the PEP propellant had higher \dot{P} and L^* extinguishment limits at a fixed pressure in comparison to the UTREZ propellant. The use of larger particle AP was also found to increase the \dot{P} required to terminate combustion at pressures above 250 psi and to decrease the \dot{P} required below 250 psi. At 200 psi, the larger particle propellant (400μ) has a critical \dot{P} approximately half that of the 200μ propellant.

2.1.3 Reduction of Experimental Data

The relationship between the observed acoustic pressure oscillations and the acoustic response function of the propellant has received considerable attention. (20,22,23,24) Although several methods have been developed to derive the acoustic response function from acoustic pressure measurements, the only method used in this study was based on growth and decay constant determination, that is,

$$\text{Re} \left(\frac{\mu}{\epsilon} \right) = \frac{P_o}{4c\rho \dot{t}_o} \left[\frac{\alpha_g}{f_g} - \frac{\alpha_d}{f_d} \right] \quad (2)$$

During the experimental program, special care was required when tests were conducted at low frequencies. Under these conditions, the combustion chamber became long and the quantity of room temperature gas required to pressurize the chamber thereby became significant. After ignition, a significant period of time was required to achieve thermal equilibrium in the combustor. However, the frequency of the pressure oscillations depended on the temperature through

the sonic velocity, i.e., $c \sim \sqrt{T}$, through the expression

$$f_g = c/2L \quad (3)$$

The sonic velocity in equation 2 results from considerations at the combustion zone and, therefore, should be evaluated from the experimental flame temperature. The approach used in this study was based on the assumption that, at high frequencies (short combustion chamber) the experimental flame temperature is established throughout the combustion chamber very rapidly. Thus, c was evaluated from equation 3 extrapolating the parameter $2Lf_g$ to high frequencies. This amounts to a partial correction of the generalized acoustic response analysis by NOTS⁽²⁵⁾ in that the common uncorrected response function is based on an average speed of sound (c_o) in the denominator of equation 2 instead of the sonic velocity of the gas in the combustion zone (c). This report suggests that the correction factor applied to the data should be based on a correction term given by $(c_o/c)^2$. Thus, if our data are to be corrected further in accordance with their results, then the numerical values of $\text{Re}(\mu/\epsilon)$ at lower frequencies should be multiplied by c_o/c and would be reduced by a small amount at low frequencies. The frequency at which the maximum occurs would not be altered by the correction term.

2.1.4 Experimental Results

Acoustic response function of propellants shown in table II were determined as a function of frequency in the T-burner. These data are presented in figures 6 through 19, using the normalized frequency $8\pi f_g / \dot{t}_o^2$ as the parameter. This form was used based on the theoretical studies of Hart⁽¹²⁾ and Friedly⁽¹⁷⁾ and

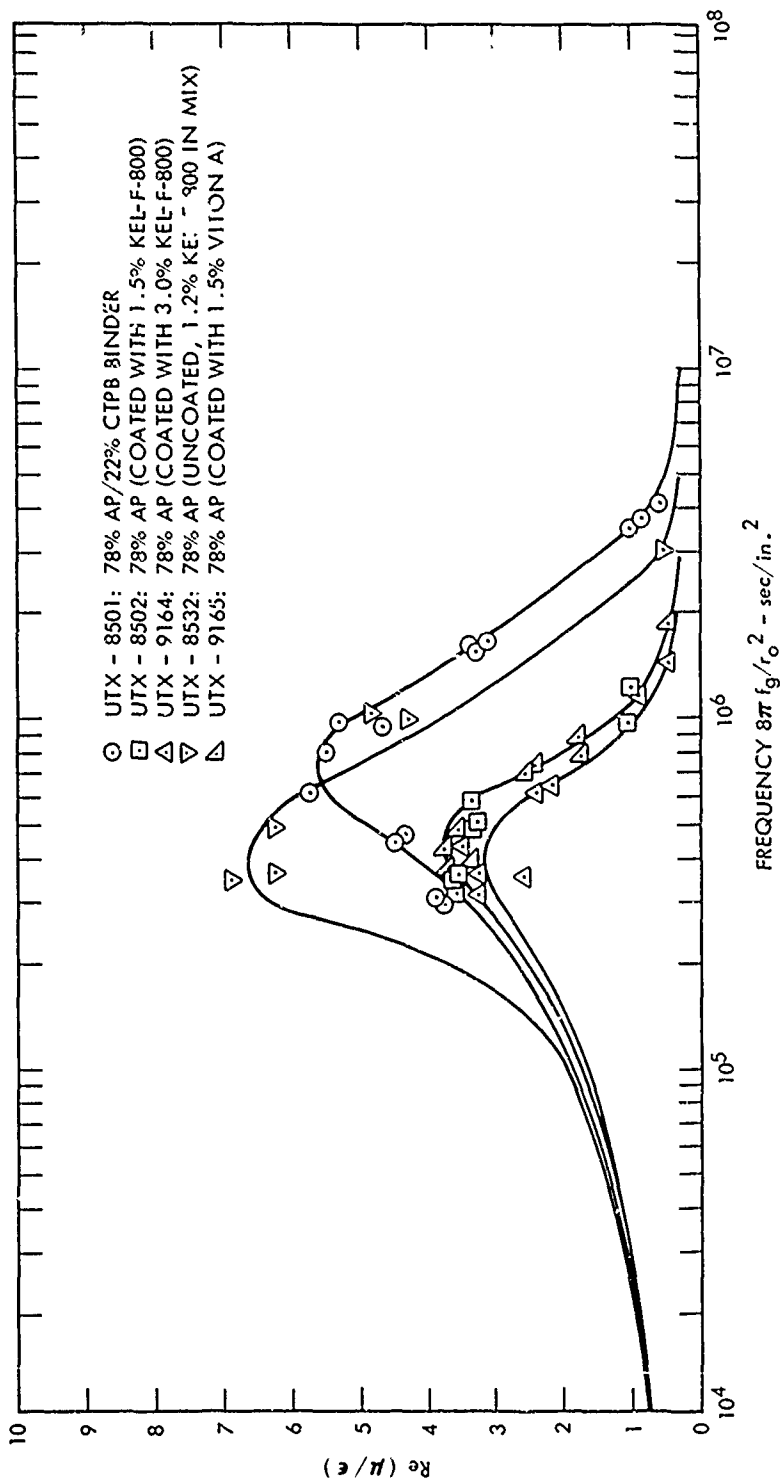


Figure 6. Effect of Kel-F and Viton Coatings on Acoustical Response

81315

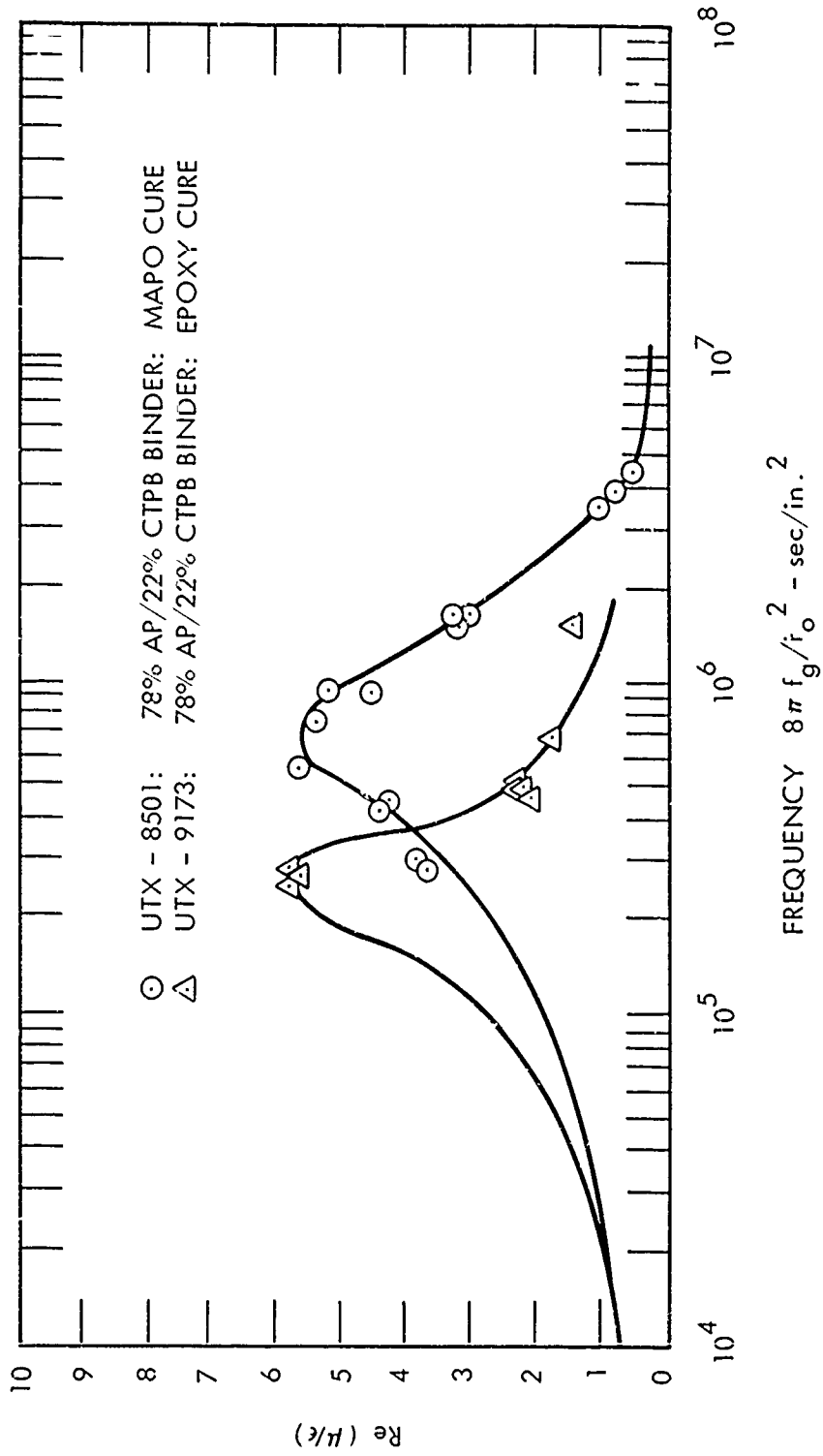


Figure 7. Effect of Cure Agents

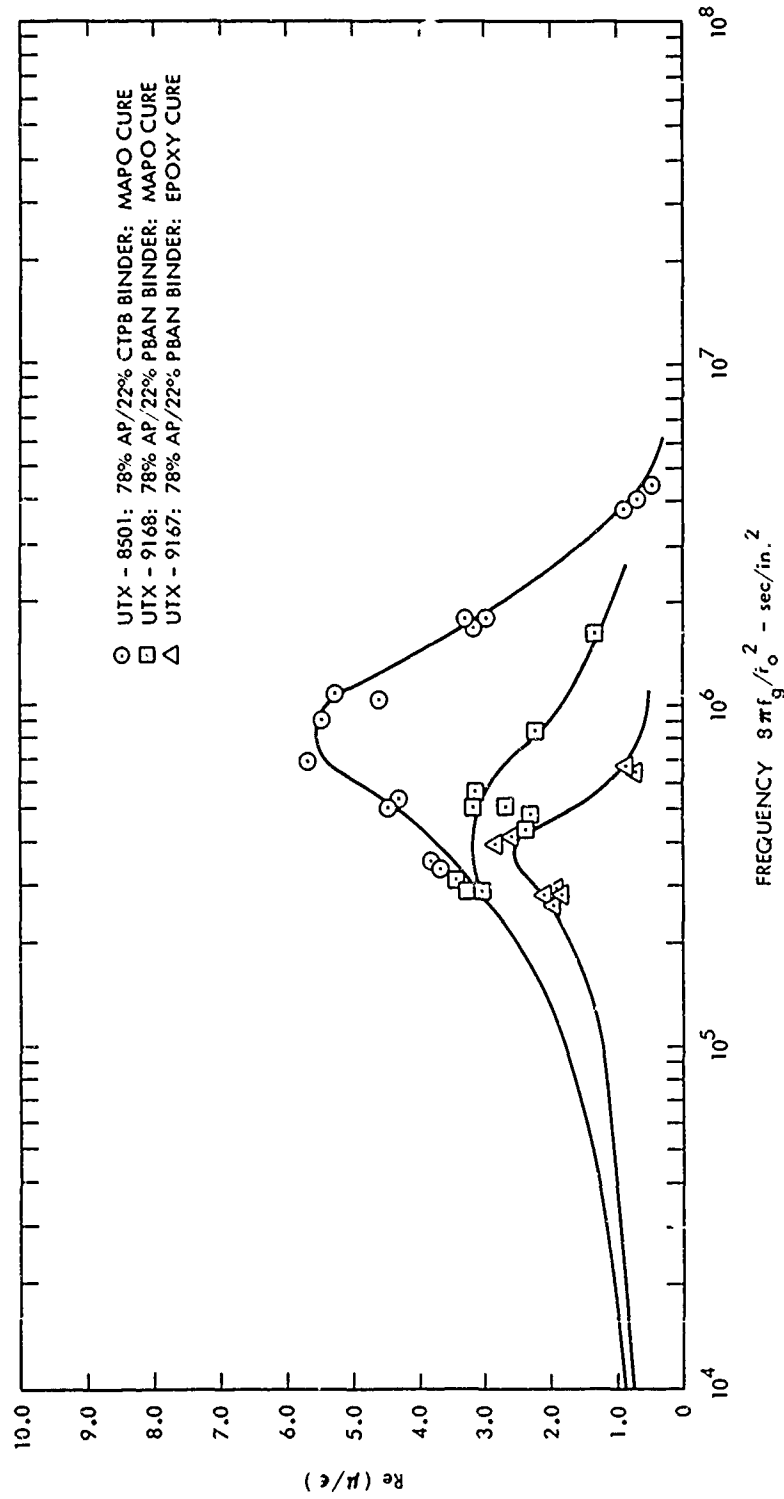
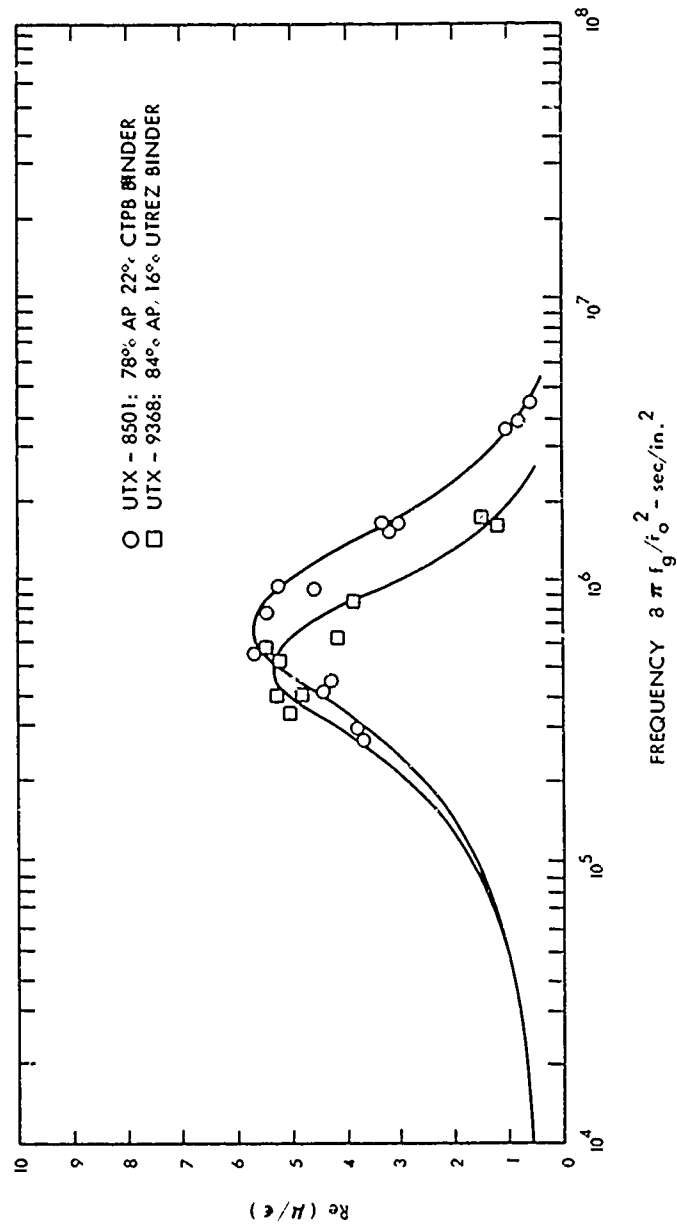
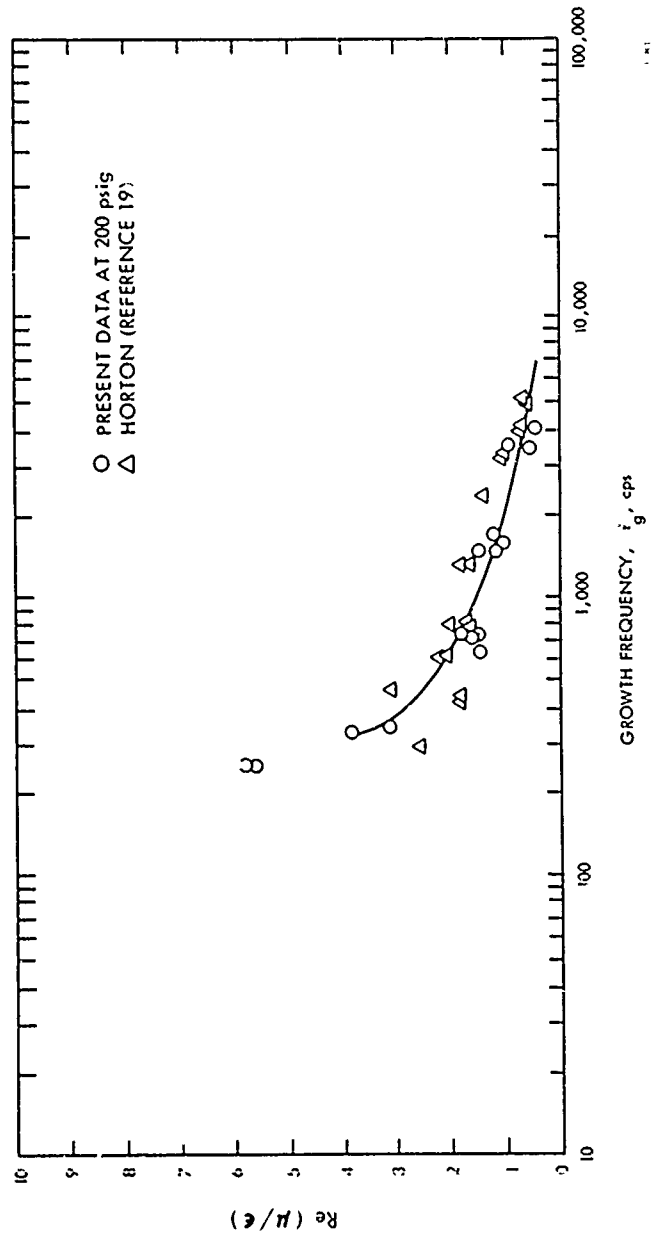


Figure 8. Effect of PBAN Binders



81317

Figure 9. Acoustic Response of CTPB and UTREZ Binders



81318

Figure 10. NOTS A-13 Propellant Data

81319

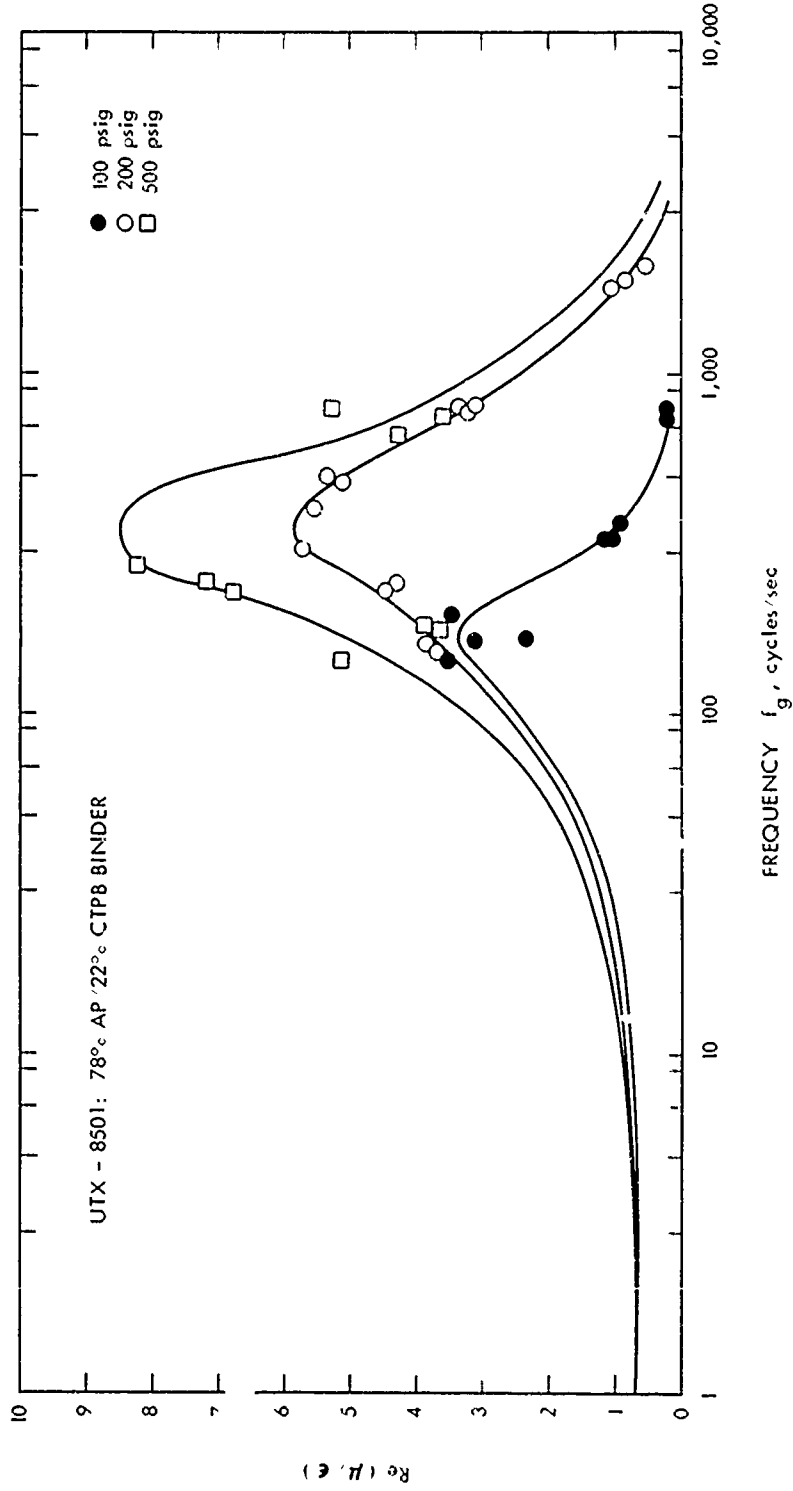


Figure 11. Effect of Pressure on Acoustic Response

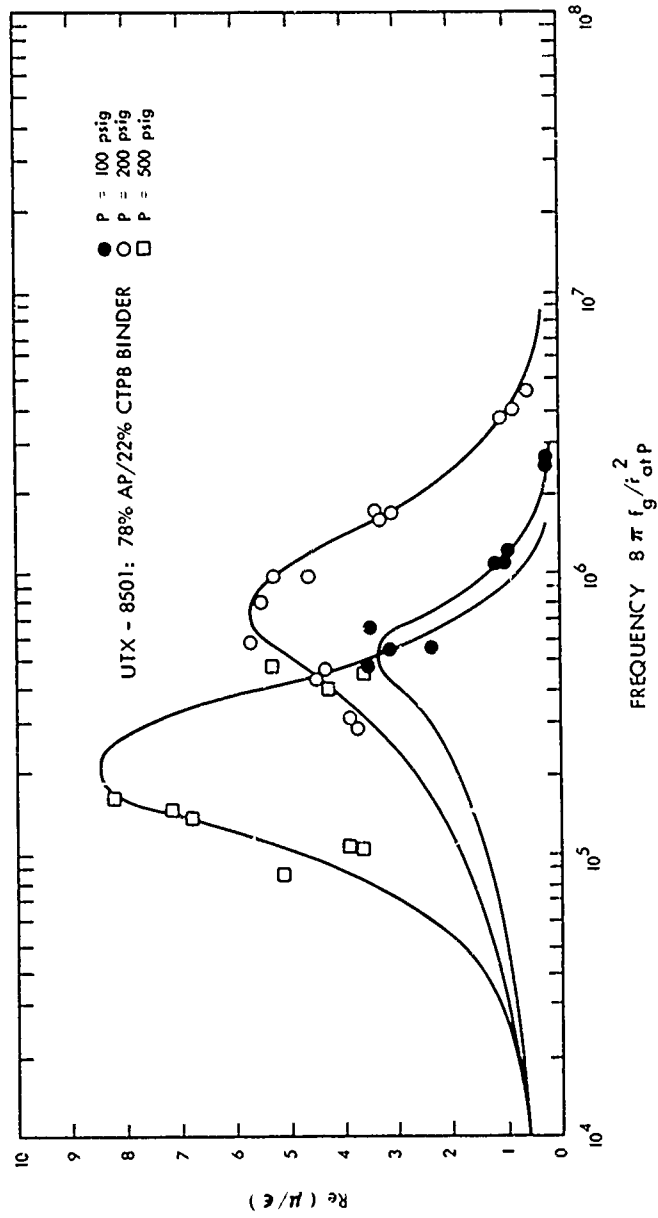


Figure 12. Effect of Pressure on Acoustic Response

81320

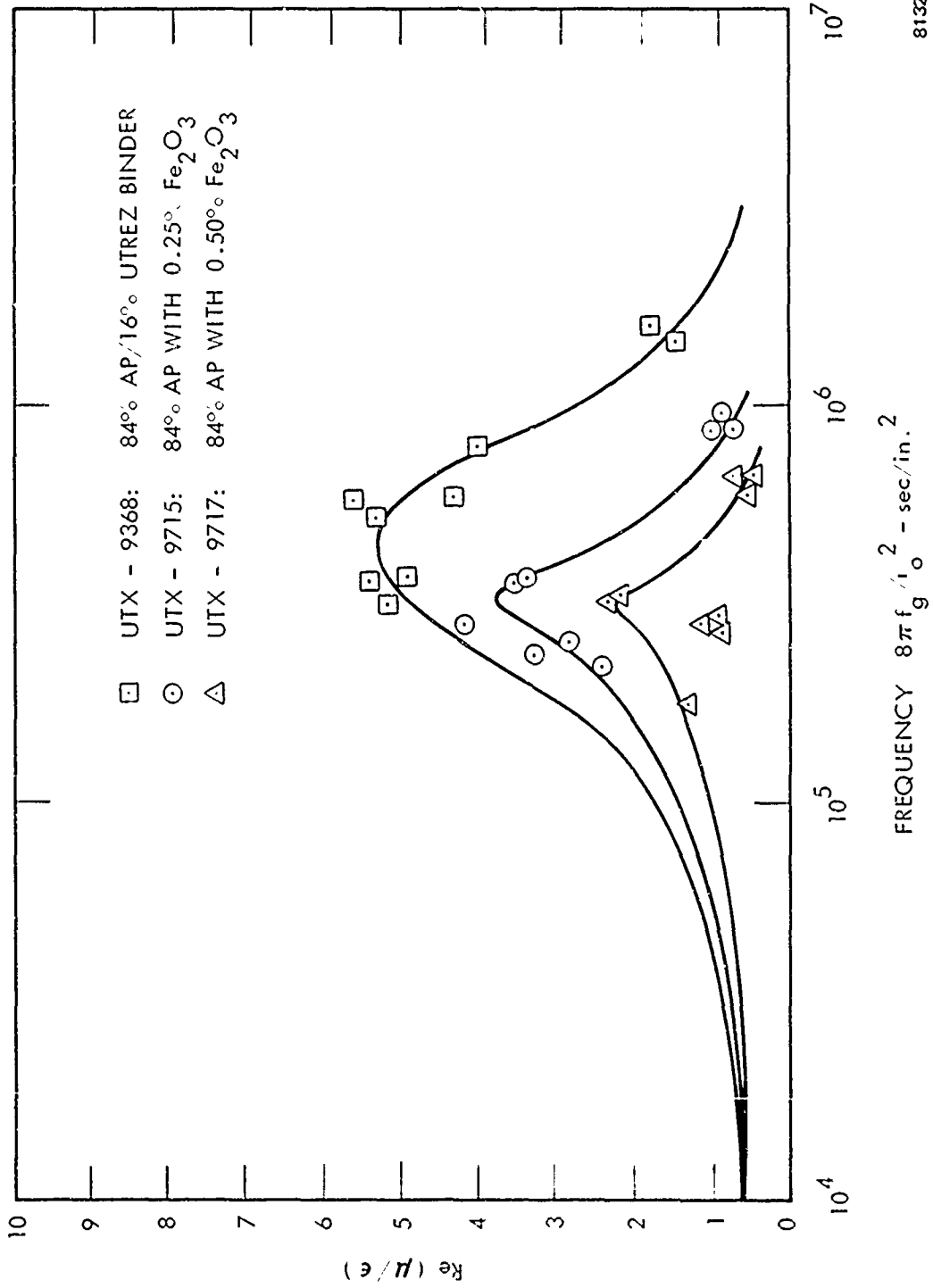
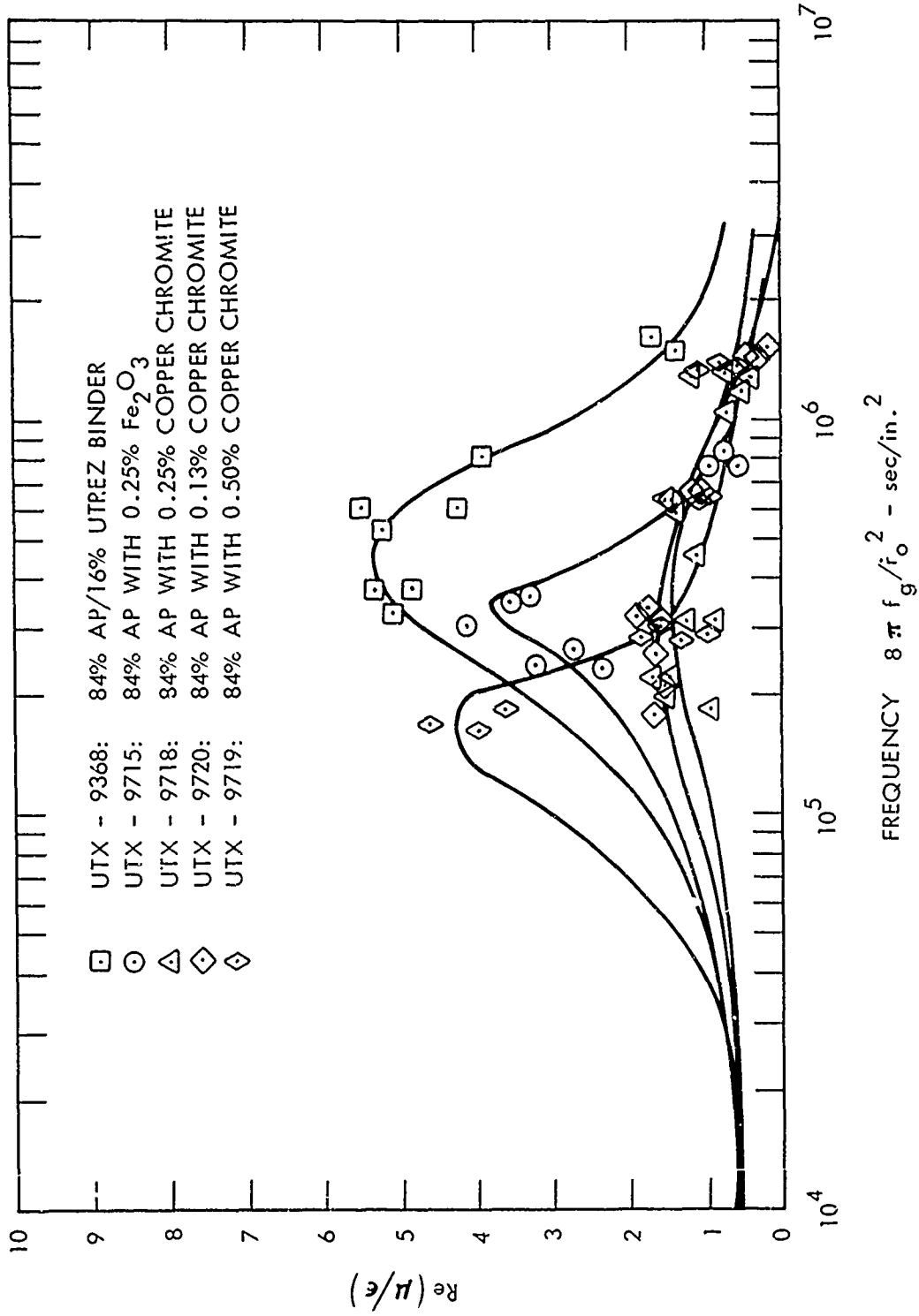


Figure 13. Effect of Ferric Oxide Catalysis



81322

Figure 14. Effect of Copper Chromite

81323

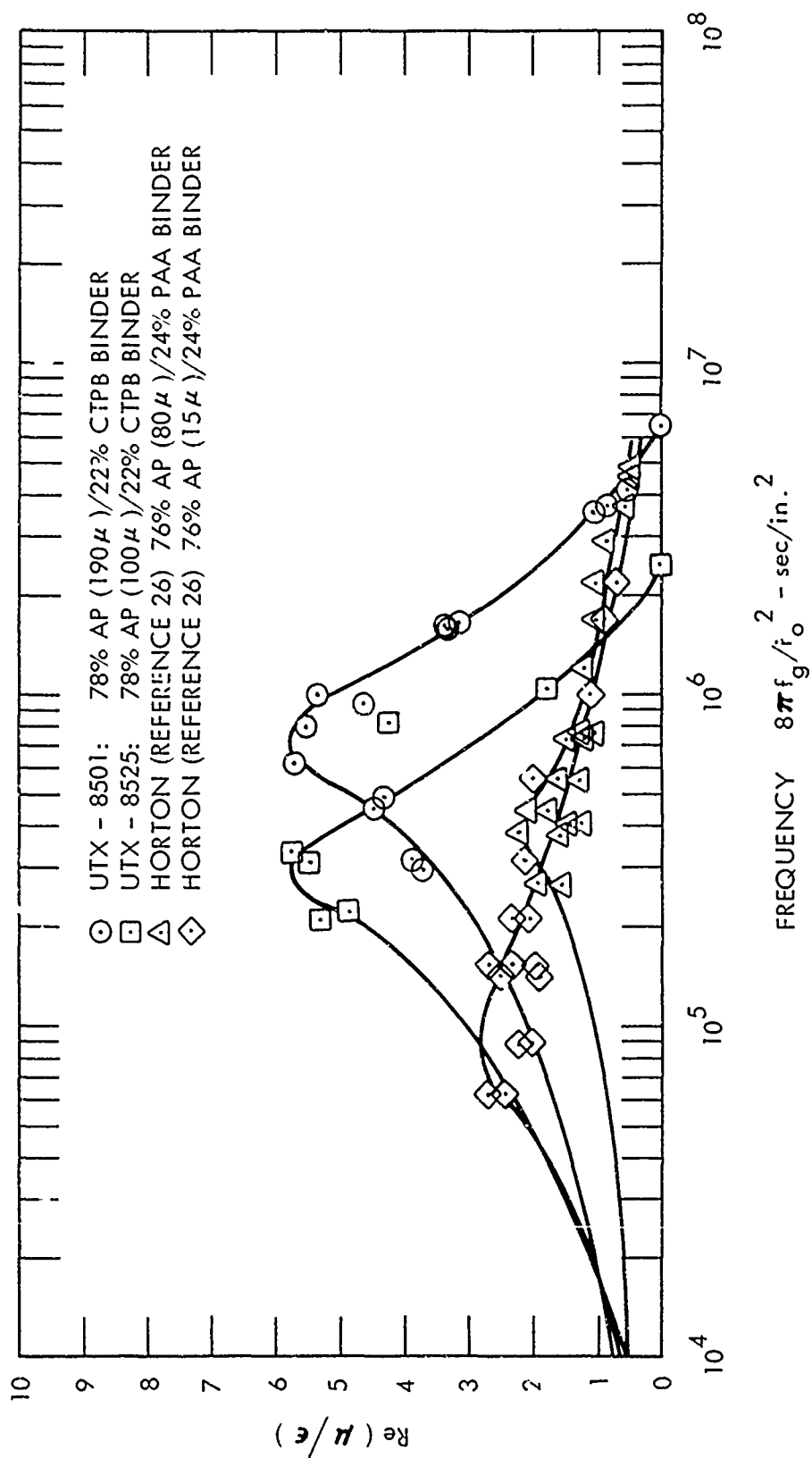


Figure 15. Effect of AP Particle Size

81324

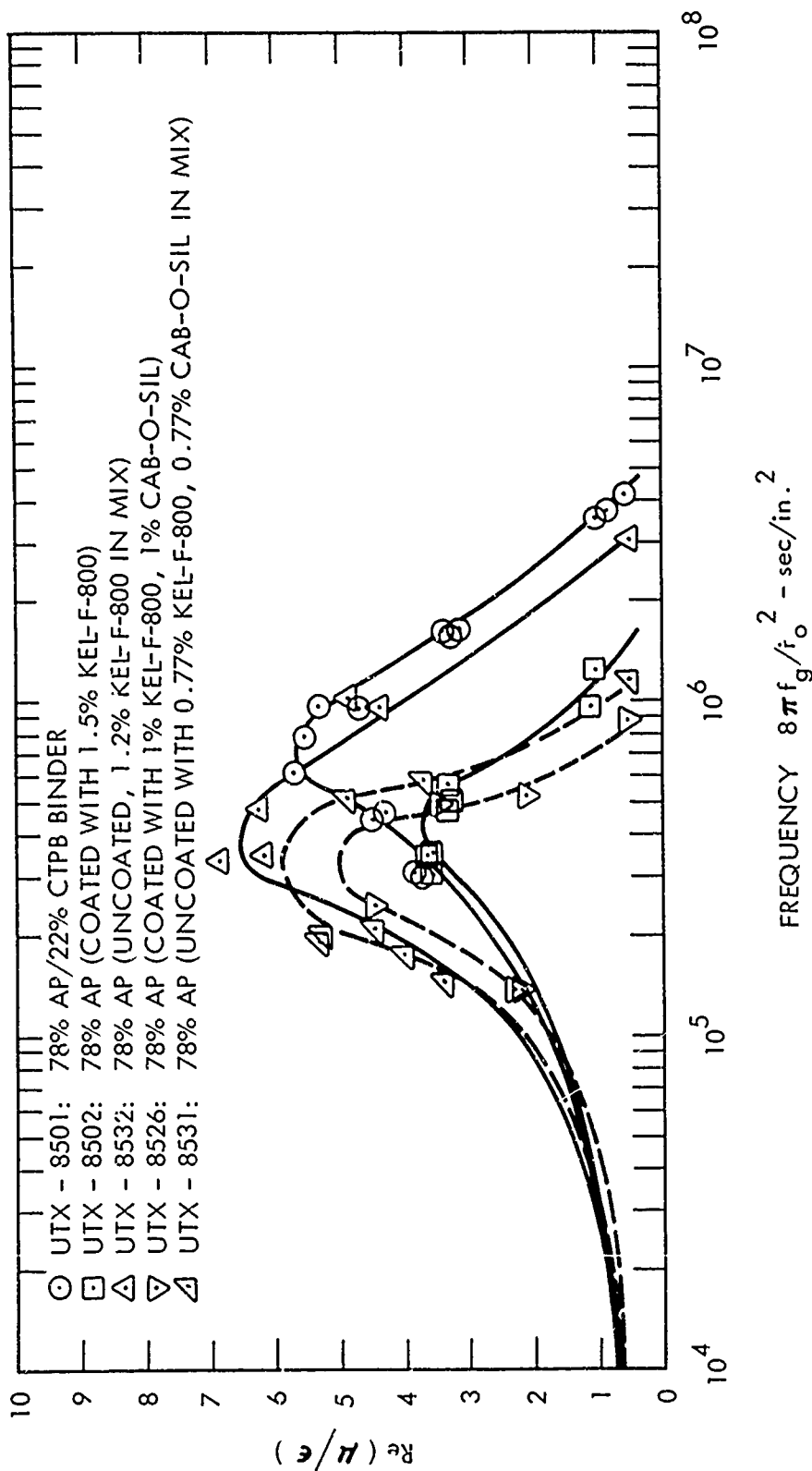


Figure 16. Effect of Coating or Addition to Propellant Mix

81325

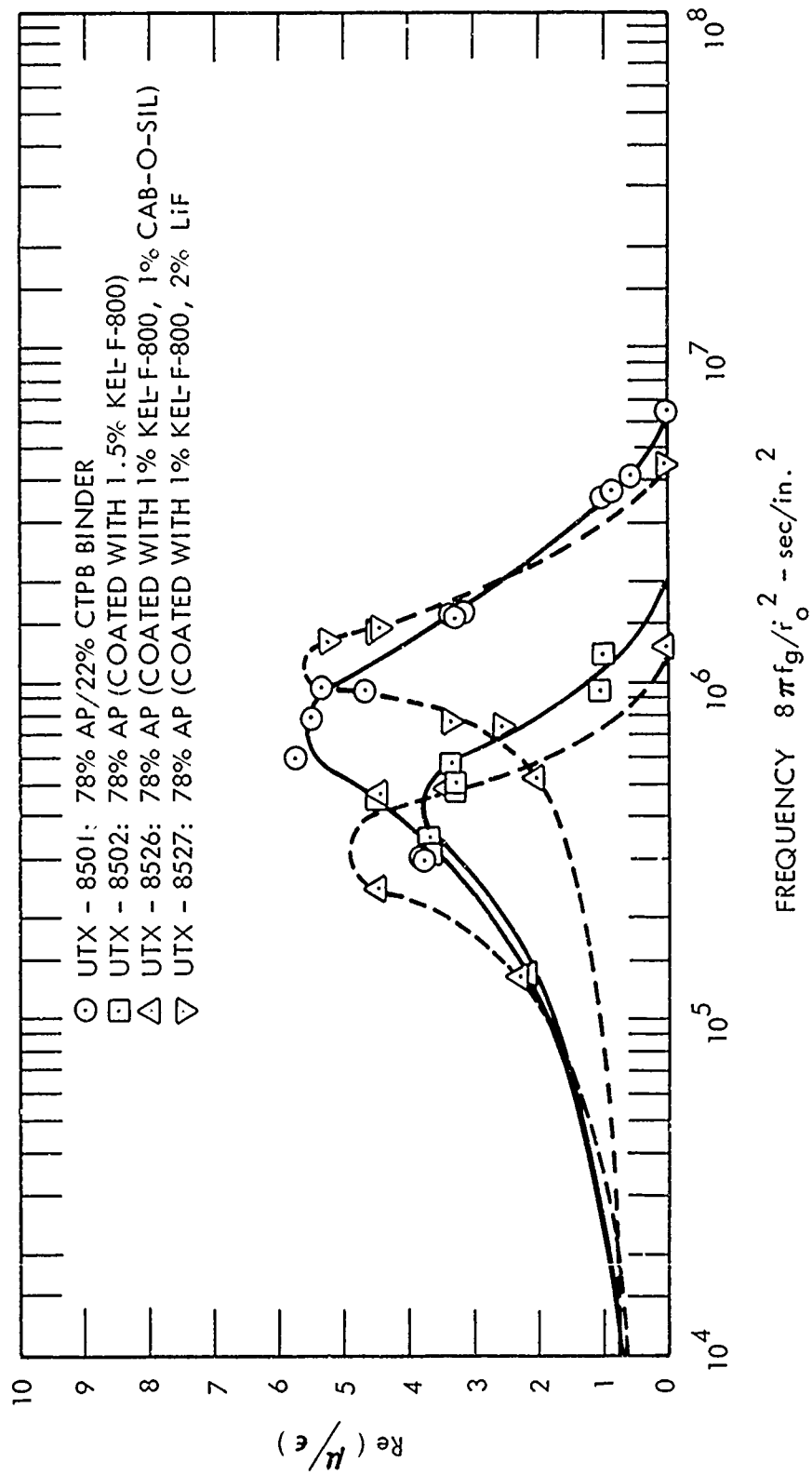


Figure 17. Effect of Kel-F Coatings

81326

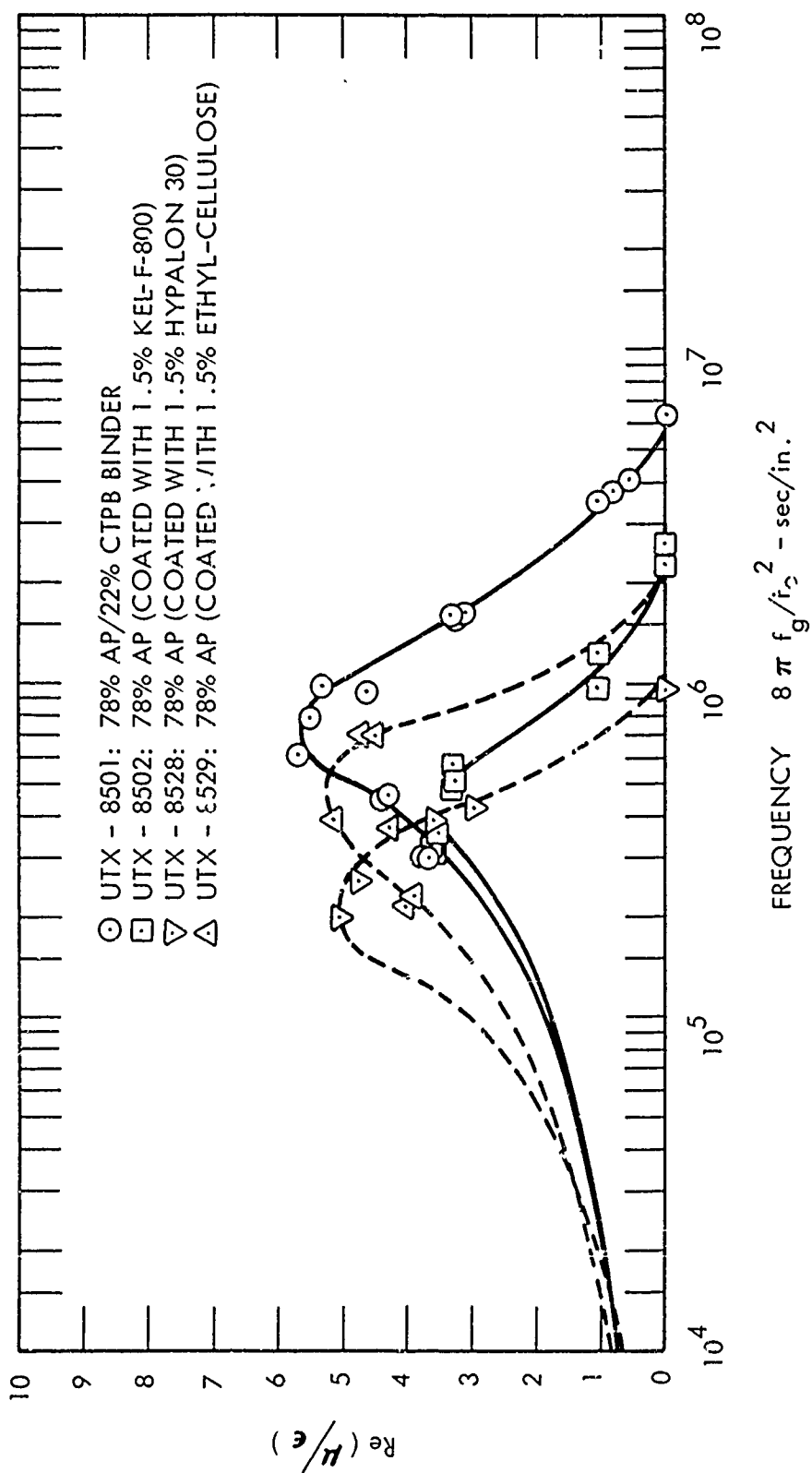
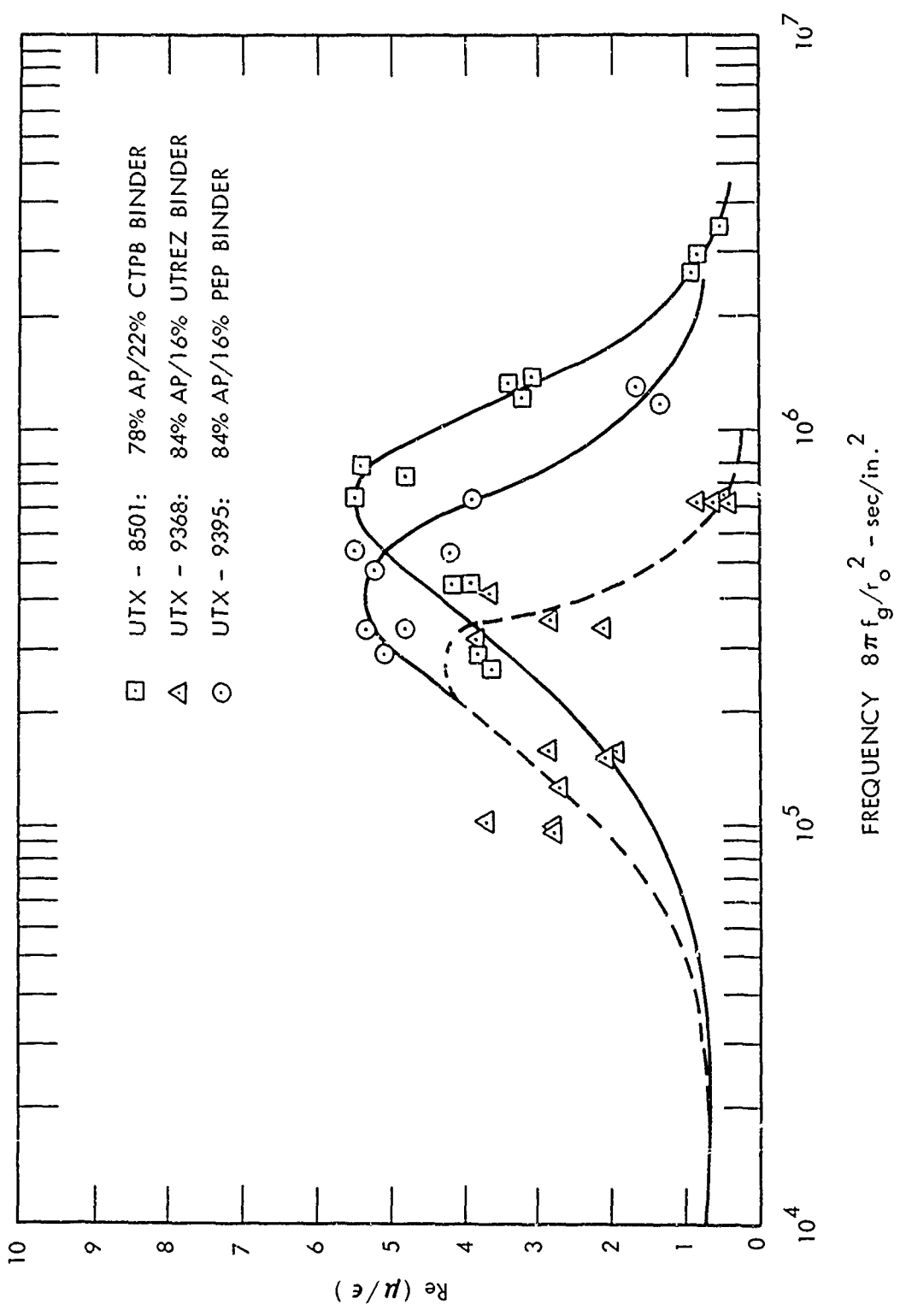


Figure 18. Effect of Various Coatings



81327

Figure 19. Effect of Binders

the theoretical studies to be discussed in the following sections. These theoretical studies suggest that the proper form for the dimensionless frequency should include the propellant thermal diffusivity. For the propellants listed, this propellant property should be relatively constant (approximately 3×10^{-4} in.²/sec); therefore it has been omitted. In addition, the definition of the acoustic response function is such that it should approach the normal burning rate pressure exponent as the frequency approaches zero; therefore, the data are reported showing the extrapolation at low frequencies to the burning rate pressure exponent obtained from the burning rate measurements.

For completeness, all the experimental data obtained for all the propellants shown in table II are presented in appendix B. The values of the growth frequency (f_g), growth rate (α_g), decay frequency (f_d), decay rate (α_d) and $\text{Re}(\mu/\epsilon)$ are reported.

It is important to note that the data are subject to significant uncertainty. The steady-state burning rates, as previously indicated, may have errors as high as $\pm 10\%$. These values enter into the calculations of the response functions, i.e., $\mu \sim 1/\dot{r}_0$, and the frequency functions, $8\pi f_g/\dot{r}_0^2$. In addition to these uncertainties, the measurements of the growth and decay rates are subject to an uncertainty of $\pm 10\%$; therefore, the absolute value of the response function μ/ϵ is valid to within $\pm 20\%$. The experimental results must be interpreted accordingly.

As part of activity associated with the ICRPG round robin group on combustion instability, the acoustic response function for A-13 propellant (an NWC

formulation) was measured at UTC. The results of these tests agree with the earlier data obtained at NWC by Horton,⁽¹⁹⁾ as shown in figure 10. Hence, it is reasonable to assume that the differences in the design of the two T-burners do not influence the experimental results.

2.2 THEORETICAL STUDIES

Before the experimental data presented in the preceding paragraphs can be analyzed, it is necessary to have some theoretical framework as a guide. To develop this framework, one can take two approaches. For the first approach, a rather complete and detailed model of the combustion process must be postulated. The various important processes are characterized mathematically and the resulting equations are solved to obtain the desired theoretical result. By comparing theoretical and experimental results, one can derive values for specific physical constants (i.e., activation energies, heats of reaction, etc.) which are presumed to characterize the combustion process. The results reflect the particular bias of the specific model, and the derived values for the various physical constants are often difficult to interpret since independent measurements are difficult to obtain.

Another approach minimizes the specific assumptions concerning the detailed structure at the combustion zone. The result is a mathematical formulation which contains a number of parameters which have no definition in physical terms. They can be derived from the experimental data and, by examination of a number of possible physical definitions, some further insight into the combustion zone can be obtained. The principal advantage of this approach is that one is not committed to a specific model; instead, the experimental evidence guides the

theoretical development. Also, by limiting the number of physical assumptions, one can better test their validity.

In the paragraphs which follow, the general analysis will be presented, and then the specific analysis developed early in the program will be derived from the general treatment.

2.2.1 General Combustion Analysis

For the purpose of analysis, the solid phase within the combustion zone is assumed to be characterized by the transient one-dimensional heat conduction equation

$$\frac{\partial T}{\partial t} = \alpha \frac{\partial^2 T}{\partial x^2} + \dot{q} \frac{\partial T}{\partial x} \quad (4)$$

The justification for this assumption has been presented in several papers and need not be presented here. However, it is recognized that this assumption still may not be valid. More discussion on this point will be presented in later paragraphs.

At the solid surface, the rate at which energy is transferred into the solid is given by

$$-k \left(\frac{\partial T}{\partial x} \right)_{x=+0} = F(T_s, P, T_f) \quad (5)$$

The function F contains the effects of energy transfer from the gas-phase combustion processes as well as the energetics of any surface reaction/vaporization processes. Also, deep within the propellant the temperature is not influenced

by the combustion process. Thus

$$T \rightarrow T_{\infty} \text{ as } x \rightarrow \infty \quad (6)$$

Within the gas phase, it is generally possible to characterize the burning rate by the general expression

$$\dot{m}_g = J(T_s, P, T_f) \cdot \rho \quad (7)$$

The specific details of the gas-phase combustion will determine the particular functional form, but most gas-phase combustion models, be they diffusion or premixed flames, will follow this general relationship.

At the solid surface, the rate of gasification can be expressed by

$$\dot{r} = H(T_s, P) = \dot{m}_s / \rho \quad (8)$$

Equations 4 through 8 constitute a general combustion model in which the only assumptions concerning the chemistry and physics of the process are that the bulk solid is homogeneous and nonreactive. These equations can now be solved for the transient burning rate and gas temperature response to a pressure disturbance. First, since $\dot{m}_g = \dot{m}_s$, equations 7 and 8 can be combined to yield an expression for the gas temperature in terms of the pressure and surface temperature

$$T_f = G(T_s, P) \quad (9)$$

Then the gas temperature can be eliminated from equation 5 using equation 9 to yield

$$-k(\partial T/\partial x)_{x=+0} = F(T_s, P) \quad (10)$$

The analysis can be simplified further by normalizing the characterizing equations using the definitions

$$\begin{aligned} \theta &= (T-T_\infty)/(T_s^\circ - T_\infty) & \zeta &= \dot{r}_0 x/\alpha \\ \tau &= r_0^2 t/4\alpha & \epsilon &= P/P_0 \end{aligned} \quad (11)$$

Hence, equations 4, 8, and 10 become

$$\frac{\partial \theta}{4\partial \tau} = \frac{\partial^2 \theta}{\partial r^2} + H_n(\theta_s, \epsilon) \cdot \frac{\partial \theta}{\partial r} \quad (12)$$

$$H_n(\theta_s, \epsilon) = \dot{r}/\dot{r}_0 \quad (13)$$

$$-(\partial \theta/\partial \zeta)_{\zeta=+0} = F/F_0 = F_n(\theta_s, \epsilon) \quad (14)$$

and

$$\theta \rightarrow 0 \text{ as } \zeta \rightarrow \infty$$

It should be noted that Hart and coworkers⁽¹⁸⁾ have used a similar approach for characterizing the gas phase portion of the combustion zone. However, they used an Arrhenius relation to characterize the surface gasification process. In view of the complexity of this process, especially in composite propellants with several ingredients decomposing and the partially molten nature of the surface, the use of a single overall pyrolysis law is an oversimplification and

seems unwarranted. Also, one does not need to make this assumption to arrive at a useful result, as the following development will show.

To solve equations 12, 13, and 14, the dependent variables can be expanded in a Taylor series, i.e.,

$$e = 1 + \Lambda e_1 + \Lambda^2 e_2 + \Lambda^3 e_3 + \dots \quad (15)$$

In a similar manner, the functions H_n , F_n and G_n can be expanded by a Taylor series to yield, for example

$$\begin{aligned} H_n(e, s, \dots) &= 1 + \Lambda e_1^\circ \left(\frac{\partial H_n}{\partial e} \right)_0 + \frac{1}{1} \left(\frac{\partial H_n}{\partial e} \right)_0 + \frac{\Lambda^2}{2} (e_1^\circ)^2 \left(\frac{\partial^2 H_n}{\partial e^2} \right)_0 \\ &+ \frac{1}{1} \left(\frac{\partial^2 H_n}{\partial e^2} \right)_0 + 2e_2^\circ \left(\frac{\partial H_n}{\partial e} \right)_0 + 2 \frac{1}{2} \left(\frac{\partial H_n}{\partial e} \right)_0 + \frac{\Lambda^3}{6} \dots \\ &= 1 + \Lambda \cdot \mu_1 + \frac{\Lambda^2}{2} \cdot \mu_2 + \dots \end{aligned} \quad (16)$$

Equations 15 and 16 can then be substituted into equations 12, 13, and 14 to yield a series of simultaneous equations characterizing the burning rate behavior.

2.2.2 Linear Response

The linear response of this set of equations can be determined by collecting terms of the order Λ , i.e.,

$$\frac{1}{4} \frac{\partial e_1}{\partial t} = \frac{\partial^2 e_1}{\partial \xi^2} + \frac{\partial e_1}{\partial \xi} + \left[e_1^\circ \left(\frac{\partial H_n}{\partial e} \right)_0 + \frac{1}{1} \left(\frac{\partial H_n}{\partial e} \right)_0 \right] \cdot \frac{\partial \theta}{\partial \xi} \quad (17)$$

$$-(\partial e_1 / \partial t)_{t=+0} = e_1^\circ \left(\frac{\partial F_n}{\partial e} \right)_0 + \frac{1}{1} \left(\frac{\partial F_n}{\partial e} \right)_0 \quad (18)$$

Assuming the pressure oscillates as

$$e_1' = p_1 \exp(i\lambda x) \quad (19)$$

the equations for the linear response (i.e., the acoustic response function)

$$\frac{u_1}{p_1} = [A_1 B_1 + Q_1 (\lambda_1 - R_1)] / [\lambda_1 + A_1 / \lambda_1 - R_1] \quad (20)$$

where

$$\lambda_1 (\lambda_1 - 1) = i\lambda / 4 \quad (21)$$

$$R_1 = [\partial F_n / \partial c]_0 \quad B_1 = [\partial F_n / \partial \rho]_0$$

$$A_1 = [\partial H_n / \partial \epsilon]_0 \quad Q_1 = [\partial H_n / \partial \epsilon]_0$$

The corresponding equations for the burning rate pressure exponent, surface temperature and flame temperature amplitudes are

$$n[1 + A_1 - R_1] = A_1 B_1 + Q_1 (1 - R_1) \quad (22)$$

$$(\dot{v}_1 / p_1) = [(u_1 / p_1) - Q_1] / A_1 \quad (23)$$

$$\frac{T_f - T_f^0}{T_f^0} = \left. \frac{T_f - T_f^0}{T_f^0} \right|_{x=0} + [(u_1 / p_1) - n] [(\partial G / \partial \epsilon)_0 / A_1] \quad (24)$$

Substituting equation 22 into equation 20 yields the familiar result

$$(u_1 / p_1) = [n(1 + A_1 - R_1) + Q_1 (\lambda_1 - 1)] / [\lambda_1 + A_1 / \lambda_1 - R_1] \quad (25)$$

It should be noted that a detailed knowledge of the structure of the gas phase combustion zone or the surface degradation process is not required to characterize the acoustic response function. The combustion parameters represent the partial derivation with respect to surface temperature and pressure of both the burning rate and the energy flux into the solid. These general definitions of the combustion parameters explain why Culick⁽²⁷⁾ was able to show that most proposed combustion models could be placed in the form of equation 25. If $Q_1 = 0$, the result reduces to the form discussed in several recent reports and papers, with a slight redefinition of the parameter B_1 .

Further manipulation of equations 19, 20, and 21 shows that the region of intrinsic stability is defined by the relations

$$4A_1 > R_1^2 \quad (26)$$

$$2A_1 > R_1(R_1 - 1) \quad (27)$$

If these conditions are not satisfied, any perturbation in the combustion process, regardless of the source, will cause runaway burning rates. They form a boundary for realistic values of A_1 and R_1 which can be ascribed to real propellants.

2.2.3 Second Order Behavior

Collecting terms of the order Λ^2 yields

$$\frac{1}{4} \frac{\partial^2 \theta_2}{\partial t^2} = \frac{\partial^2 \theta_2}{\partial r^2} + \frac{\partial^2 \theta_2}{\partial r^2} + u_1 \frac{\partial \theta_1}{\partial r} + \left| \frac{\mu_2}{2} \right| \frac{d\theta_0}{dr} \quad (28)$$

$$\begin{aligned}
 -\left(\frac{\partial \theta_2}{\partial t}\right)_{t=0} &= \frac{(\theta_1^0)^2}{2} \frac{\partial^2 F_n}{\partial \theta^2} \Big|_0 + \theta_1^0 \left(\frac{d^2 F_n}{d\theta dt}\right) \Big|_0 + \frac{1}{2} \left(\frac{d^2 F_n}{dt^2}\right) \\
 &+ \theta_2^0 \left(\frac{\partial F_n}{\partial \theta^0}\right) \Big|_0 + \theta_2^0 \left(\frac{dF_n}{dt}\right) \Big|_0
 \end{aligned} \tag{29}$$

These equations are linear in the unknown θ_2 , but nonlinearities appear in the form of the cross products of first order terms. In the solution of the first order problem, the dimensionless temperature was given by

$$\theta_1^0 = \epsilon_1 \exp(i\lambda \tau)$$

However, equations 28 and 29 were derived using the real part of θ_1^0 . Hence, as Friedly⁽²⁸⁾ has shown, the cross products of the first order terms must be considered as

$$[\text{Re}(\theta_1^0)]^2 = \frac{\text{Re}(\theta_1 \cdot \theta_1^*)}{2} + \text{Re} \frac{(\theta_1)^2}{2} \exp(2i\lambda \tau) \tag{30}$$

where θ_1^* is the complement of θ_1 .

Hence the solution of the dependent parameters in equations 28 and 29 must have the form

$$\text{Re}(\theta_2) = \text{Re}(\theta_2^m) + \text{Re}[\theta_2^{sc} \exp(2i\lambda \tau)] \tag{31}$$

Equations 30 and 31 show that the solution of the second order problem can be divided into two parts and solved separately. One part reflects the change in the time average burning rate and the other reflects the component which oscillates with the second harmonic frequency.

After making the appropriate substitutions into equations 28 and 29, the change in the time average surface temperature and hence the time average burning rate can be determined.

$$\dot{r}/\dot{r}_0 = 1 + E(\lambda) \cdot \lambda^2 = 1 + \lambda^2 \operatorname{Re}(u_2^m / c_1^2) \quad (32)$$

The detailed expression for $E(\lambda)$ is presented in appendix C. It should also be noted that

$$E(0) = n(n-1)/4 \quad (33)$$

2.2.4 Third Order Behavior

Collecting terms of the order λ^3 yields

$$\frac{1}{4} \frac{\partial e_3}{\partial \tau} = \frac{\partial^2 e_3}{\partial r^2} + \frac{\partial e_3}{\partial r} + \frac{\mu_1^2 \partial e_2}{\partial r} + \frac{\mu_2 \partial \theta_1}{\partial r} + \mu_3 \frac{de_0}{dr} \quad (34)$$

$$\begin{aligned} -(\partial e_3 / \partial r)_{\xi=+0} &= \frac{(e_1^0)^3}{6} R_3 + \frac{(e_1^0)^2}{2} D_{12} + \frac{e_1^0}{2} D_{21} + \frac{c_1^3 B_3}{6} \\ &+ \left(\frac{1}{2} e_2^0 + e_1^0 \right) D_{11} + e_1^0 e_2^0 R_2 + \frac{1}{2} B_2 + e_3^0 R_1 + \frac{1}{3} B_1 \end{aligned} \quad (35)$$

The proper formulation of the cross products in equations 34 and 35 must be made in a manner similar to equation 30. It can readily be shown⁽²⁸⁾ that

$$\text{Re}[\theta_1^\circ] \cdot \text{Re}[\theta_2^\circ] = \text{Re} \left\{ \left[\bar{e}_2^m \theta_1^\circ + \frac{sc}{2} \theta_1^{\circ*} \right] \exp(i\lambda\tau) \right\} + \text{terms in } \exp(3i\lambda\tau) \quad (36)$$

$$\text{Re}[\theta_1^\circ]^3 = \text{Re} \left[\frac{3(e_1^\circ)^2}{4} (\theta_1^\circ)^* \exp(i\lambda\tau) \right] + \text{terms in } \exp(3i\lambda\tau) \quad (37)$$

This suggests that the solution for θ_3 should take the form

$$\text{Re}[\theta_3] = \text{Re}[\bar{e}_3^\circ \exp(i\lambda\tau)] + \text{terms in } \exp(3i\lambda\tau) \quad (38)$$

Thus the solution for \bar{e}_3° , and the third order burning rate response, consists of two terms, one which oscillates with the first harmonic and one which oscillates with the third. The first term, the one oscillating at the first harmonic, is of particular interest because it represents the change in the first order response with pressure amplitudes. Thus

$$\text{Re}(\mu/c_1) = \text{Re}(\mu_1/c_1) + c_1^2 F(\lambda) \quad (39)$$

where $F(\lambda)$ represents the component of μ_3 oscillating with $\exp(i\lambda\tau)$. The solution of equations 34 and 35 for $F(\lambda)$ is presented in appendix C.

It should be noted that the principal assumptions in the preceding analysis are that the solid is homogeneous and nonreacting and that the time constants for the gas phase processes are sufficiently fast so that the gas phase is always in equilibrium with the instantaneous pressure and solid surface conditions.

2.2.5 Utility of General Model

Another interesting point is that equations 20, 22, 32, and 39 can be used to describe the linear and nonlinear combustion characteristics of any combustion model fitting within the framework of equations 8, 12, and 13. The simplified model developed early in this program may be used as an example. In that analysis

$$-k \frac{dT}{dx} \Big|_{x=0} = K + Z_4 P \exp(-E_4/RT) - \Delta H_V \dot{r} \quad (40)$$

(1) (2) (3)

The terms on the right-hand side of equation 40 represent

- (1) = heat supplied from the flame zone (gas-phase reaction zone a finite distance away from the surface)
- (2) = heat generated at the surface by heterogeneous reactions between the solid oxidizer decomposition gases and the exposed fuel matrix
- (3) = heat released because of gasification of the propellant at the surface

In addition

$$K = K_o (P/P_o)^n \quad (41)$$

$$\dot{r} = Z_2 \exp(-E_2/RT_s) \quad (42)$$

For this particular case

$$A_1 = E_2 (T_s^\circ - T_\infty) / R (T_s^\circ)^2 \quad (43)$$

$$Q_1 = 0 \quad (44)$$

$$R_1 = (\Gamma - f) / s_1 \quad (45)$$

$$B_1 = (n' + \Gamma) / (1 - \phi) \quad (46)$$

Similarly, one could write the equations for the linear and nonlinear behavior for many of the combustion models previously reported in the literature.

2.3 COMPARISON OF THEORY AND EXPERIMENT

A comparison of the experimental results described in section 2.1 was made with equations 20 and 22 for two reasons: (1) these comparisons yield values of the linear combustion parameters (A_1 , B_1 , Q_1 and R_1), and a study of the effect of propellant formulation changes on these parameters will provide additional insight into the combustion process; and (2) these comparisons provide some idea of the validity of the basic assumption used to derive equations 20 and 22.

2.3.1 Method for Deriving Combustion Parameters

A parameteric study of equations 20 and 22 shows that the maximum value of the acoustic response function depends on both Q_1 and R_1 and that the frequency at which this maximum occurs depends on A_1 and Q_1 . In these calculations, n was held constant and B_1 was determined from equation 22 for the particular set of A_1 , R_1 , Q_1 . Since there is no simple method for deriving the set of combustion parameters graphically, the best set of A_1 , R_1 , Q_1 was selected by the least-squares approach based on a comparison of the measured and predicted real parts of the response function. The best set of combustion parameters derived for each propellant is shown in tables III and IV. All the data shown in tables III and IV were obtained using a value of the thermal diffusivity of 3.0×10^{-4} in.²/sec. The effect of this assumption will be discussed in section 2.3.5.

TABLE III
 LINEAR COMBUSTION PARAMETERS AT 200 PSIG

<u>Propellant No.</u>	<u>Formulation No.</u>	<u>$A_1 \pm 2$</u>	<u>$R_1 \pm 0.2$</u>	<u>$Q_1 \pm 0.2$</u>	<u>B_1</u>
1	8501	60	7.0	-0.3	0.41
2	8502	32	4.4	-0.3	0.46
3	8525	24	5.2	0.2	0.48
4	8526	26	5.0	-0.4	0.45
5	8527	No unique solution			
6	8528	14	4.4	1.0	0.62
7	8529	30	4.6	1.6	
		18	2.0	3.6	0.57
8	8531	12	3.2	2.4*	0.95
9	8532	36	6.2	1.3	0.55
10	9164	34	3.6	-0.5	0.43
11	9165	28	5.2	-0.1	0.37
12	9167	24	1.8	-0.3	0.47
13	9168	14	3.0	1.0	0.57
14	9173	18	5.8	0.6*	0.47
15	9368	38	7.6	0.6*	0.35
16	9379	36	6.7	-0.5*	0.23
17	9395	8	3.4	1.0*	0.45
18	9715	22	5.4	0.1	0.31
19	9717	10	4.2	0.1*	0.29
20	9718	18	-0.4	0.0	0.53
21	9719	12	4.6	0.3*	0.45
22	9720	28	0.4	-0.7*	0.50
23	9754	20	6.2	1.3*	0.47

* Significant at 95% confidence level.

TABLE IV
 EFFECT OF PRESSURE ON COMBUSTION PARAMETERS
 (UTX-8501)

<u>Pressure psia</u>	<u>$A_1 \pm 0.2$</u>	<u>$R_1 \pm 0.2$</u>	<u>$Q_1 = \pm 0.2$</u>	<u>B_1</u>
100	40	7.8	-0.7*	0.27
200	60	7.0	-0.3	0.41
500	20	5.2	0.0	0.39

* Significant at 95% confidence level.

Because equations 20 and 22 are nonlinear in the combustion parameters, the process of selecting the minimum value of the error estimate (i.e., the sum of squares) is not straightforward. Of the several methods for minimizing a nonlinear function, the grid approach was selected as being the simplest and most straightforward. The region of A_1 , R_1 , Q_1 most likely to contain the minimum was mapped, and the set of A_1 , R_1 , Q_1 yielding the minimum error estimate was determined. This result represents a "local" minimum which may not be the "universal" minimum which represents a different "best" set. This is illustrated by the fact that two solutions were obtained for propellant No. 7. In this case, the solution $A_1 = 18$, $R_1 = 2.0$, $Q_1 = 3.6$ yielded the lower error estimate.

Propellant No. 5 illustrates another problem which can be encountered. Only four measurements were obtained for this propellant: two each at two different frequencies. Unfortunately, there was not a significant difference in the measured response functions at the two frequencies. Thus, one could draw the response function-frequency curve with the maximum between the two sets of points, or one could consider that there is a large error between the sets and draw the curve most anywhere. Therefore, no best solution could be found for this propellant.

In an effort to ensure that the "universal best" set of combustion parameters was determined, a wide range of values was examined. However, there is always the possibility that the grid was too large and that points of low error estimates were overlooked. It should also be noted that propellants where the maximum response function was clearly determined did not present any problem, but those without a clearly established maximum did present difficulties.

All of the values presented in tables III and IV satisfy the stability criteria defined by equations 26 and 27 and, thus, represent values which are in the region of inherent stability.

2.3.2 Statistical Significance of Q_1

Many of the values of Q_1 in tables III and IV are negative, which is difficult to explain on physical ground. However, it is possible that the values of Q_1 presented in tables III and IV are not significantly different than zero.

To test the hypothesis, the data were examined by the grid approach for the case of $Q_1 = 0$. The values of A_1 , R_1 , and B_1 obtained for this special case are shown in tables V and VI. The error estimates for the general case and for the case where Q_1 is zero were compared statistically using the "F" test. At the 95% confidence level, propellants No. 8, 14, 15, 16, 17, 19, 21, 22, and 23 (i.e., those marked with a flag in tables III and IV) have values of Q_1 significantly different than zero. In all the other cases, one cannot separate the derived values of Q_1 from zero.

2.3.3 Comparison of Data Reduction Method with Other Approaches

Several alternate data reduction approaches to the one used in this program have been proposed by other investigators. With the exception of the limited efforts of Hart and coworkers,⁽¹⁸⁾ these comparisons have all been made assuming $Q_1 = 0$. As shown in section 2.3.2, this is valid in some, but not all, cases.

If $Q_1 = 0$, then one approach to the comparison of equation 20 with experimental data involves determining both the real and the imaginary parts of the

TABLE V
 LINEAR COMBUSTION PARAMETERS AT 200 PSIG
 ($Q_1 = 0$)

<u>Propellant No.</u>	<u>Formulation No.</u>	<u>$A_1 \pm 2$</u>	<u>$R_1 \pm 0.2$</u>	<u>B_1</u>
1	8501	56	6.6	0.44
2	8502	28	4.2	0.49
3	8525	24	5.4	0.43
4	8526	24	4.6	0.52
5	8527	No unique solution		
6	8528	20	5.2	0.41
7	8529	40	6.8	0.44
8	8531	20	5.6	0.48
9	8532	52	8.4	0.36
10	9164	30	3.0	0.48
11	9165	26	5.4	0.37
12	9167	20	1.6	0.49
13	9168	28	3.2	0.46
14	9173	24	6.0	0.33
15	9368	40	8.2	0.25
16	9379	32	5.6	0.32
17	9395	26	6.2	0.17
18	9715	22	5.6	0.29
19	9717	12	4.0	0.29
20	9718	18	-0.4	0.53
21	9719	14	4.6	0.38
22	9720	16	1.6	0.42
23	9754	36	7.8	0.15

TABLE VI
 EFFECT OF PRESSURE ON COMBUSTION PARAMETERS
 (UTX-8501 with $Q_1 = 0$)

<u>Pressure, psig</u>	<u>$A_1 \pm 2$</u>	<u>$R_1 \pm 0.2$</u>	<u>B_1</u>
100	44	7.8	0.42
200	56	6.6	0.44
500	20	5.2	0.39

response function from experimental data. For the T-burner, Strittmater,⁽²⁰⁾ Friedly⁽²²⁾ and Beckstead⁽²³⁾ have shown in earlier work

$$\frac{\mu}{\epsilon} \approx \frac{P}{40c\dot{r}_0} \left[\frac{\alpha_g + \alpha_d}{f_d} + 2\pi i \frac{(f_g - f_d)}{f_d} \right] \quad (47)$$

Since the growth and decay constants (i.e., α_g and α_d) and the corresponding frequencies are determined experimentally for each point, equating the real and imaginary parts of equations 25 and 47 provides the two expressions in terms of R_1 and A_1

$$\begin{aligned} A_1 \left\{ \operatorname{Re}(\mu/\epsilon) - n\lambda_1^r \right\} &= R_1 \left\{ \lambda_1^r [\operatorname{Re}(\mu/\epsilon) - n] - \operatorname{Im}(\mu/\epsilon) \lambda_1^i \right\} \\ &= \left\{ n\lambda_1^r + 2\operatorname{Im}(\mu/\epsilon) \lambda_1^i \lambda_1^r - \operatorname{Re}(\mu/\epsilon) [(\lambda_1^r)^2 - (\lambda_1^i)^2] \right\} \end{aligned} \quad (48)$$

$$\begin{aligned} A_1 \left\{ \operatorname{Im}(\mu/\epsilon) - n\lambda_1^i \right\} &= R_1 \left\{ \lambda_1^i [\operatorname{Re}(\mu/\epsilon) - n] + \operatorname{Im}(\mu/\epsilon) \lambda_1^r \right\} \\ &= \left\{ n\lambda_1^i - 2\operatorname{Re}(\mu/\epsilon) \lambda_1^i \lambda_1^r - \operatorname{Im}(\mu/\epsilon) [(\lambda_1^r)^2 - (\lambda_1^i)^2] \right\} \end{aligned} \quad (49)$$

Hence, values of A_1 and R_1 can be derived for each data point.

This approach to the analysis of T-burner data has a serious limitation resulting from experimental uncertainties. For the propellants, shown in table II, the imaginary part of equation 47 becomes

$$\operatorname{Im}(\mu/\epsilon) \approx 400 (f_g - f_d)/f_d \quad (50)$$

Since f_g and f_d have similar magnitudes, the experimental errors in both f_g and f_d are magnified in the calculation of $\operatorname{Im}(\mu/\epsilon)$. This results in significant

uncertainties in R_1 and A_1 when they are derived from equations 48 and 49. Thus, it was concluded that this method of data reduction, though more rigorous, is too sensitive to small errors in the frequency measurements. For this reason, the analysis of the imaginary part of the response function was not included in the data reduction procedure.

In an effort to circumvent this difficulty, Beckstead and Culick⁽²³⁾ have modified this approach. Instead of using the imaginary part of the response function in equations 48 and 49, they assigned $\text{Im}(\mu/\epsilon) = 0$. To determine the effect of this assumption, some of the data obtained in this program were reduced both ways. For frequencies below 800 to 1,000 cps, the two methods yield comparable values of A_1 , but some significant changes in R_1 were noted. At higher frequencies significant differences in both A_1 and R_1 were noted, thereby casting doubt on the general validity of the modified approach.

This approximate method is open to further question since Beckstead⁽²³⁾ found that the linear combustion parameters for A-13 propellant fell outside the region of intrinsic stability. This result is clearly not satisfactory on physical grounds. The method described in section 2.3.1 resulted in $A_1 = 16$, $R_1 = 4.6$, and $Q_1 = 0.5$. The value of Q_1 was also found to be significantly different than zero. These values are well within the region of intrinsic stability. Even if the results were based on $Q_1 = 0$, this would still be the case. Therefore, the data reduction process can bias the derived result to the extent that erroneous conclusions can be drawn.

In another study, Oberg⁽²⁹⁾ has compared experimental data with equation 20 using only the real part of the response function. He concluded that both the T-burner data obtained by Horton⁽²⁶⁾ and the L* data obtained by Beckstead⁽³⁰⁾ can be adequately correlated by equation 20.

2.3.4 Approximate Method for Data Reduction

In the course of studying various data reduction methods, a quick and accurate method was developed in which $Q_1 = 0$ is assumed. Under these conditions, parametric solutions of equation 25 show that, to a good approximation, the response is a maximum when $\text{Im}(\mu_1/\epsilon_1) = 0$. Hence,

$$A_1 = \frac{i}{\lambda_1} / 4(\lambda_1^r - 1) \quad (51)$$

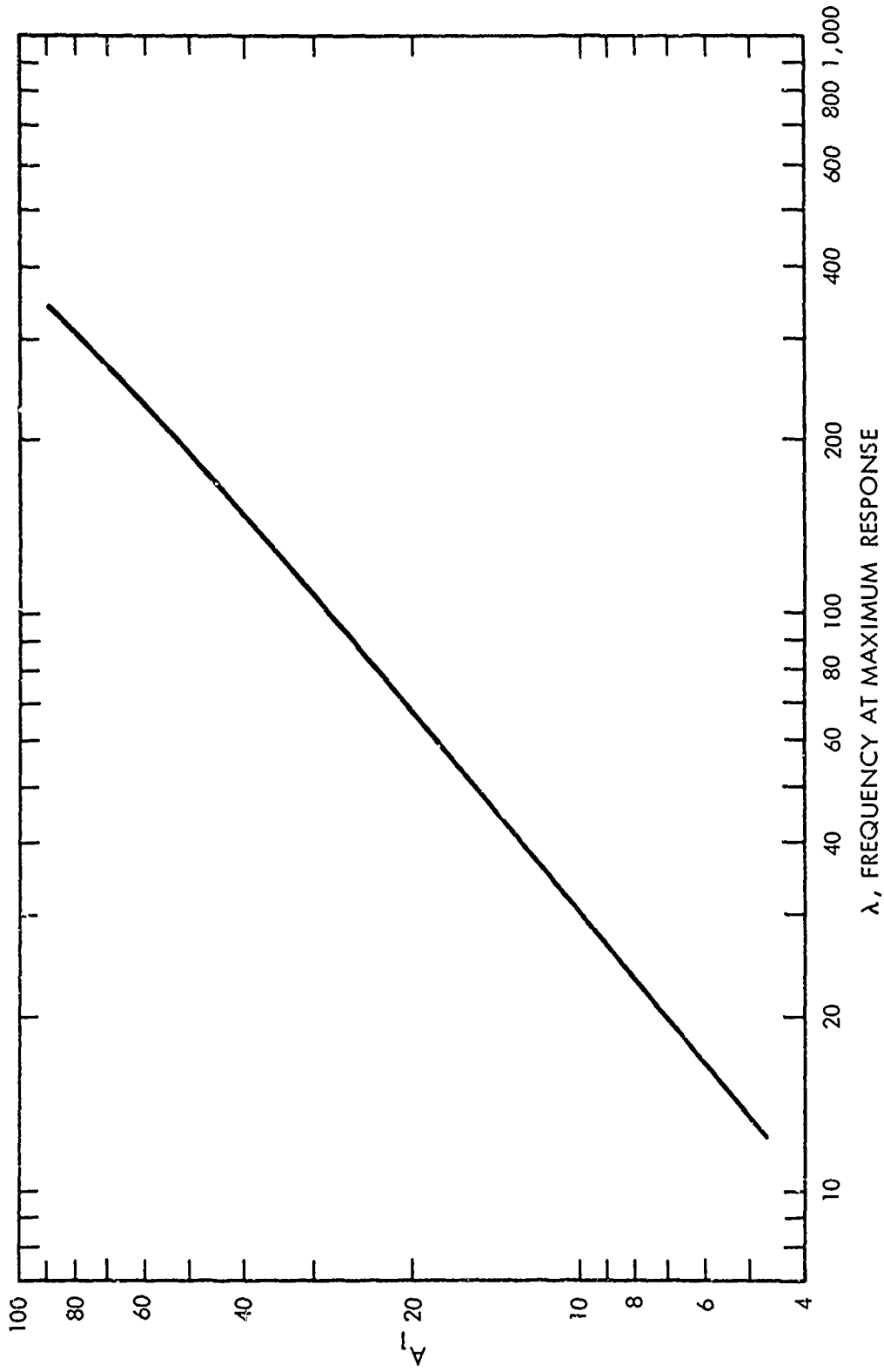
where λ_1 is evaluated at the frequency of maximum response.

A plot of equation 51 is shown in figure 20 where R_1^c is the critical value of R_1 for intrinsic stability determined in equation 27. Therefore, the parameter A_1 can be determined directly from experimental data by noting the dimensionless frequency at which $\text{Re}(\mu/\epsilon)$ becomes a maximum. The parameter R_1 can then be determined from the maximum response function and burning rate pressure exponent by substituting equation 51 into equations 20 and 22, yielding

$$\frac{1}{n} \cdot \text{Re}(\mu/\epsilon)_{\text{max}} = (1 - R_1 + A_1) / \left\{ \lambda_1^r - R_1 + 4A_1 \lambda_1^i / \lambda_1 \right\} \quad (52)$$

Equation 52 is shown graphically in figure 21.

The values derived by this method are nearly identical to those presented in tables V and VI which were derived by the least-squares approach.



81328

Figure 20. Frequency of Maximum Acoustic Response vs A_1

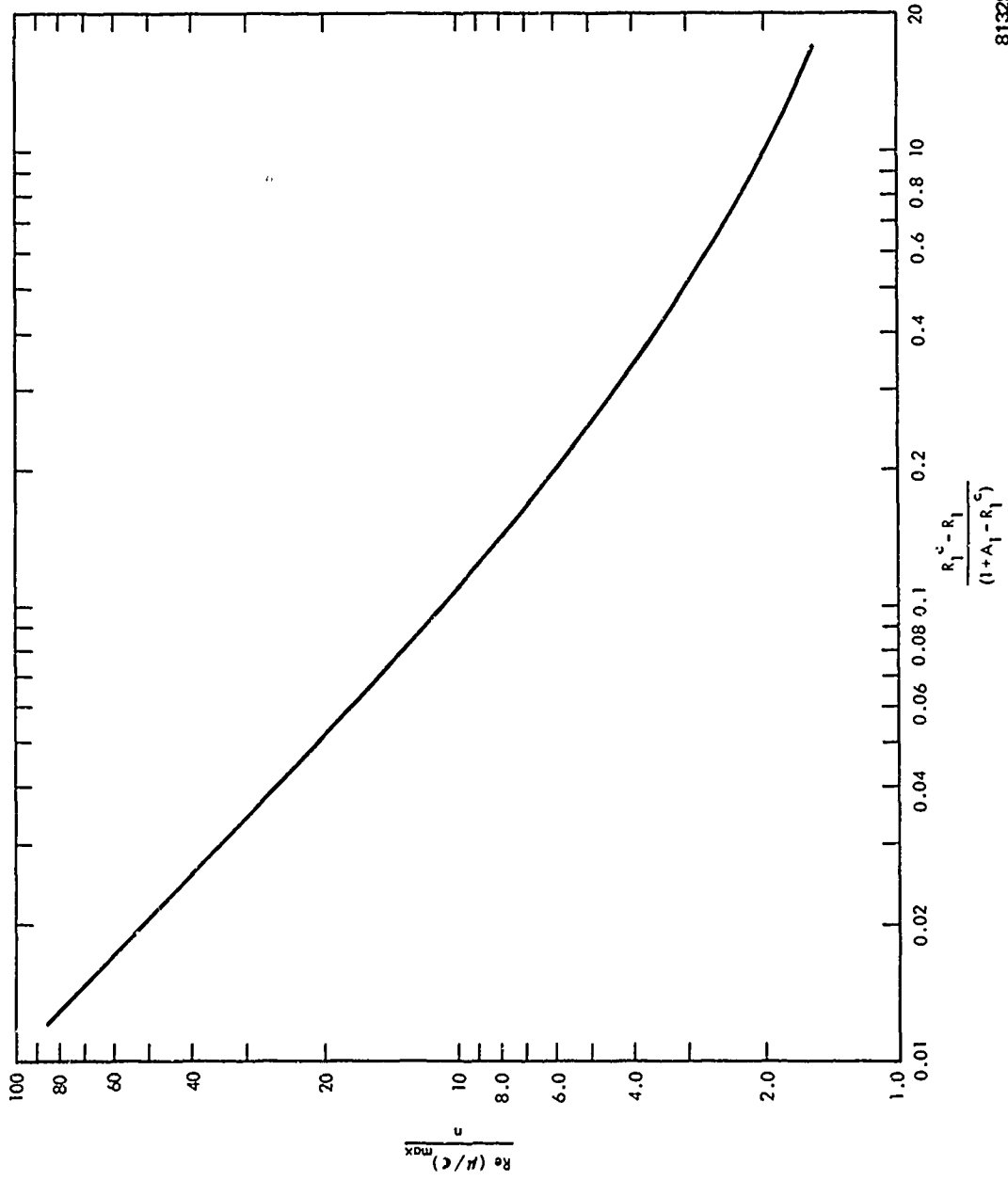


Figure 21. Maximum Value of Acoustic Response Function

2.3.5 Analysis of Error Effects

For reasons of simplicity and economy, the approximate method presented in section 2.3.4 was used in this part of the study. The effect of errors in the dimensionless frequency at the maximum response (i.e., burning rate, diffusivity, and dimensional frequency errors) were determined by an arbitrary 16% reduction in α and, therefore, the dimensionless frequency at the maximum response. The results show that an error of 16% in λ results in a 16% error in A_1 and an 8% error in R_1 .

Arbitrary changes in $Re(\mu/\epsilon)$ and n were evaluated and the resulting effect on R_1 is shown in table VII. Note that A_1 is determined by λ alone and is not subject to these errors.

TABLE VII

EFFECT OF n AND $Re(\mu/\epsilon)_{max}$ ON R_1

		<u>$Re(\mu/\epsilon)_{max}$</u>			
		5.5	5.7	5.9	
n	0.49	R_1	6.60	6.77	6.93
	0.55		6.00	6.19	6.37
	0.60		5.43	5.70	5.90

The results show that errors in the experimental measurements, i.e., λ , n , and $Re(\mu/\epsilon)_{max}$, result in approximately the same percentage error in the derived combustion parameters. Hence, the procedure for deriving the combustion parameters does not significantly amplify or attenuate experimental uncertainties.

The response function-frequency curve was calculated for propellant No. 1 using the derived combustion parameters shown in table IV. Figure 22 shows that the shape of the predicted response-frequency curve is not significantly altered by an error in α . Figure 23 shows the effect of n and $Re(\mu/\dot{v})_{\max}$ on the predicted response function frequency curve. The pressure exponent, n , influences the shape of the curve at the frequency extremes but has little influence near the maximum; $Re(\mu/\dot{v})_{\max}$ has more influence on the peak region of the curve but little influence on the frequency extremes.

Figures 22 and 23 show that the response function derived from equations 20 and 22 adequately predicts the observed shape of the frequency-response function curve. Other comparisons between the data on the curves predicted by equations 20 and 22 using the combustion parameters shown in table III are in agreement. This leads to the conclusion that equations 20 and 22 adequately represent the linear combustion behavior of the propellants listed in table II.

It would be interesting to compare equations 20 and 22 with the extensive data obtained at NWC, but these data have not been publicly distributed.

2.3.6 Interpretation of Combustion Parameters

It is interesting to speculate on the physical significance of the various linear combustion parameters and the numerical values of the associated physical parameters. The parameters associated with the burning rate of the solid phase, i.e., the function $H(T_s, P)$, can be considered. If one supposes that

$$\dot{r}_s = H(T_s, P) = Z_2 P_1^{n_1} \exp(-E_2/RT_s) \quad (53)$$

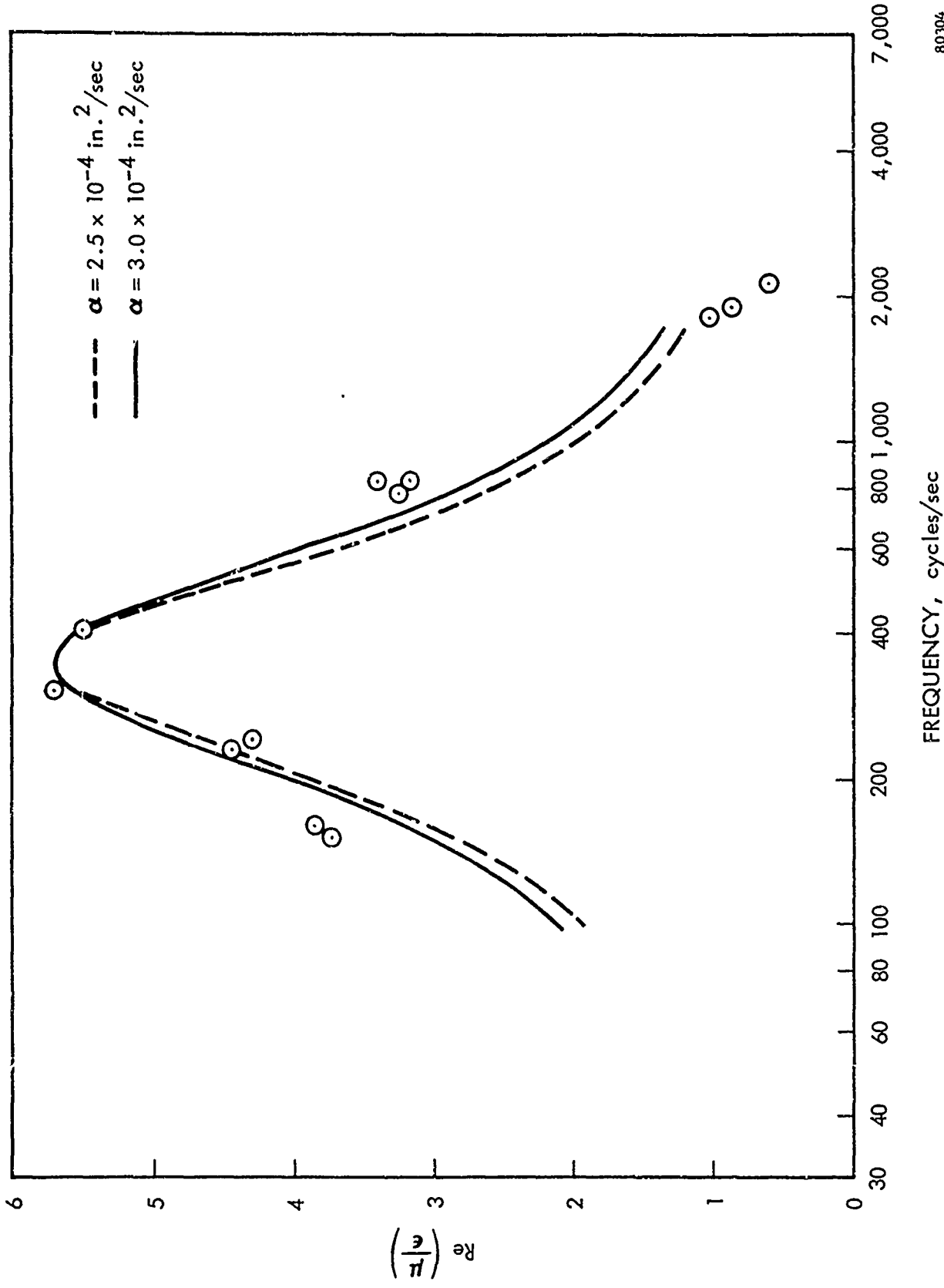
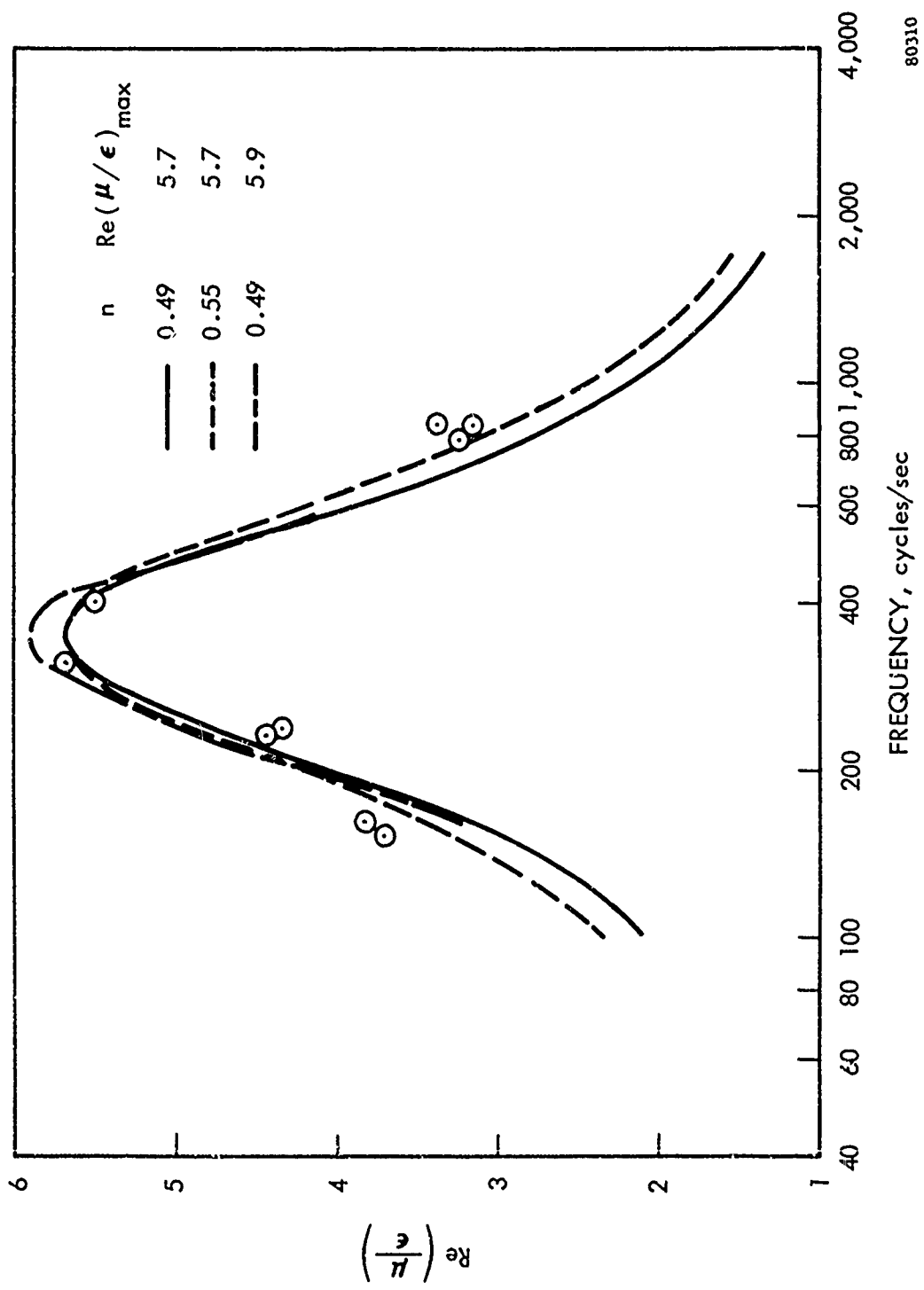


Figure 22. Effect of Thermal Diffusivity on Shape of Response-Frequency Curve



80310

Figure 23. Effect of Steady-State Burning Rate Exponent and $Re(\mu/\epsilon)_{max}$ on Shape of Response-Frequency Curve

(a form which has been proposed in almost all combustion models but which has not been convincingly justified), then

$$A_1 = E_2(T_s^\circ - T_\infty^\circ) / RT_s^2 \quad (54)$$

$$B_1 = n_1 \quad (55)$$

Given equation 53, the parameter A_1 is a measure of the surface temperature and actuation energy of the reaction. Assuming an initial propellant temperature of 300°K and a steady-state surface temperature of 750°K, a value of A_1 equal to 30 corresponds to an E_2 of 74.5 Kcal/mole. If the surface temperature is assumed to be 850°K, than an A_1 of 30 corresponds to an E_2 of 78.1 Kcal/mole. Thus, in the case of equation 53, the variations in A_1 shown in table III and IV reflect formulation effects on E_2 versus the effects on the surface temperature. At a 750°K surface temperature, the activation energies derived from table I range from 20 Kcal/mole for propellant No. 17 to 145 Kcal/mole for propellant No. 1. These are extremely high, especially in view of the values reported for the decomposition and gasification of various ingredients. The results, though consistent with nonacoustic combustion instability data,⁽²³⁾ suggest that if equation 53 applies there is a complex series of surface reactions and that the formulation changes shift the balance rather drastically.

Further evidence of this shift in the reaction process is provided by the catalyst data in table III. These data show the addition of catalysts to the formulation decreases the value of A_1 ; the higher the catalyst concentration the lower the value of A_1 . At the same time, Q_1 is increased from -0.5 to approximately 0.1 when the catalysts are present in concentrations greater than

0.25%. Since the parameters A_1 and Q_1 reflect the solid phase contribution to the mass burning rate, the effect of burning rate catalysts influence this part of the combustion process in addition to the gas phase reaction effects.

The data in table III indicate that the effect of pressure is significant at the higher solids loading. At 78% oxidizer loading, only two of the propellants showed Q_1 values significantly different than zero. At 84%, however, only two of the nine propellants had Q_1 values of zero. Thus, the coatings had little effect on the pressure dependence of the solid phase aspects of the mass burning rate.

A perplexing aspect of these data is the fact that some of the significant nonzero values of Q_1 are negative, while they are greater than one in other cases. The latter result may be somewhat surprising, but it can be explained in terms of possible chemical reaction mechanisms. The explanation of the former result (i.e., that $Q_1 < 0$) is not possible in this manner. This difficulty in explaining the activation energy and the order of the reaction leads one to suspect the validity of equation 53 in characterizing propellant combustion. However, logical alternates to equation 53 are equally difficult to propose.

As further evidence of the complexity of physically interpreting equation 8, consider the results presented in table IV. The effect of pressure on Q_1 suggests that as the pressure is increased, Q_1 becomes less negative (therefore more positive). At first, one would ascribe this change to the increasing rate of the self combustion of the ammonium perchlorate at the higher pressure. The effect of pressure on A_1 also supports the concept of a shifting reaction

mechanism with pressure. However, one is still faced with the difficulty of explaining negative values of Q_1 at the lower pressures and the parabolic effect of pressure on A_1 .

The situation regarding R_1 and B_1 is even more complex. To demonstrate this point, the first order Taylor expression of equation 5 is

$$dK = \left(\frac{\partial K}{\partial T_s} \right)_o dT_s + \left(\frac{\partial K}{\partial P} \right)_o dP + \left(\frac{\partial K}{\partial T_f} \right)_o dT_f \quad (56)$$

Equation 56 can then be combined with the first order expansions of equations 7 and 8 to provide alternate definitions of R_1 and B_1 in terms of the functions $K(T_s, P, T_f)$, $H(T_s, P)$, and $J(T_s, P, T_f)$.

$$R_1 = \left\{ \frac{(\partial K / \partial T_s)_o (\partial J / \partial T_f)_o + (\partial K / \partial T_f)_o [(\partial H / \partial T_s)_o - (\partial J / \partial T_s)_o]}{\dot{r}_o \rho C_p (\partial J / \partial T_f)_o} \right\} \quad (57)$$

$$B_1 = P_o \left\{ \frac{(\partial K / \partial P)_o (\partial J / \partial T_f)_o + (\partial K / \partial T_f)_o [(\partial H / \partial P)_o - (\partial J / \partial P)_o]}{\dot{r}_o \rho C_p (T_s - T_\infty) (\partial J / \partial T_f)_o} \right\} \quad (58)$$

Considering the wide range of proposed definitions for the parameters in equation 56 one finds that generally $(\partial H / \partial T_s) > (\partial J / \partial T_s)$, that $(\partial K / \partial T_f) > 0$, and that $(\partial J / \partial T_f) > 0$. Hence, one can conclude that if $R_1 < 0$, then $(\partial K / \partial T_s) < 0$. This would be the case, for example, if equation 53 applies and the process is endothermic. However, since the experimental value of $R_1 > 0$, this implies that approximately $(\partial K / \partial T_s) \geq 0$. This then suggests that the surface processes are at least nearly thermally neutral (i.e., $\frac{\partial K}{\partial T_s} \approx \left(\frac{\partial K}{\partial T_f} \right) \left[\frac{\partial H}{\partial T_s} - \frac{\partial J}{\partial T_s} \right] / \left(\frac{\partial J}{\partial T_f} \right)$)

or perhaps even somewhat exothermic. The magnitude of the various partial derivatives determine the extent to which this is true. However, it would appear that the values of R_1 are reasonable in terms of the various proposed definitions from the several available combustion models. Similarly, the values of B_1 derived from the data are also quite reasonable. Either the granular diffusion visible or the laminar premixed flame model predicts pressure indices between 0 and 1, which is consistent with the observations.

Examination of the effects of the various formulation changes on R_1 and B_1 yields some interesting results. The effect of coatings on the solid oxidizer can be considered first. The coatings reduced the temperature sensitivity of the heat transfer into the solid phase. Viton A was the least effective, and Kel-F, Hypalon, and ethyl cellulose all had nearly the same effect. It is, of course, impossible to determine whether the effect is the result of a reduction in possible exothermic surface reactions (the original intent of the experiment) or the result of decreased mixing within the gas phase reaction zone. There appears to be little effect of the coatings on B_1 , so no clues can be obtained from studying those results. It should also be noted that the coatings were porous, thereby lessening the resulting effects in comparison to a nonporous coating.

The influence of the catalysts is also interesting to consider. In all cases, the values of R_1 were substantially reduced by the addition of the catalysts. When combined with their influence on the activation energy of the surface gasification process, the data suggest the effect is to reduce the activation energies of the various reactions. An additional influence, which

effects R_1 but not A_1 , results from increasing the gas phase damping. Both catalysts exist as solids within the gas phase combustion zone and could behave in much the same manner as aluminum.

Another aspect of the catalyst data is that the addition of copper chromite results yield substantially lower values of R_1 and higher values of B_1 . It may be that copper chromite influences different processes characterized in R_1 and B_1 than iron oxide.

The influence of pressure on R_1 and B_1 , at least for propellant No. 1, seems to be counter to expectations. Increasing the pressure appears to decrease R_1 in the region where one would expect the self-deflagration of AP to increase R_1 . However, the shift in the complex reaction path and the resulting change in activation energies could cause the effect to be opposite to the anticipated effect.

2.3.7 Nonlinear Behavior

The nonlinear behavior of the combustion model has also been examined. The original approach to the study of the nonlinear constants was to attempt their derivation by extrapolating the linear results. However, the lack of decisive linear results made this approach impractical. Therefore, two alternatives were available: (1) studying the effects of the nonlinear constants separately; (2) studying the nonlinearities within the context of one particular combustion model. Both approaches have been attempted, and the results from each approach are presented in the following paragraphs.

2.3.7.1 Parametric Studies of General Analysis

Equations 20, 22, 32, and 39 show that a large number of constants are required to characterize the complete behavior. However, a parametric study of the shift in time average burning rate is straightforward if one keeps the linear behavior fixed. Equation 32 shows that if $\epsilon_2 = 0$, which is reasonable in the T-burner, then only two second order constants, X_1 and W_1 , are required. Calculations were then made assuming $A_1 = 20$, $n = 0.40$, $R_1 = 4.0$, and $Q_1 = 0$. The effect of X_1 and W_1 is shown in figure 24.

These results show that both increases and decreases in the time average burning rate can be explained within this analytical framework depending on the nonlinear constants. It should be noted that in both cases the zero frequency corresponds to the shift consistent with the equation 33. Only limited experimental data are available with which to compare these predicted results. Eisel⁽³¹⁾ has found that $-0.5 E(\lambda) \sim 0$ for both composite and double-base propellants. When compared with figure 24 and other parametric results not shown, the data indicate that W_1 is less than 200 for these propellants.

Turning to third order effects, parametric studies show that $F(\lambda)$ can have a wide range of values depending on both second and third order constants. The effects are too numerous for a meaningful study of the behavior.

2.3.7.2 Parametric Study for a Particular Combustion Model

The model selected to study the nonlinear combustion behavior was the simplified model presented in section 2.2.2. This model does have its limitations, particularly in the analysis of the transient flame temperature. However, the derivation of equation 25 shows that this effect can be treated separately

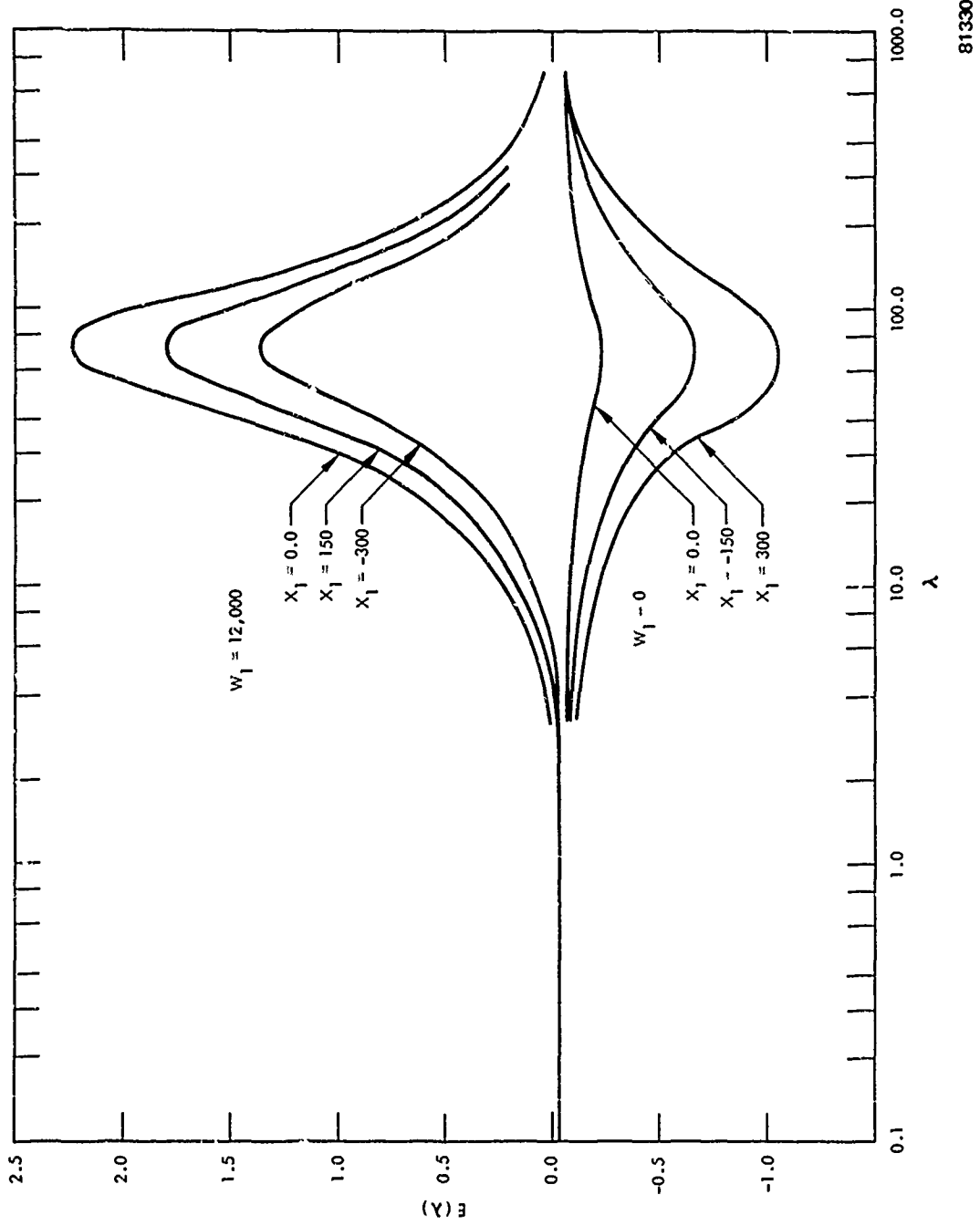


Figure 24. Nonlinear Effect on Burning Rate Shift

81330

from the analysis of the transient burning rate. Therefore, the results of this nonlinear analysis are somewhat more general than the combustion model suggests.

An examination of the higher order equations 28 through 39 reveals that six combustion parameters are required to characterize the nonlinear behavior of the simplified model and, as long as they represent an independent set, any combination of six is sufficient. In the present studies, the three parameters characterizing the linear behavior were retained. The three remaining parameters are the surface temperature ratio ($\phi = T_{\infty} / T_s^{\circ}$), the pressure exponent of the gas phase heat flux (n'), and the ratio of activation energy of exothermic surface reaction to that of the overall pyrolysis reaction at the surface ($\Lambda = E_4 / E_2$). These three additional parameters represent physical characteristics of the combustion process which can be estimated within reasonable bounds. For example, it is generally believed that typical surface temperatures are of the order of 750°K ,⁽³²⁾ thereby providing a reasonable estimate for ϕ . Likewise, n' must lie between zero and one. Λ is the least known parameter, but in the light of the high values of E_2 , Λ should also lie between zero and one.

A parameteric study of the higher order effect has been made using this set of combustion parameters. The results are shown in figures 25 through 27 for the case where the linear response (acoustic response function) corresponds to propellant No. 1 in table II. Figures 25 and 26 show $E(\lambda)$ is always negative and follows the inverse frequency-acoustic response function pattern (i.e., $E(\lambda)$ is small at low and high frequencies) and reaches a minimum at the same frequency in which the response function is a maximum. The results show the minimum value

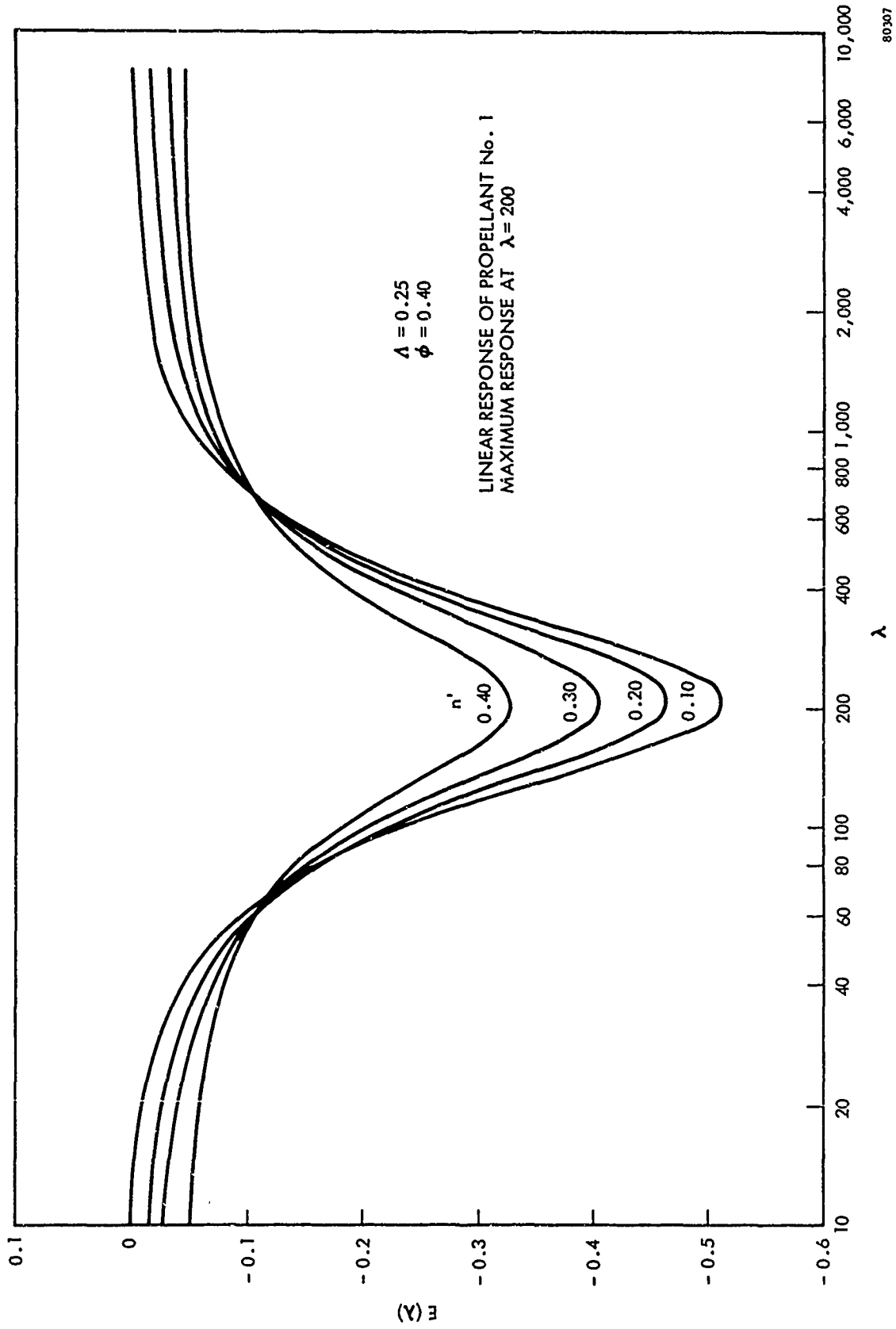


Figure 25. Effect of Gas Phase Pressure Exponent on Burning Rate Change

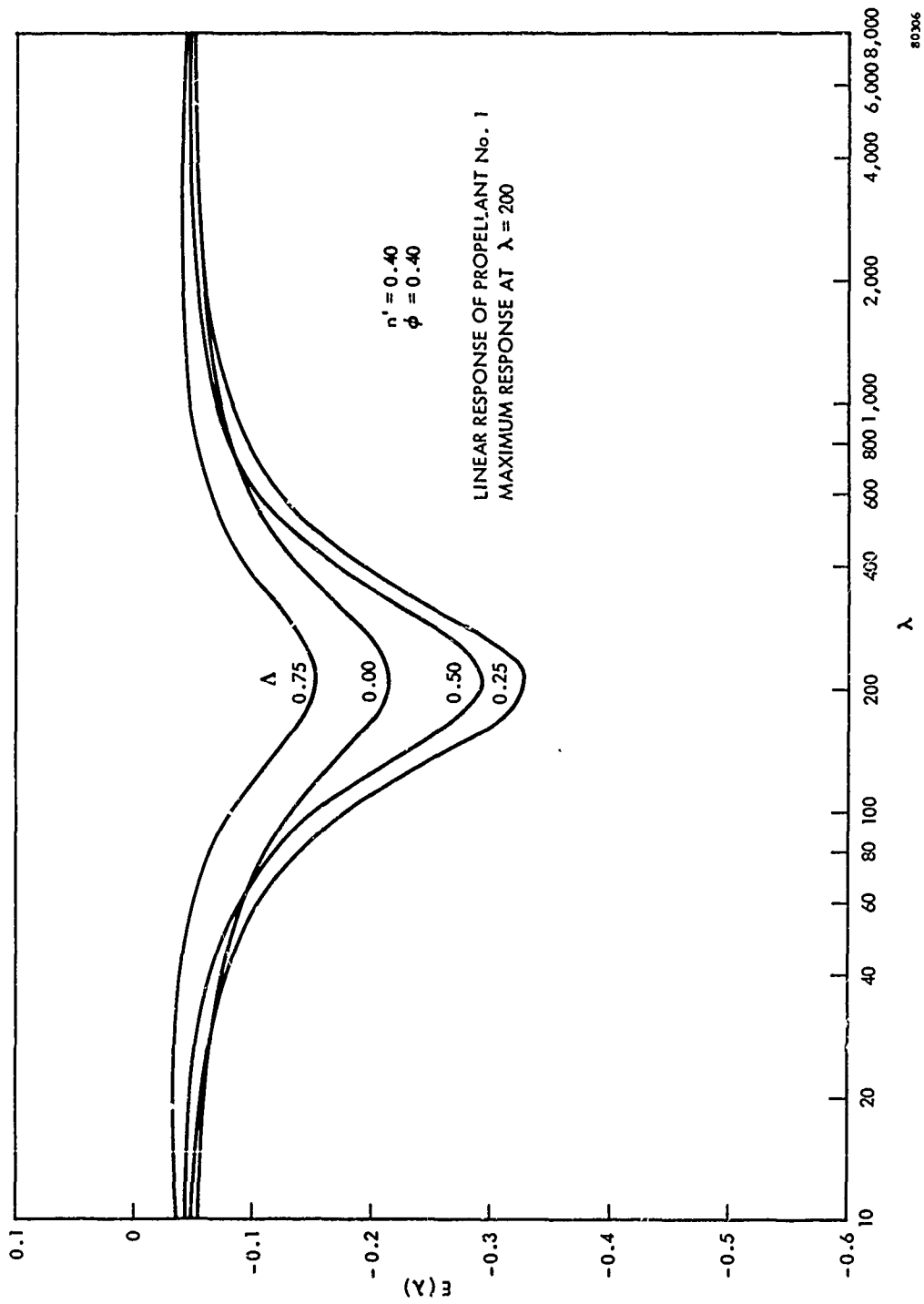


Figure 26. Effect of Activation Energy Δ on Burning Rate Change

of $E(\lambda)$ becomes increasingly negative for decreasing values of the gas phase pressure exponent (n'), as shown in figure 25. The effect of Λ on $E(\lambda)$, which is shown in figure 26, is more complex. For $\Lambda > 0.25$ the minimum value of $E(\lambda)$ increases with increasing values of the activation energy ratio Λ . For $\Lambda < 0.25$, the minimum value of $E(\lambda)$ increases with decreasing values of Λ . Other calculations show that the temperature ratio, θ , has little effect on $E(\lambda)$.

These results can be explained in terms of the physics of the combustion model. If n' is less than unity, the energy transfer from the gas phase will not be symmetric about the mean value during one pressure cycle. In fact, there will be a net decrease in energy transfer, depending on n' , which results in the decrease in steady burning rate. The effect of Λ results from the asymmetry of the surface heat liberation term as a consequence of the surface temperature contribution. If Λ is significantly less than unity, the increase in surface temperature does not increase the burning rate and energy liberation in direct proportion. The effect of Λ is complicated by the fact that the heat release from surface reactions depends on both surface temperature and pressure. This dual dependence accounts for the nonmonotonic effect of Λ . For $\Lambda = 0$, the surface reaction effect depends only on pressure to the first power and it oscillates symmetrically about the mean. This symmetric effect counters the asymmetric behavior of the gas phase flux and reduces the overall asymmetry of the energy transfer to the solid.

The behavior at the frequency extremes can also be explained on this basis. At low frequencies, asymmetry results because the burning rate pressure exponent

is less than one. At the high frequency, asymmetry results from the behavior of the gas phase flux alone, since the surface temperature can not follow the pressure oscillations (i.e., $\text{Re}(\mu/\epsilon) \rightarrow 0$ as $\lambda \rightarrow \infty$). This contrasts the high-frequency behavior reported by Friedly.⁽²⁸⁾

Similar calculations were made for the corresponding PBAN/AP propellant (i.e., propellant No. 13). The results show similar behavior to that shown in figures 25 and 26, except that the magnitude of the effects are approximately half that shown in these figures. Therefore, the parameters which characterize the linear behavior, particularly R_1 , have a significant influence on the non-linear behavior as well.

The maximum change in $E(\lambda)$, shown in figures 25 and 26, represents a small shift in burning rate. Typical values for ϵ_1 in the T-burner are 0.1 to 0.3, and the maximum decrease in burning rate is approximately 2%. This value is of the same order of magnitude as the experimental observations of Eisel.⁽³¹⁾ Furthermore, the change in burning rate is shown to be quadratic in pressure amplitude, which also agrees with experimental results. Unfortunately, the accuracy of the data is not sufficient to make meaningful quantitative comparisons with theory.

Another aspect of the nonlinear studies concerns the changes which occur in the acoustic response function with increasing pressure amplitudes. The effects of ϕ , n' , and Λ on $F(\lambda)$ were determined through equation 23, using the values of R_1 , A_1 , and n for propellant No. 1 (thereby matching the experimentally determined linear response). Figure 27 shows the effect of Λ on $F(\lambda)$. The effects of n' and ϕ are found to be essentially negligible. It should be noted

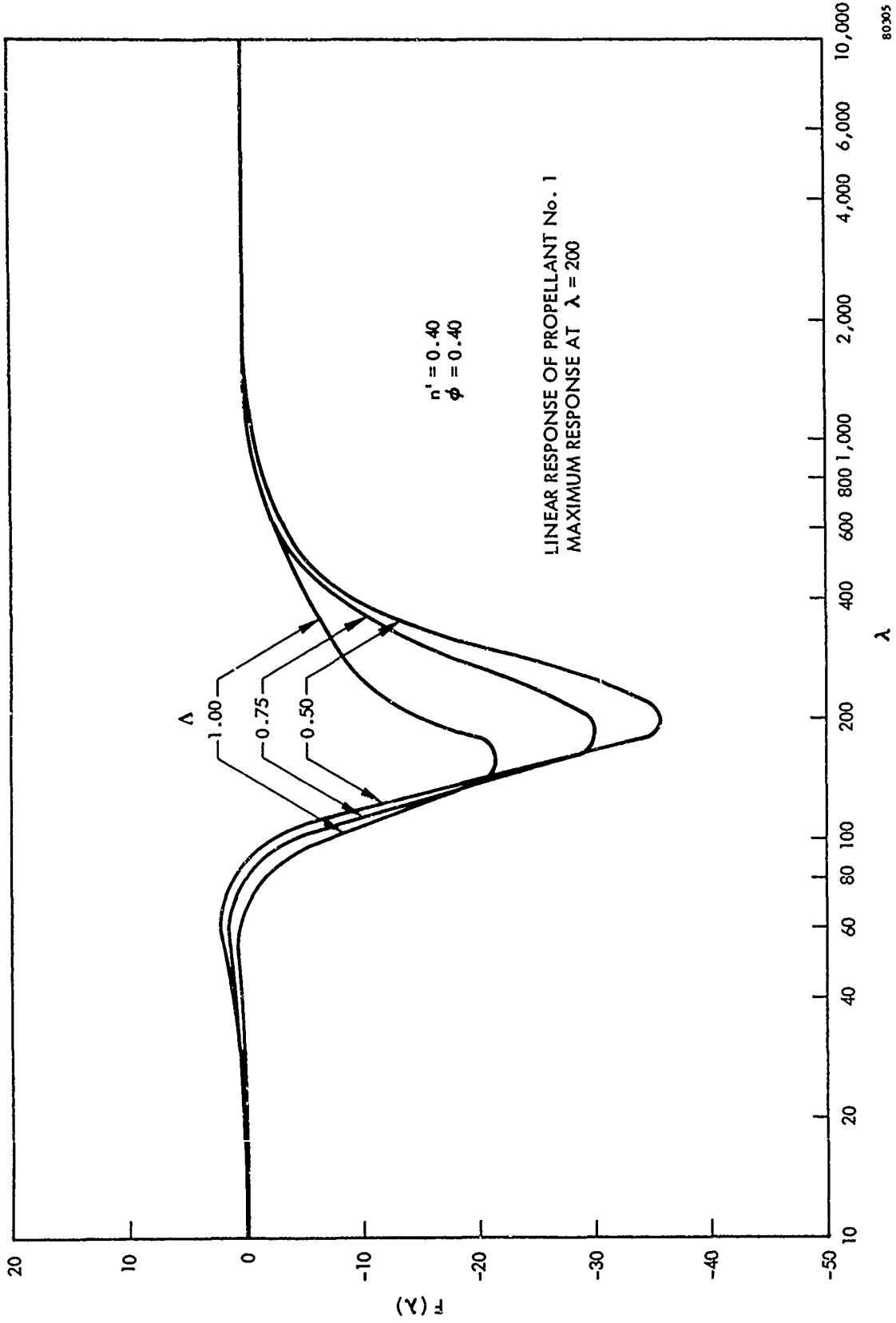


Figure 27. Effect of Activation Energy Δ on Change in Acoustic Response

that the curves for $0 < \Lambda < 0.50$ cannot be distinguished from the curve for $\Lambda = 0.50$. The results also show that $F(\lambda)$ approaches zero at both high and low frequency. The high-frequency behavior results from the inability of the solid to respond to the pressure oscillations while the low-frequency limit indicates that the burning rate pressure exponent n is independent of pressure.

The results shown in figure 27 are similar to Friedly's⁽³³⁾ predictions, although there are some important differences. $F(\lambda)$ is negative at frequencies which are less than the frequency at which the maximum response occurs. Friedly's results would lead to the opposite conclusion. One possible explanation is that different methods were used to solve the differential equations and calculate $F(\lambda)$: Friedly used the approximate method of discretization, in contrast to the exact variation of parameters approach used in this study.

The large negative values in the intermediate pressure region show that the combustion process is self-limiting in the T-burner configuration. As the pressure amplitude increases because of the linear behavior in the T-burner, the response function decreases. This reduces the energy input driving the acoustic pressure and eventually results in an upper limit in the acoustic pressure. By setting $\text{Re}(\mu/\epsilon)$ equal to zero in equation 39, these limiting pressure amplitudes have been calculated for the cases shown in figure 27. The results, which are shown in figure 28 reveal that limiting amplitudes of 0.4 would be expected on the basis of combustion behavior alone at typical T-burner frequencies. Since these calculations do not consider the effect of acoustic losses, the predictions are reasonable in the light of experimentally observed limit amplitudes. Furthermore, calculations show the effect of n' and θ to be insignificant, and the effect of Λ on the limit amplitude can be anticipated from figure 27.

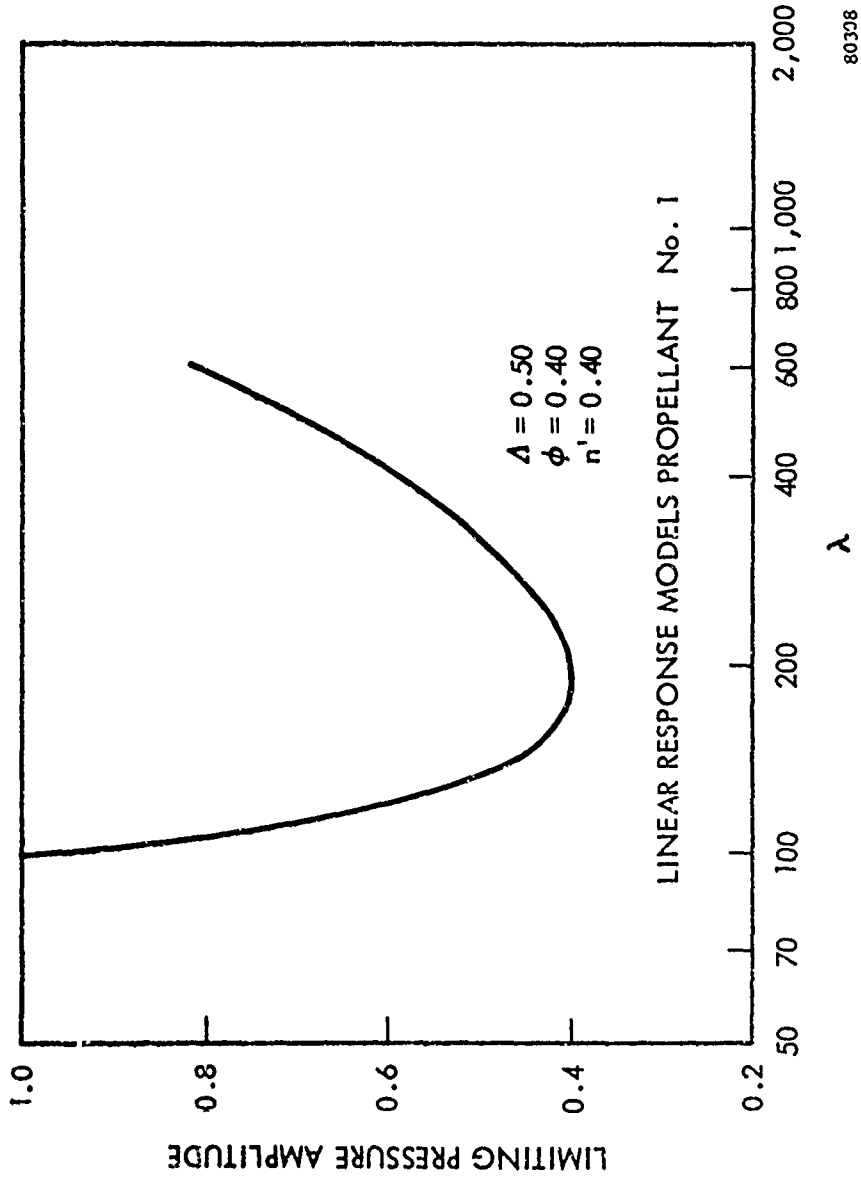
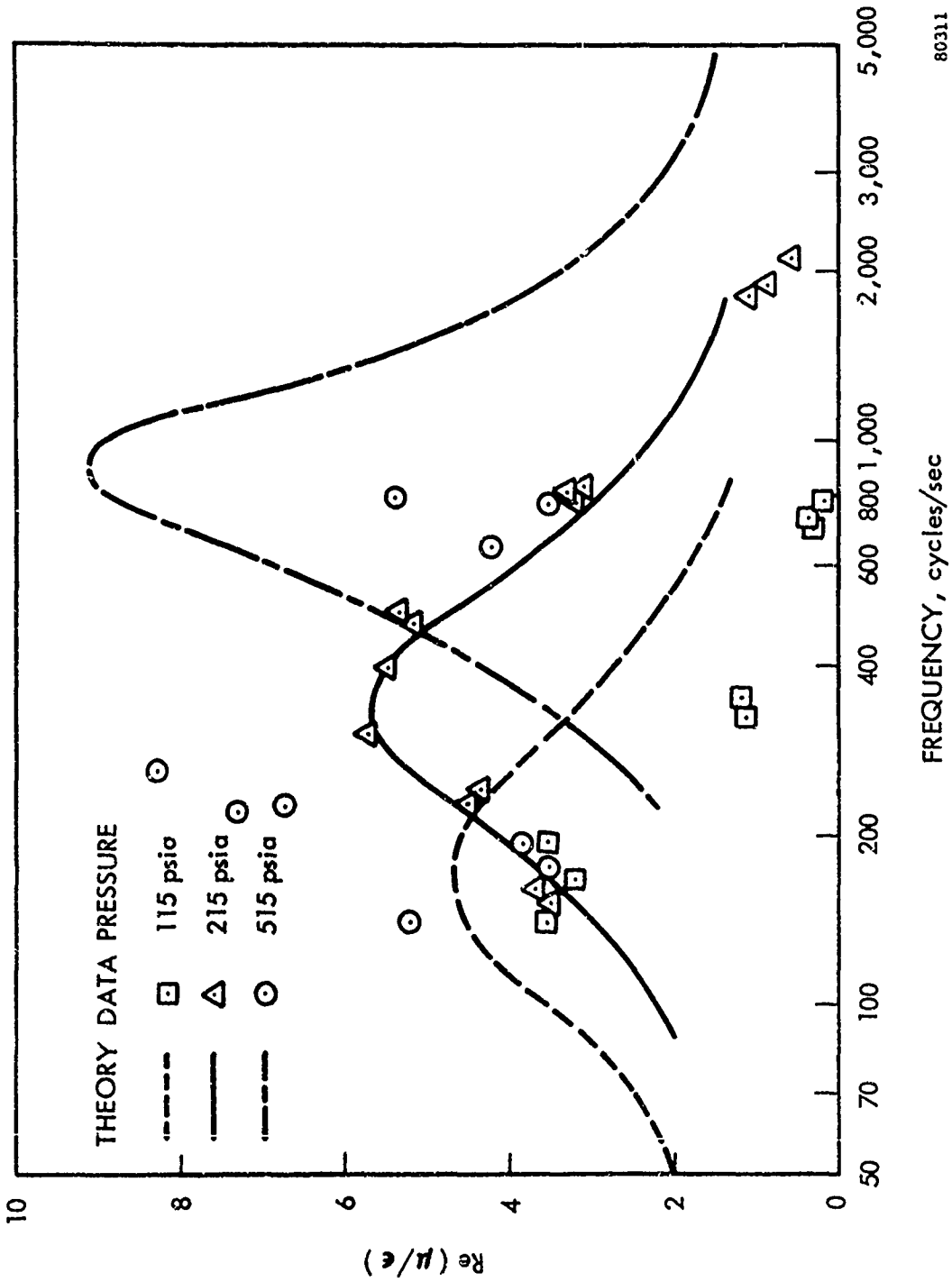


Figure 28. Limit Amplitude of Combustion Zone

2.3.8 Effect of Pressure

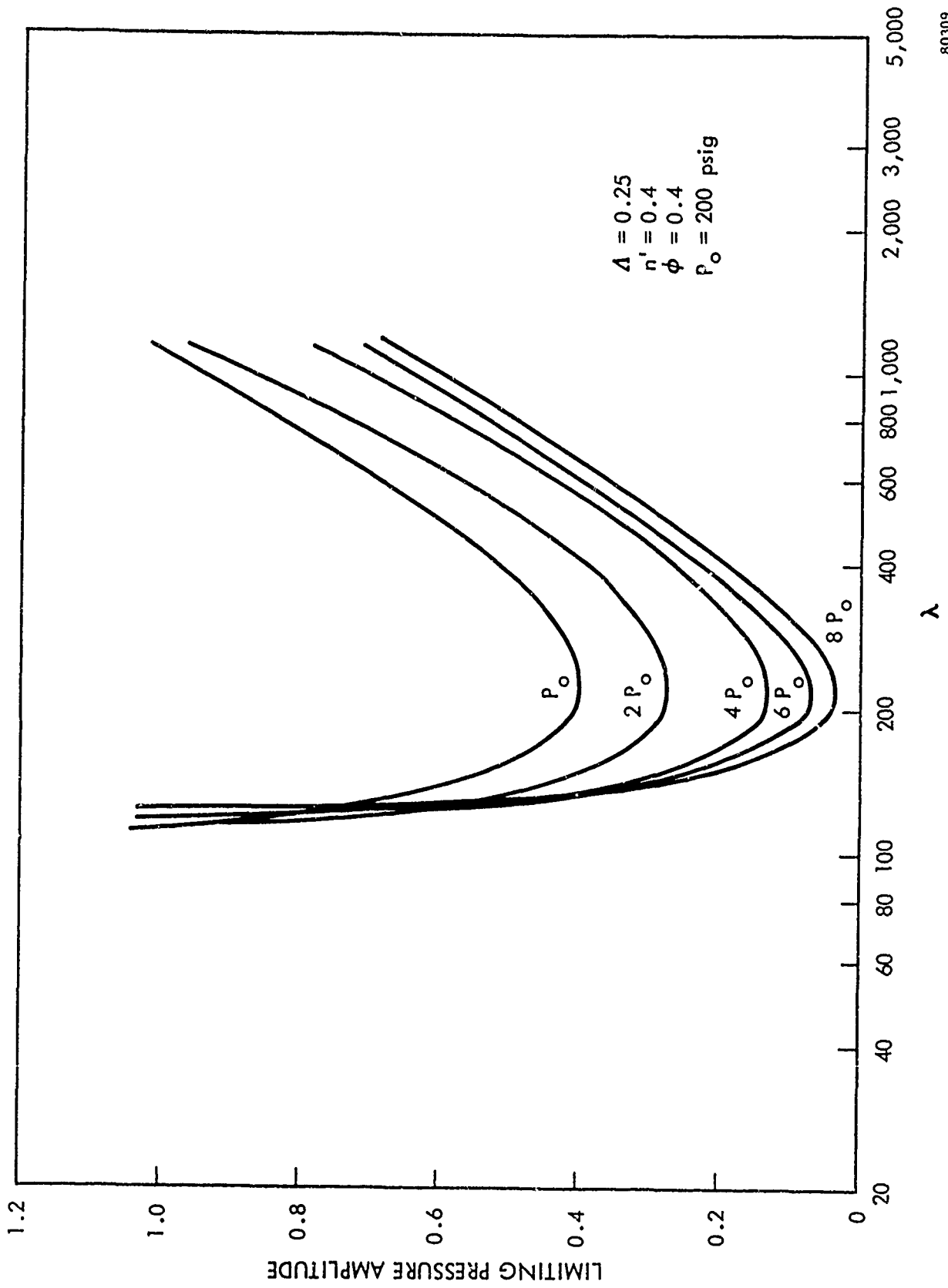
The effect of pressure on the transient behavior is also of interest in light of the data of Ibiricu.⁽³⁴⁾ This effect can only be studied using a specific combustion model. This was done with the model described by equations 40, 41, and 42 because of the simplicity and economy of calculations. This combustion model predicts that the response function increases with pressure and that the frequency at which the maximum response occurs also increases without limit. Using the previously reported method to correct for changes in propellant surface temperature with pressure⁽²⁾ the predicted result of increasing pressure is shown in figure 29 for propellant No. 1. In this calculation $\Lambda = 0.25$, $n' = 0.40$, and $\phi = 0.40$, while the values of R_1 , A_1 , and n at 200 psi are those shown in table II. This effect is consistent with the stability behavior observed by Ibiricu⁽³⁴⁾ at the lower pressures. However, at the higher pressure, Ibiricu observed the response function to pass through a maximum and then to decrease with further increases in pressure. The linear behavior shown in figure 29 shows no such maximum.

Further study of the pressure influence on the nonlinear behavior reveals a partial explanation of this dichotomy. The effect of pressure on the limiting pressure amplitudes for propellant No. 1 using the values of Λ , n' , and ϕ is shown in figure 30. From this plot, it is apparent that increasing the pressure sharply reduces the limiting pressure amplitude.



80311

Figure 29. Predicted Effect of Pressure on Response Function



80309

Figure 30. Effect of Pressure on Limit Amplitude

These results now provide a possible explanation for the data of Ibiricu. At the lower pressure (i.e., approximately 200 psia) the limiting pressure amplitudes are sufficiently large to permit meaningful measurement of the amplitude growth constants in the linear region. Therefore, the reported response functions are truly characteristics of the propellant behavior. In this area Ibiricu's data and the data obtained for propellant No. 1 in the course of this study are consistent with the predicted linear behavior.

As the pressure is increased, however, the limiting acoustic pressure amplitude decreases. Considering the fact that nonlinear effects become significant when the pressure amplitude reaches 50% of the limiting value, the region in which meaningful response function measurements can be made is sharply reduced with increasing pressure. Furthermore, if nonlinear effects are mistakenly included in the linear interpretation of the data, equation 39 shows that the resulting response function will be less than the true value. Hence, it is possible that the measurements reported by Ibiricu⁽³⁴⁾ might reflect the apparent response function and not the true response function.

To determine if the magnitude of this effect is sufficient to account for the data, equations 2 and 27 have combined to yield the following expression for the growth of the acoustic pressure amplitude in the T-burner

$$c'_g = \frac{df_n(\epsilon)}{dt} = \frac{4 \cdot \dot{r}_o \cdot c}{g P_o} [\text{Re}(\nu/\epsilon), + \epsilon^2 F(\lambda)] - c'_d \tag{59}$$

Experimental results from T-burner measurements have indicated that, as a first approximation, $c'_d = K f_d^{3/4} / (P_o)^{1/4}$.⁽³⁵⁾ An integration of equation 59 yields

the amplitude of the acoustic pressure as a function of time. Values of the apparent response function were derived from these predicted curves by measuring the apparent growth constant at a pressure amplitude of 5 psi. The difference between the resulting apparent response function and the true value (determined at zero pressure amplitude) was negligible over a wide pressure region.

This calculation is somewhat inconclusive, since the effect of pressure on the combustion parameters was determined by the limited specific combustion model. Thus, one can conclude that this specific model does provide the magnitude of the pressure effect required to account for Tbiricu's observations. However, other combustion models which consider the transient flame temperature behavior might account for the experimental observations.

3.0 CONCLUSIONS

- A. Transient combustion of composite solid propellants can be characterized by assuming the transient behavior of the solid phase to be that of a homogeneous nonreacting solid.
- B. The gasification of the solid phase was found to be an extremely complex process. For all propellants tested, this process was found to be strongly dependent upon surface temperatures, more so than could be accounted for by an Arrhenius expression with a reasonable activation energy. For propellants having an 84% loading of AP, the gasification process was also dependent on pressure and surface temperature. Some propellants showed the gasification increasing with pressure, while others showed a decrease.
- C. The rate of energy transfer into the solid was found to increase with increasing surface temperature and increasing pressure. The temperature effect is characteristic of a thermally neutral or slightly exothermic surface. The pressure effect is consistent with that predicted by laminar premixed and granular diffusion flame models. Coating the solid oxidizer reduced the temperature sensitivity of the energy transfer, with the magnitude of the effect depending on the coating. However, coatings had little effect on the pressure sensitivity.

- D. Parametric studies were conducted in which the linear behavior was held constant and the effects of the second and third order coefficients were determined. The results show that both positive and negative values of $E(\lambda)$ can be obtained, depending on the magnitude of the constants. Since Eisel has observed $E(\lambda)$ to be negative in his studies, this defines the region of reasonable second order coefficients. Additional studies show that $F(\lambda)$ is negative for reasonable second and third order coefficients. Therefore, the combustion process itself can limit the acoustic pressure amplitude in the T-burner. On the basis of these calculations, limiting amplitudes of 0.1 to 0.5 can be expected without consideration of acoustic losses.

REFERENCES

1. Wenograd, J., "Solid Propellant Combustion Studies," presented at the Combustion Symposium, Cambridge, England, July 1964.
2. Most, M. J., and J. Wenograd, "Solid Propellant Combustion Mechanism Studies," Seventeenth Progress Report, Contract No. Nor 1858(32), Princeton University, June 1965.
3. Steinz, J. A., and M. Summerfield, "Solid Propellant Combustion Mechanism Studies," Eighteenth Progress Report, Contract No. Nor 1858(32), Princeton University, July 1965.
4. Anderson, R., R. S. Brown, G. T. Thompson, and R. W. Ebeling, "Theory of Hypergolic Ignition of Solid Propellants," presented at the AIAA Meeting, Palm Beach, Florida, December 1963.
5. Anderson, R., and R. S. Brown, "The Role of Heterogeneous Reactions in Composite Solid Propellant Combustion, Termination and Instability," presented at the Combustion Instability Symposium, Orlando, Florida, November 1964.
6. Brown, R. S., and R. Anderson, "Pressure Coupling with Chemical Mechanism of Combustion Zone of Composite Solid Propellant Burning," presented at the Combustion Instability Symposium, Orlando, Florida, November 1964.
7. Novikov, S. S. and Yu. S. Fyazantsev, "The Theory of the Steady-State Propagation Velocity of an Exothermic Front in the Condensed Phase." Shur. Prik. Mekh. and Tekh. Fiziki. 3: 43-48, 1965.
8. Summerfield, M., G. S. Sutherland, M. J. Webb, H. J. Tabach, and K. P. Hall, "Burning Mechanism of Ammonium Perchlorate Propellants," Solid Propellant Rocket Research, edited by M. Summerfield. New York: Academic Press, 1960. pp. 141-182.
9. Nachbar, W., "A Theoretical Study of the Burning of a Solid-Propellant Sandwich," Solid-Propellant Rocket Research, edited by M. Summerfield. New York: Academic Press, 1960. pp. 207-226.
10. Rosen, G., "Burning Rates of Solid Propellants." J. Chem. Phys. 32: 89-93, 1960.
11. Spaulding, D. B., "The Theory of Burning of Solid and Liquid Propellants." Combustion and Flame. 4: 59-76, 1960.
12. McClure, F. T., R. W. Hart, and J. F. Bird, "Solid Propellant Rocket Motors as Acoustic Oscillators," Advances in Astronautics and Rocketry, Vol I, edited by M. Summerfield. New York: Academic Press, 1960. p.295.

13. Krier, H., J. S. Tien, W. A. Sirignano, M. Summerfield, "Non-Steady Burning Phenomenon of Solid Propellants." AIAA Journal. 6: 278-285 (1968)
14. Denison, M. R., and E. Baum, "A Simplified Model of Unstable Burning in Solid Rocket Propellants." ARS Journal. 3: 1112-1121, 1961.
15. Marxman, G. A., and C. E. Wooldridge, "Effect of Surface Reactions on the Solid Propellant Response Function." AIAA Journal. 6: 471-479, 1968.
16. Culick, F. E. C., "Calculations of the Admittance Function for a Burning Surface," presented at the 3rd ICRPG Combustion Conference, Cocoa Beach, Florida, October 1966.
17. Friedly, J. C., and E. E. Peterson, "Influence of Combustion Parameters on Instability in Solid Propellant Motors. Part I: Development of Model and Linear Analysis." AIAA Journal. 4: 1605-1610, 1966.
18. Hart, R. W., R. A. Farrell, and R. H. Cantrell, "Theoretical Study of a Solid Propellant Having a Homogeneous Surface Reaction. Part I: Acoustic Response, Low and Intermediate Frequencies." Combustion and Flame. 10: 367-380, 1966.
19. Horton, M. D., "Testing the Dynamic Stability of Solid Propellants: Techniques and Data," Report NOTS TP 3610, U. S. Naval Ordnance Test Station, August 1964.
20. Strittmater, R., L. Watermeier, and S. Pfaff, "Virtual Specific Acoustic Admittance Measurements of Burning Solid Propellant Surface by a Resonant Tube Technique," Ninth Symposium (International) on Combustion. New York: Academic Press, 1963. pp. 311-315.
21. Jensen, G. E., "A Stop-Start Study of Solid Propellants," Final Report, Contract No. NAS 1-6601, November 1967.
22. Friedly, J. C., "A Theoretical Analysis of Intermediate Frequency Instabilities During the Combustion of a Solid Propellant," Ph.D. Thesis, University of California, Berkeley, 1964.
23. Beckstead, M. W., and F. E. C. Culick, "A Comparison of Analysis and Experiment for Solid Propellant Combustion Instability," NWC Report TP 4531, May 1968.
24. Coates, R. L., N. W. Ryan, and M. D. Horton, "The T-Burner Method for Determining the Acoustic Admittance of Burning Propellants," AIAA Preprint No. 64-137, January 1964.
25. Price, E. W., et al, "Combustion of Solid Propellants and Low Frequency Combustion Instability," NOTS Report TP 4244, June 1967.
26. Horton, M. D., and D. H. Rice, "The Effects of Compositional Variables on Oscillatory Combustion of Solid Rocket Propellants." Combustion and Flame. 8: 21-28, 1964.

27. Culick, F. E. C., "A Review of Calculations of the Admittance Function for a Burning Surface," presented at the ICRPG/AIAA 2nd Solid Propulsion Conference, Anaheim, California, June 1967.
28. Friedly, J. C., and E. E. Peterson, "Influence of Combustion Parameters on Instability in Solid Propellant Motors. Part II: Nonlinear Analysis." AIAA Journal. 4: 1932, 1966.
29. Olberg, C. L., "Combustion Instability. The Relation Between Acoustic and Non-Acoustic Instability." AIAA Journal. 6:265-271, 1968.
30. Beckstead, M. W., N. W. Ryan, and A. D. Baer, "Non-Acoustic Instability of Composite Propellant Combustion." AIAA Journal. 4:1622-1628, 1966. Also Beckstead, M. W., and E. W. Price, "Non-Acoustic Combustor Instability." AIAA Journal. 5:1966-1989, 1967.
31. Eisel, J. L., "The Effect of Acoustic Pressure on the Burning Rate of Solid Rocket Propellants." Pyrodynamics. 1:61-70, 1964.
32. Sabadell, A. J., J. Wenograd and M. Summerfield, "Measurement of Temperature Profiles through Solid-Propellant Flames Using Fine Thermocouples." AIAA Journal. 3:1580-1584, 1965.
33. Friedly, J. C. and E. E. Peterson, "A Mathematical Analysis of the Non-Linear Dynamics of Solid Propellant Combustion: An Application of the Method of Discretization," presented at the International Control Conference, London, June 1966.
34. Ibiricu, M. M., "Stable and Unstable Regimes in Solid Propellant Combustion," Proceedings of the XVII Congress of the International Astronautical Federation, Gordon and Breach: New York, 1967. pp. 183-9.
35. Ibiricu, M. M., Ballistics Research Laboratory, Aberdeen Proving Ground, Maryland, Private Communication, May 1968.

APPENDIX A. ADDITIONAL EXPERIMENTAL STUDIES

1.0 PHOTOGRAPHIC STUDIES

A sample holder was constructed with viewing windows, as shown schematically in figure A-1. The 1.5-in.-diameter propellant disk was located in the center, and a purge system was located between the sample and the windows. Tests were conducted using both Vycor and Plexiglas windows with and without the purge system. The windows were sealed to their mounting with gaskets. A photograph of the final assembly is shown in figure A-2.

The camera used in these studies was a Hycon 16-mm rotary prism camera with a framing rate capacity to 4,000 frames/sec, which will provide several frames during a complete cycle at the lower frequencies. The initial photographs were taken at a framing rate of 500 frames/sec. A quartz-iodine lamp was used for backlighting the viewing section.

The greatest problem encountered in the photographic studies was the rapid buildup of carbonaceous material on the windows. To eliminate this problem, several changes were made in the experiments. A clean-burning propellant consisting of 84[~] AP was selected. The burning rate at 200 psig was 0.130 in./sec. The windows were also recessed from the tube walls to allow the nitrogen window purge to operate efficiently. The amount of ground propellant placed over the ignition wires was reduced to minimize the effects of the additional mass ejected during the ignition phase and subsequent clouding of the windows.

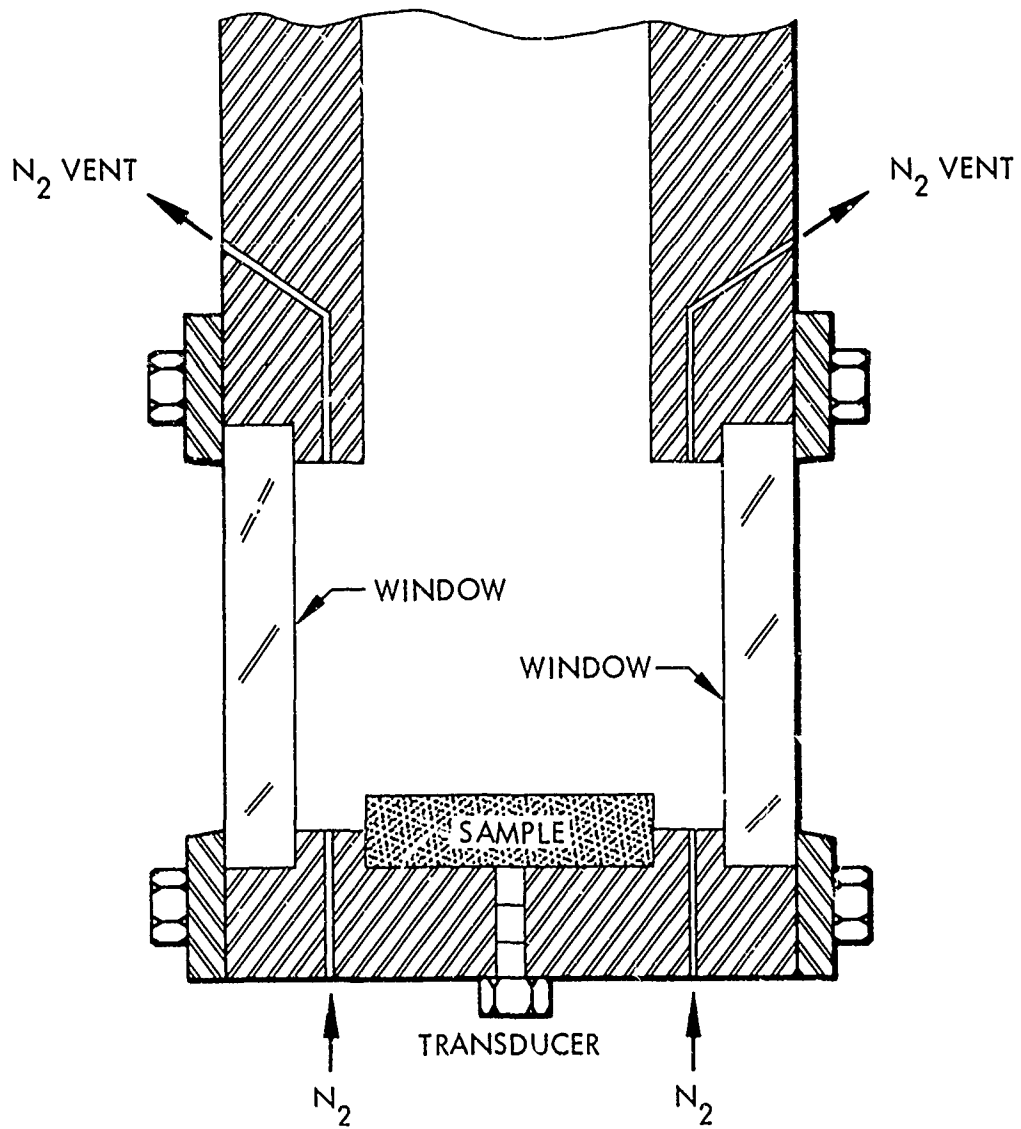


Figure A-1. Schematic of Viewing Section

81331



81332

Figure A-2. Viewing Section

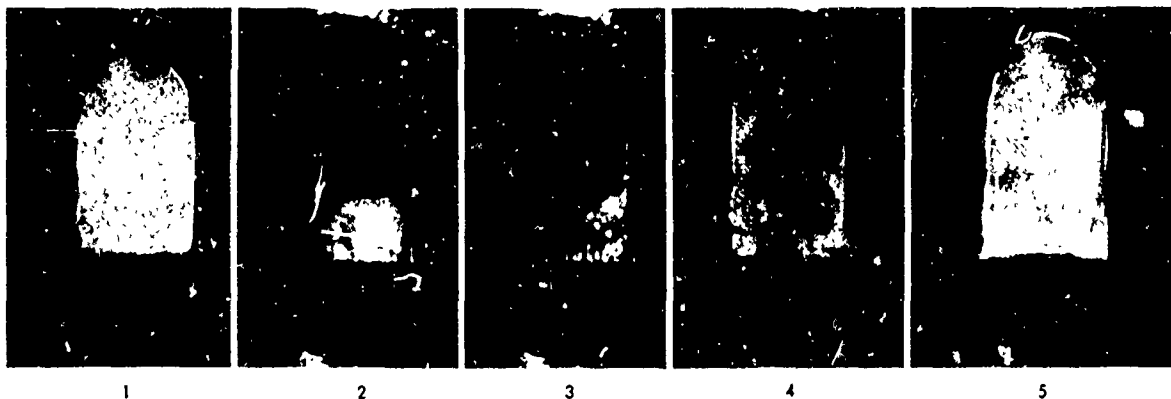
These changes significantly improved the initial photographic results and made it possible to observe the propellant surface during a large portion of the run. During the early stages, a film of opaque material was temporarily deposited on the windows, preventing observation of the initial stages of the instability process. Methods of solving this problem are currently being considered.

A typical film sequence is shown in figure A-3 for the 84% AP propellant. The sides of the test sample were inhibited before firing, and a nitrogen purge was used in this test. The photographs were taken from the 16-mm color film, and the original film displays greater detail than appears in figure A-3. Random frames were selected to display various features of the combustion process. The first frame shows the test section before firing, and the next frame shows the ignition process. Ignition is obtained by electrically heating the nichrome wire secured to the propellant surface, and this appears as a blue flash (i.e., bright flash near surface in frame 2) when the electrical contact is broken. Once ignition has occurred, mass is evolved from the surface, as displayed by the luminous streaks near the surface in frame 3. At a later time the propellant started to burn around the inhibitor, as shown in frames 4 and 5.

2.0 PHASE SHIFT STUDIES

A series of preliminary experiments was conducted in which the combustion process was altered by phase shifting the pressure oscillations with electrical feedback into the combustion chamber. When oscillations occur, the output pressure signal is passed through a phase inverter and then back into

GRAPHIC NOT REPRODUCIBLE



81333

Figure A-3. Combustion Process in T-Burner Viewing Section

the combustion chamber through a probe located inside the chamber. This technique provides a possible method of investigating temperature oscillations or entropy waves in the T-burner and may also moderate or eliminate combustion instability in motors.

A schematic of the feedback loop previously developed in connection with flame acoustic studies at UTC is shown in figure A-4. The pressure transducer (A) senses any pressure fluctuations which are then amplified (B) and inverted in phase by 180° (C). The final signal is then fed into the combustion chamber through a probe (D) located above the propellant surface and utilizes the case walls as the ground electrode.

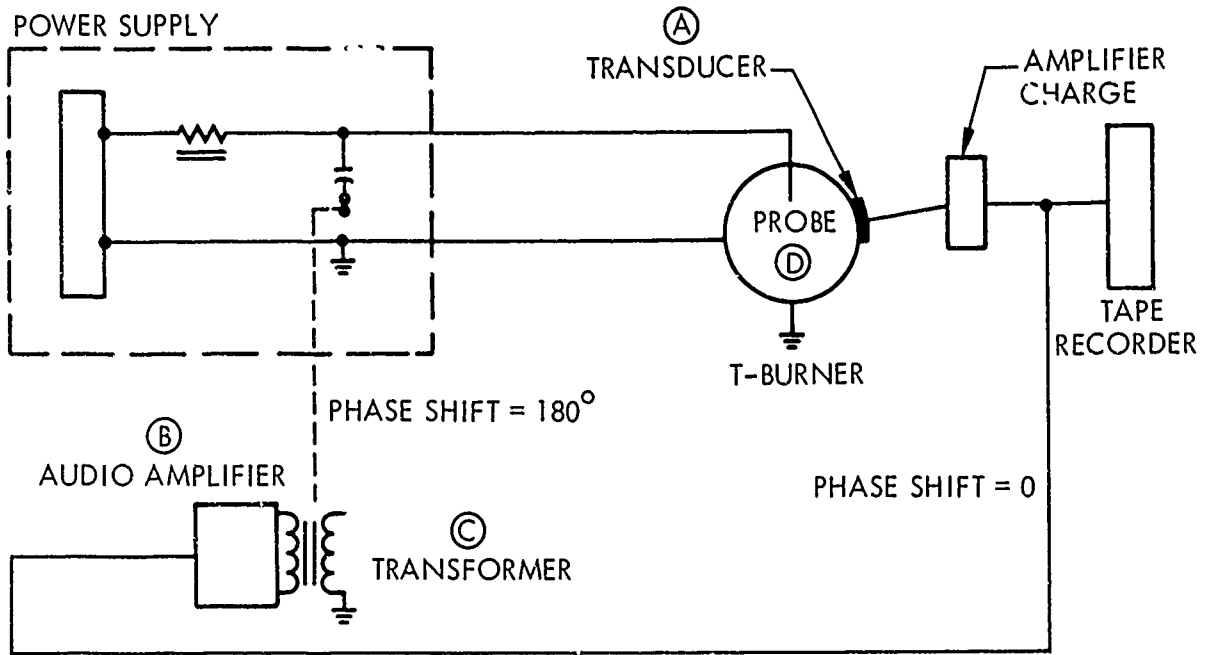
The probe was a tungsten rod with a ceramic shield in a connax fitting. It was located about 1 in. from the surface of one of the propellant samples

in the double-ended T-burner and protruded into the center of the tube.

The propellant used in these preliminary tests contained 82% AP, 2% CsNO_3 , and 16% UTREZ binder. The seeding material, along with the high oxidizer loading, was used to increase the conductivity of the gases. The current, in turn, was related to the conductivity and voltage across the electrodes. In the present system with 500 vdc across the electrode to ground, a nominal 0.3 amp were obtained during the tests. As the voltage fluctuated out-of-phase with the pressure due to the feedback mechanism, the current fluctuated in-phase with the pressure, and simultaneous recordings were made of the pressure, voltage, and current on the CEC recorder.

These studies were made at a fundamental oscillating mode of approximately 350 cps. Although it was difficult to obtain reproducible results from these initial studies, several important qualitative observations were observed. The results, based on measurements of the chamber pressure with the probe in the system compared with and without the 500 vdc and zero gain on the feedback amplifier, showed no significant change in the measured signal. This indicates that there was no interference between the electronics and the recorded pressure. Small amplitude oscillations appeared in the current trace and were in-phase with the pressure oscillations, which is a result of temperature oscillations that appear in the T-burner (i.e., $\Delta \text{current} \propto \Delta \text{conductivity} \sim (\Delta \text{temperature})^{10}$).

Measurements of the chamber pressure, made with the probe in position, were also compared with and without the feedback mechanism in operation. The results indicate that both the absolute magnitude in the time varying pressure



81308

Figure A-4. Schematic of Feedback Loop

oscillations (ΔP) and the sensitivity of the propellant specified in terms of the acoustic response function ($\mu/\epsilon = \frac{\Delta \dot{r}}{\dot{r}_0} \cdot \frac{P_0}{\Delta P_0}$) were reduced.

APPENDIX B. EXPERIMENTAL DATA

Data for the propellants tested on this program are tabulated in this appendix. The specific formulations are described in table II.

TABLE B-I. UTX-8501 PROPELLANT

Density: 0.063 lb/in.³

Velocity of Sound: 36,500 in./sec

Run No.	Mean Pressure	Growth Frequency	Growth Rate, γ_g	Decay Frequency	Decay Rate, α_d	Re(μ/ϵ)
1	100 psig	163	3.76	180	4.48	2.38
2		137	4.03	184	7.76	3.54
3		167	6.18	193	4.86	3.13
4		195	2.35	205	11.90	3.49
5		333	5.30	320	1.01	0.95
6		327	5.88	296	0.97	1.05
7		320	4.53	291	2.24	1.08
8		728	2.20	667	1.72	0.29
9		762	2.16	762	2.60	0.31
10		100 psig	728	1.81	695	2.33
1	200 psig	151	4.72	151	2.27	3.72
2		160	4.24	144	3.11	3.85
3		228	9.42	242	3.48	4.46
4		239	10.20	266	2.92	4.31
5		400	13.47	219	7.76	5.54
6		307	18.81	285	2.83	5.72
7		477	27.40	785	5.13	5.15
8		500	28.55	741	7.21	5.37
9		816	18.77	579	11.56	3.37
10		784	18.42	615	10.52	3.26
11		816	8.98	563	15.68	3.13
12		1,904	13.51	1,818	6.33	0.85
13		1,812	13.29	1,904	10.04	1.02
14		200 psig	2,105	10.34	1,904	4.33
1	500 psig	140	2.96	164	4.76	5.20
2		186	3.57	126	2.37	3.95
3		177	1.47	166	4.24	3.51
4		226	9.78	216	4.78	6.75
5		220	10.88	242	5.16	7.32
6		260	12.80	270	8.40	8.33
7		762	7.14	728	17.90	3.52
8		667	5.00	762	35.10	4.17
9		500 psig	800	5.30	762	34.70

TABLE B-II. UTX-8502 PROPELLANT

Density: 0.063 lb/in.³

Velocity of Sound: 34,000 in./sec

Run No.	Mean Pressure	Growth Frequency	Growth Rate, % _g	Decay Frequency	Decay Rate, % _d	Re(μ/c)
1	200 psig	190	5.50	164	2.23	3.55
2	↑ ↓	188	2.69	161	4.72	3.65
3		168	3.94	160	3.20	3.63
4		271	4.08	313	7.41	3.23
5		307	4.56	290	7.18	3.30
6		242	4.95	313	5.94	3.28
7		667	4.49	635	3.57	1.04
8	200 psig	513	6.77	769	1.00	1.19

TABLE B-III. UTX-8525 PROPELLANT

Density: 0.063 lb/in.³

Velocity of Sound: 36,500 in./sec

Run No.	Mean Pressure	Growth Frequency	Growth Rate, % _g	Decay Frequency	Decay Rate, % _d	Re(μ/c)
1	200 psig	146	5.18	131	4.49	4.90
2	↑ ↓	137	5.00	139	5.46	5.33
3		220	8.59	223	9.60	5.77
4		210	8.43	218	8.06	5.43
5		685	13.47	647	3.43	1.75
6		755	3.21	631	13.38	1.77
7		200 psig	1,620	Could not measure a growth curve on several runs		

TABLE B-IV. UTX-8526 PROPELLANT

Density - 0.063 lb/in³ Velocity of Sound - 36,000 in./sec

Run No.	Mean Pressure	Growth Frequency	Growth Rate, %/g	Decay Frequency	Decay Rate, %/d	Re(μ/ϵ)
1	200 psig	160	4.51	210	2.35	2.14
2	↑ ↓	160	5.11	202	1.98	2.27
3		280	17.80	285	5.37	4.48
4		600	16.67	770	7.35	2.04
5		570	25.88	636	11.74	3.46
6	200 psig	1500	Could not measure a growth curve on several runs			

TABLE B-V. UTX-8527 PROPELLANT

Density - 0.063 lb/in³ Velocity of sound: 36,000 in.sec

Run No.	Mean Pressure	Growth Frequency	Growth Rate, %/g	Decay Frequency	Decay Rate, %/d	Re(μ/ϵ)
1	200 psig	120	1.23	165	1.14	2.53
2	↑ ↓	123	1.41	170	1.97	3.37
3		231	3.59	275	3.82	4.30
4		216	5.76	263	2.35	5.22
5		200 psig	700	Could not measure a growth curve on several runs		

TABLE B-VI. UTX-8528 PROPELLANT

Density: 0.063 lb/in.³ Velocity of Sound: 36,000 in./sec

Run No.	Mean Pressure	Growth Frequency	Growth Rate, %/g	Decay Frequency	Decay Rate, %/d	Re(μ/c)
1	200 psig	166	4.95	146	5.25	4.75
2	↕	127	3.64	143	5.96	5.06
3		256	9.72	245	2.67	3.52
4		296	4.28	256	6.77	2.95
5	200 psig	600	Could not measure a growth curve on several runs			

TABLE B-VII. UTX-8529 PROPELLANT

Density: 0.063 lb/in.³ Velocity of Sound: 36,000 in./sec

Run No.	Mean Pressure	Growth Frequency	Growth Rate, %/g	Decay Frequency	Decay Rate, %/d	Re(μ/c)
1	200 psig	174	4.65	176	5.55	3.92
2	↕	163	5.20	161	4.51	4.05
3		256	15.29	285	4.81	5.16
4		244	9.79	284	6.47	4.23
5		525	31.32	730	5.76	4.54
6		527	32.70	784	6.91	4.76
7	200 psig	1,690	Could not measure a growth curve on several runs			

TABLE B-VIII. UTX-8531 PROPELLANT

Density: 0.063 lb/in.³

Velocity of Sound: 36,000 in./sec

Run No.	Mean Pressure	Growth Frequency	Growth Rate, % _g	Decay Frequency	Decay Rate, % _d	Re(μ / ϵ)
1	200 psig	147	3.66	167	5.50	3.38
2	↑ ↓	172	4.65	170	7.00	3.98
3		190	9.23	215	9.16	5.33
4		210	8.63	265	9.10	4.42
5		200	7.48	254	13.88	5.39
6		583	31.55	750	5.85	3.62
7	514	514	32.10	611	12.73	4.87
8	200 psig	1,800	Could not measure a growth curve on several runs			

TABLE B-IX. UTX-8532 PROPELLANT

Density: 0.063 lb/in.³

Velocity of Sound: 36,000 in./sec

Run No.	Mean Pressure	Growth Frequency	Growth Rate, % _g	Decay Frequency	Decay Rate, % _d	Re(μ / ϵ)
1	200 psig	165	5.83	135	6.26	6.83
2	↑ ↓	175	5.69	136	5.64	6.20
3		233	9.83	232	7.41	6.22
4		490	18.31	755	15.27	4.82
5		475	21.51	690	4.42	4.32
6	200 psig	1,500	3.15	1,700	7.11	0.52

TABLE B-X. UTX-9164 PROPELLANT

Density: 0.063 lb/in.³ Velocity of Sound: 34,000 in./sec

Run No.	Mean Pressure	Growth Frequency	Growth Rate, %	Decay Frequency	Decay Rate, %	Re(μ/c)
1	200 psig	200	1.38	182	4.26	2.56
2	↑ ↓	205	2.09	190	3.02	2.27
3		291	10.30	302	3.41	3.95
4		291	7.25	341	2.60	2.85
5		333	1.49	296	9.10	2.98
6		364	4.05	314	9.57	3.81
7		372	3.66	262	4.07	2.20
8		696	4.31	696	2.43	0.84
9	200 psig	727	1.60	762	2.38	0.47

TABLE B-XI. UTX-9165 PROPELLANT

Density: 0.063 lb/in.³ Velocity of Sound: 34,000 in./sec

Run No.	Mean Pressure	Growth Frequency	Growth Rate, %	Decay Frequency	Decay Rate, %	Re(μ/c)
1	200 psig	191	5.11	170	3.06	3.76
2	↑ ↓	190	3.66	174	3.09	3.11
3		174	4.93	174	2.46	3.56
4		190	4.46	170	3.40	3.66
5		170	4.62	178	1.83	3.15
6		320	2.43	250	3.97	1.97
7		320	3.30	222	2.72	1.89
8		347	3.06	235	3.00	1.81
9	↓	320	2.23	242	5.09	2.35
10		200 psig	750	3.24	750	2.56

TABLE B-XII. UTX-9167 PROPELLANT

Density: 0.063 lb/in.³

Velocity of Sound: 36,500 in./sec


Run No.	Mean Pressure	Growth Frequency	Growth Rate, α_g	Decay Frequency	Decay Rate, α_d	Re(μ/c)
1	200 psig	228	3.61	170	2.67	1.98
2		216	3.57	170	2.34	1.90
3		222	4.48	186	1.98	1.94
4		223	3.60	211	3.63	2.10
5		333	7.44	222	3.77	2.46
6		320	4.68	222	6.04	2.70
7		800	3.52	800	6.03	0.75
8	200 psig	800	3.17	730	6.82	0.84

TABLE B-XIII. UTX-9168 PROPELLANT

Density: 0.063 lb/in.³

Velocity of Sound: 36,500 in./sec



Run No.	Mean Pressure	Growth Frequency	Growth Rate, α_g	Decay Frequency	Decay Rate, α_d	Re(μ/c)
1	200 psig	200	3.36	163	5.12	3.41
2		195	2.96	157	4.65	3.17
3		191	1.69	145	5.43	3.28
4		333	5.38	250	7.15	3.16
5		333	2.58	210	6.15	2.61
6		320	2.65	265	6.52	2.32
7		286	3.24	308	6.93	2.37
8		533	10.95	730	7.08	2.16
9		696	10.20	800	3.50	1.35

TABLE B-XIV. UTX-9173 PROPELLANT

Density: 0.063 lb/in.³

Velocity of Sound: 36,500 in./sec

Run No.	Mean Pressure	Growth Frequency	Growth Rate, % _g	Decay Frequency	Decay Rate, α_d	Re(μ/ϵ)
1	200 psig	210	9.54	200	8.60	5.80
2	↑ ↓	210	8.53	200	9.71	5.85
3		216	5.79	160	9.80	5.80
4		381	9.16	348	3.98	2.32
5		381	9.03	348	4.16	2.33
6		360	5.40	276	4.58	2.08
7		382	6.59	260	4.91	2.37
8		800	5.25	806	16.56	1.79
9	200 psig	552	11.30	843	5.88	1.81

TABLE B-XV. UTX-9368 PROPELLANT

Density: 0.064 lb/in.³

Velocity of Sound: 36,500 in./sec

Run No.	Mean Pressure	Growth Frequency	Growth Rate, % _g	Decay Frequency	Decay Rate, α_d	Re(μ/ϵ)
1	200 psig	239	14.78	267	2.94	5.23
2	↑ ↓	220	13.38	267	2.41	5.05
3		239	13.21	276	3.10	4.80
4		372	24.90	762	8.68	5.55
5		400	14.75	727	7.94	4.15
6		533	22.70	800	8.47	3.82
7		1,010	6.15	1,145	12.40	1.21
8	200 psig	1,080	8.32	1,250	15.20	1.43

TABLE B-XV. UTX-9368 PROPELLANT

Density: 0.064 lb/in.³ Velocity of Sound: 36,500 in./sec

Run No.	Mean Pressure	Growth Frequency	Growth Rate, α_g	Decay Frequency	Decay Rate, α_d	Re(μ/c)
1	200 psig	239	14.78	267	2.94	5.23
2	↑ ↓	220	13.38	267	2.41	5.05
3		239	13.21	276	3.10	4.80
4		372	24.90	762	8.68	5.55
5		400	14.75	727	7.94	4.15
6		533	22.70	800	8.47	3.82
7		1,010	6.15	1,145	12.40	1.21
8	200 psig	1,080	8.32	1,250	15.20	1.43

TABLE B-XVI. A-13 (NOTS PROPELLANT)

Density: 0.057 lb/in.³ Velocity of Sound: 36,500 in./sec

Run No.	Mean Pressure	Growth Frequency	Growth Rate, α_g	Decay Frequency	Decay Rate, α_d	Re(μ/ϵ)
1	200 psig	242	6.4	157	10.3	5.64
2	↑ ↓	243	5.4	182	13.2	5.81
3		320	6.5	314	13.5	3.88
4		333	7.2	286	8.6	3.17
5		640	5.2	572	8.7	1.43
6		696	5.5	552	10.4	1.64
7		728	6.9	762	12.3	1.57
8		728	7.1	572	11.1	1.79
9		800	5.2	800	17.5	1.74
10		1,430	11.0	1,820	20.6	1.16
11		1,430	9.5	1,504	25.4	1.44
12		1,540	14.4	1,740	13.2	1.04
13		1,670	10.4	1,820	24.6	1.21
14		3,300	4.3	3,330	23.0	0.51
15		3,300	9.2	2,850	37.3	0.97
16		200 psig	4,000	22.3	4,450	5.4

TABLE B-XVII. UTX-9379 PROPELLANT

Density: 0.064 lb/in.³

Velocity of Sound: 36,500 in./sec

Run No.	Mean Pressure	Growth Frequency	Growth Rate, γ_g	Decay Frequency	Decay Rate, α_d	Re(μ/c)
1	200 psig ↑	205	6.45	154	2.46	3.28
2		200	5.79	167	1.84	2.78
3		191	4.66	170	1.52	2.33
4		228	7.62	165	4.58	4.27
5		335	10.22	281	4.06	3.15
6		308	15.3	262	2.49	4.13
7		308	16.16	291	3.31	4.45
8	↓ 200 psig	842	1.16	800	3.71	0.418
9		855	2.58	855	3.58	0.501
10		842	1.18	842	2.75	0.328
11		842	2.67	762	2.20	0.418

TABLE B-XVIII. UTX-9395 PROPELLANT

Density: 0.064 lb/in.³

Velocity of Sound: 36,500 in./sec

Run No.	Mean Pressure	Growth Frequency	Growth Rate, γ_g	Decay Frequency	Decay Rate, α_d	Re(μ/c)
1	200 psig ↑	254	6.93	210	10.15	2.35
2		250	5.67	222	11.63	2.83
3		258	13.36	193	13.02	3.78
4		381	10.27	286	7.77	2.04
5		391	11.71	391	8.82	1.99
6		341	14.22	334	9.88	2.69
7		391	22.85	308	5.45	2.88
8		876	18.65	800	44.1	2.88
9		915	24.5	855	60.8	3.69
10		790	68.65	627	10.55	3.91
11		842	29.88	687	14.8	2.16
12	↓ 200 psig	1,880	16.55	1,780	10.00	0.55
13		1,780	14.8	1,780	14.95	0.63
14		1,780	23.35	1,730	22.00	0.92
15		1,780	11.15	1,780	7.7	0.40

TABLE B-XIX. UTX-9715 PROPELLANT

Density: 0.064 lb/in.³ Velocity of Sound: 36 500 in./sec

Run No.	Mean Pressure	Growth Frequency	Growth Rate, α_g	Decay Frequency	Decay Rate, α_d	Re(μ/ϵ)
1	200 psig ↑ ↓ 200 psig	228	10.50	235	7.73	4.56
2		266	6.62	222	8.40	3.63
3		242	7.62	235	7.62	3.85
4		276	6.54	205	9.76	4.14
5		235	7.91	191	8.41	4.50
6		336	7.50	314	11.75	3.47
7		381	7.25	348	13.85	3.42
8		348	9.40	286	7.10	3.01
9		763	5.24	696	3.41	0.69
10		844	6.27	667	3.38	0.73
11		762	4.20	842	8.75	0.90
12		842	3.37	842	2.30	0.38

TABLE B-XX. UTX-9717 PROPELLANT

Density: 0.064 lb/in.³ Velocity of Sound: 36,500 in./sec

Run No.	Mean Pressure	Growth Frequency	Growth Rate, α_g	Decay Frequency	Decay Rate, α_d	Re(μ/ϵ)
1	200 psig ↑ ↓ 200 psig	239	5.25	222	2.82	1.67
2		203	9.97	225	1.11	2.55
3		232	5.8	236	4.45	2.12
4		372	3.21	302	3.09	0.91
5		364	4.39	291	3.10	1.10
6		364	6.19	320	3.19	1.29
7		381	3.71	287	3.22	1.58
8		854	4.93	782	4.56	0.559
9		728	4.39	762	4.03	0.545
10		842	1.34	800	2.48	0.505
11		842	4.75	696	4.14	0.559

TABLE B-XXI. UTX-9718 PROPELLANT

Density: 0.064 lb/in.³ Velocity of Sound: 36,500 in./sec

Run No.	Mean Pressure	Growth Frequency	Growth Rate, α_g	Decay Frequency	Decay Rate, α_d	Re(μ/ϵ)
1	200 psig	250	4.62	296	3.22	1.49
2	↑ ↓	242	2.38	286	1.87	0.83
3		267	5.0	281	4.33	1.73
4		272	3.23	239	3.65	1.38
5		571	5.79	421	5.43	1.16
6		410	3.75	364	3.83	0.99
7		422	5.08	422	7.88	1.55
8		422	6.94	410	3.52	1.27
9		390	5.91	258	4.14	1.58
11		382	6.58	291	5.88	1.89
12		800	15.65	667	6.98	1.52
13		842	13.53	941	7.58	1.22
14		762	16.0	616	3.82	1.38
15		762	13.15	640	5.3	1.34
16		1,730	17.18	1,830	22.45	1.18
17		1,490	12.1	1,600	10.32	0.73
18	1,830	12.28	1,940	11.05	0.63	
19	1,780	9.93	1,880	9.75	0.60	
20	200 psig	1,830	6.9	1,775	3.75	0.25

TABLE B-XXII. UTX-9719 PROPELLANT

Density: 0.064 lb/in.³ Velocity of Sound: 36,500 in./sec

Run No.	Mean Pressure	Growth Frequency	Growth Rate, α_g	Decay Frequency	Decay Rate, α_d	Re(μ/ϵ)	
1	200 psig	246	11.47	281	7.35	3.62	
2	↑ ↓	226	12.27	235	9.09	4.6	
3		219	11.74	250	6.69	3.99	
4		391	3.12	281	3.29	0.98	
5		380	5.83	286	3.59	1.38	
6		381	7.08	281	5.49	1.89	
7		421	5.38	421	7.02	1.46	
8		854	9.83	705	5.18	0.94	
9		865	14.9	695	4.22	1.18	
10		842	14.34	680	6.5	1.33	
11		1,830	15.37	1,560	8.11	0.68	
12		1,939	21.3	1,489	7.65	0.81	
13		1,780	19.55	1,989	23.60	1.14	
14		200 psig	1,880	14.21	1,680	4.22	0.47

TABLE B-XXIII. UTX-9720 PROPELLANT

Density: 0.064 lb/in.³ Velocity of Sound: 36,500 in./sec

Run No.	Mean Pressure	Growth Frequency	Growth Rate, % _g	Decay Frequency	Decay Rate, % _d	Re(u/c)
1	200 psig	254	2.25	222	3.64	1.35
2	↑ ↓	254	3.25	229	3.92	1.58
3		211	3.61	235	3.34	1.66
4		411	7.55	327	4.86	1.78
5		372	7.1	364	6.21	1.9
6		390	5.28	281	4.86	1.63
7		372	5.37	291	4.2	1.52
8		762	16.2	667	2.8	1.4
9		800	14.14	695	3.38	1.18
10		800	12.8	667	2.99	1.08
11		890	10.42	667	2.54	0.82
12		1,730	5.8	1,640	4.9	0.33
13		1,775	10.5	1,680	5.65	0.49
14		1,830	9.35	1,775	5.15	0.15
15		200 psig	1,775	6.9	1,680	6.3

TABLE B-XXIV. UTX-9754 PROPELLANT

Density: 0.064 lb/in.³ Velocity of Sound: 36,500 in./sec

Run No.	Mean Pressure	Growth Frequency	Growth Rate, % _g	Decay Frequency	Decay Rate, % _d	Re(u/c)
1	200 psig	188	4.27	162	1.52	2.9
2	↑ ↓	154	5.68	158	2.62	3.93
3		156	4.67	162	3.24	4.52
4		145	6.19	133	1.74	5.04
5		286	3.13	246	3.19	2.16
6		239	6.31	226	2.33	3.33
7		250	5.72	276	1.12	2.43
8		271	9.09	262	2.49	3.9
9	200 psig	577	4.68	696	7.43	1.68

APPENDIX C
EQUATIONS FOR NONLINEAR BEHAVIOR

The second order behavior of the general analysis is given by

$$E(\lambda) = \text{Re} \left\{ \frac{1}{4(1+A_1-R_1)} \left[\left(\frac{e_1^0}{\epsilon_1} \right) \left(\frac{e_1^0}{1} \right)^* W_1 + 2 \left(\frac{e_1^0}{\epsilon_1} \right) X_1 + Y_1 + 4 \left(\frac{\epsilon_2^m}{\epsilon_1^2} \right) Z_1 - 2 \left(\frac{\mu_1}{\epsilon_1} \right)^* \left(\frac{e_1^0}{\epsilon_1} \right) A_1 \right] \right\} \quad (\text{C-1})$$

where

$$W_1 = (1-R_1) \left[\frac{\partial^2 H_n}{\partial \theta^2} \right]_0 + A_1 \left[\frac{\partial^2 F_n}{\partial \theta^2} \right]_0 = (1-R_1)A_2 + A_1 R_2 \quad (\text{C-2})$$

$$X_1 = (1-R_1) \left[\frac{\partial^2 H_n}{\partial \theta \partial \epsilon} \right]_0 + A_1 \left[\frac{\partial^2 F_n}{\partial \theta \partial \epsilon} \right]_0 = (1-R_1)C_{11} + A_1 D_{11} \quad (\text{C-3})$$

$$Y_1 = (1-R_1) \left[\frac{\partial^2 H_n}{\partial \epsilon^2} \right]_0 + A_1 \left[\frac{\partial^2 F_n}{\partial \epsilon^2} \right]_0 = (1-R_1)Q_2 + A_1 B_2 \quad (\text{C-4})$$

$$Z_1 = [(1-R_1)Q_1 + A_1 B_1] \quad (\text{C-5})$$

However, by extrapolating $E(\lambda)$ to $E(0)$ one of the constants can be eliminated. Assuming $\epsilon_2 = 0$ as $\lambda \rightarrow 0$, the resulting expression becomes

$$E(0) = \frac{n(n-1)}{4} = \frac{1}{4(1+A_1-R_1)} \left\{ \left(\frac{n-Q_1}{A_1} \right)^2 W_1 + 2 \left(\frac{n-Q_1}{A_1} \right) X_1 + Y_1 - 2n \left(\frac{n-Q_1}{A_1} \right) A_1 \right\} \quad (\text{C-6})$$

Thus, Y_1 can be eliminated from equation C-1 yielding an equation which contains three additional parameters (X_1 , W_1 , and Z_1) beyond those required to characterize the linear region and the steady-state behavior.

The corresponding solution for $\mu_2^{sc} / \epsilon_1^2$, the component of μ_2 which oscillates at the second harmonic, is

$$\frac{\mu_2^{sc}}{\epsilon_1^2} (\lambda_2 + A_1 / \lambda_2 - R_1) = \left\{ \frac{(\theta_1^0 / \epsilon_1)^2 [W_1 + A_2 (\lambda_2 - 1)] + 2(\theta_1^0 / \epsilon_1) [X_1 + C_{11} (\lambda_2 - 1)] + [Y_1 + Q_2 (\lambda_2 - 1)]}{4} \right\} + \frac{\epsilon_2^{sc}}{\epsilon_1^2} \left\{ n(H + A_1 - R_1) + Q_1 (\lambda_2 - 1) \right\} + \frac{(\mu_1 / \epsilon_1) (\theta_1^0 / \epsilon_1)}{2\lambda_1 (\lambda_1 - 1)^2} A_1 \left\{ \frac{Dm(\lambda) - \lambda_2 (\lambda_2 - \lambda_1)}{\lambda_2} \right\} \quad (C-7)$$

where

$$D \equiv (\mu_2 / \epsilon_1) / (\theta_1^0 / \epsilon_1) \quad m(\lambda) \equiv (\lambda_1 - 1)(\lambda_2 + 1 - 2\lambda_1)$$

$$\lambda_2 (\lambda_2 - 1) = i\lambda / 2$$

The third order behavior is given by the equations

$$F(\lambda) [\lambda_1 + A_1 / \lambda_1 - R_1] = A_1 [A_{11} (\lambda_1 - 1) + A_{12} + A_{13} - A_{14} (\lambda_2 - \lambda_1) - A_{17} (\lambda_1^* - \lambda_1)] + \left[\frac{\theta_1^0}{\epsilon_1} \right]^2 \left[\frac{\theta_1^0}{\epsilon_1} \right]^* \frac{[(\lambda_1 - R_1)A_3 + A_1 R_1]}{8} + \left[\left(\frac{\theta_1^0}{\epsilon_1} \right)^2 + 2 \left(\frac{\theta_1^0}{\epsilon_1} \right) \left(\frac{\theta_1^0}{\epsilon_1} \right)^* \right] \frac{[(\lambda_1 - R_1)C_{12} + A_1 D_{12}]}{8} + 2 \left[\left(\frac{\theta_1^0}{\epsilon_1} \right) + \left(\frac{\theta_1^0}{\epsilon_1} \right)^* \right] \frac{[(\lambda_1 - R_1)C_{21} + A_1 D_{21}]}{8} + \frac{[(\lambda_1 - R_1)Q_3 + A_1 B_3]}{8} + \left[\left(\frac{\theta_1^0}{\epsilon_1} \right) \left(\frac{\theta_2^0}{\epsilon_2} \right)^m + \left(\frac{\theta_1^0}{\epsilon_1} \right)^* \frac{\epsilon_2^{sc}}{\epsilon_1^2} \right] \frac{[(\lambda_1 - R_1)A_2 + A_1 R_2]}{2} + \left[\left(\frac{\theta_2^0}{\epsilon_2} \right)^m + \left(\frac{\theta_2^0}{\epsilon_2} \right)^* \right] \frac{[(\lambda_1 - R_1)Q_2 + A_1 B_2]}{2}$$

$$\begin{aligned}
 & + \left\{ \left(\frac{\theta_1^o}{\epsilon_1} \right) \left(\frac{\mu_2^m + \mu_2^*}{\epsilon_1} \right) + \left(\frac{\theta_1^o}{\epsilon_1} \right) \left(\frac{\mu_2^{sc}}{\epsilon_1} \right) + \left(\frac{\mu_2^o + \mu_2^*}{\epsilon_1} \right) + \left(\frac{\theta_2^{sc}}{\epsilon_1} \right) \right\} \frac{[(\lambda_1 - R_1)C_{11} + A_1 D_{11}]}{2} \\
 & + \left(\frac{\epsilon_3}{\epsilon_1} \right) [(\lambda_1 - R_1)Q_1 + A_1 B_1] \tag{C-8}
 \end{aligned}$$

where

$$A_{13} \lambda_1 (\lambda_1 - 1) = - (\mu_1 / \epsilon_1) [K_5 + K_5^*] / 2 \tag{C-9}$$

$$\begin{aligned}
 A_{11} \lambda_1 (\lambda_1 - 1) &= \frac{(\mu_1 / \epsilon_1) [K_5 + K_5^*]}{2 \lambda_1 (\lambda_1 - 1)} + \left(\frac{\mu_1}{\epsilon_1} \right) \frac{[(\mu_2^m / \epsilon_1^2) + (\mu_2^* / \epsilon_1^2)^*]}{4 \lambda_1 (\lambda_1 - 1)} \\
 &- \left(\frac{\mu_1}{\epsilon_1} \right)^* \frac{(\mu_2^{sc} / \epsilon_1^2)}{4 \lambda_1 (\lambda_1 - 1)} + \left(\frac{\mu_1}{\epsilon_1} \right) \\
 &\left\{ \frac{(K_5 + K_5^*) + (K_6 + K_6^*) - [(\mu_2^m / \epsilon_1^2) + (\mu_2^* / \epsilon_1^2)^*]}{2} \right\} - \left(\frac{\mu_1}{\epsilon_1} \right)^* \frac{A_{23}}{2} \tag{C-10}
 \end{aligned}$$

$$A_{12} (2\lambda_1 - 1) = - \left(\frac{\theta_1^o}{\epsilon_1} \right) \frac{\lambda_1 [(\lambda_1 - 1) + D] [(\mu_2^m / \epsilon_1^2) + (\mu_2^* / \epsilon_1^2)^*]}{4 \lambda_1 (\lambda_1 - 1)} \tag{C-11}$$

$$A_{14} \lambda_1 (\lambda_1 - 1) = \left(\frac{\mu_1}{\epsilon_1} \right)^* \frac{[(\theta_2^{sc} / \epsilon_1^2) - A_{23} - A_4] \lambda_2}{2} \tag{C-12}$$

$$A_{17} \lambda_2 (\lambda_2 - 1) = \left(\frac{\mu_1^o}{\epsilon_1} \right) K_6^* \lambda_1^* + \left(\frac{\epsilon_1}{\epsilon_1} \right)^* \frac{\lambda_1^* [\lambda_1^* (\lambda_1^* - 1) + D^*]}{4 \lambda_1^* (\lambda_1^* - 1)} \left[\mu_2^* / \epsilon_1^2 \right] \tag{C-13}$$

$$A_{23} \lambda_2 (\lambda_2 - 1) = \frac{(\mu_1 / \epsilon_1)^2}{2 \lambda_1 (\lambda_1 - 1)} - (\mu_2^* / \epsilon_1^2)^{sc} \tag{C-14}$$

$$A_4 = - \left(\frac{\mu_1}{\epsilon_1} \right) \left(\frac{\theta_1^0}{\tau_1} \right) \frac{\lambda_1 [\lambda_1 (\lambda_1 - 1) + D]}{2 [\lambda_1 (\lambda_1 - 1)]^2} \quad (C-15)$$

$$K_5 = \frac{(\mu_1 / \epsilon_1)^* (\mu_1 / \epsilon_1)}{2 \lambda_1 (\lambda_1 - 1)} - (\mu_2 / \tau_1^2) \quad (C-16)$$

$$K_6 = \frac{(\mu_1 / \epsilon_1)^* (\theta_1^0 / \epsilon_1) \lambda_1 [(\lambda_1 - 1) + D]}{2 [\lambda_1 (\lambda_1 - 1)]^2} \quad (C-17)$$

APPENDIX D

THEORETICAL ANALYSIS OF SUBSURFACE REACTIONS AND NONLINEAR EFFECTS
USING FINITE DIFFERENCE TECHNIQUES

The equations used to develop the nonlinear algorithm are essentially identical to those being studied for the linear behavior. The principal difference between the two is the manner in which the subsurface reaction term is handled. In the studies using the perturbation technique, this term is neglected; in studies using the finite difference approach, this term can be considered.

Using the variables expressed in nondimensional form

$$\theta = T/T_{\infty} \quad (D-1)$$

$$\theta_0 = T_s^{\circ}/T_{\infty} \quad (D-2)$$

$$\tau = t(\dot{r}_0)^2/\alpha \quad (D-3)$$

$$r = x r_0/\alpha \quad (D-4)$$

where \dot{r}_0 is the steady-state combustion velocity and $\alpha = k/C_p$, equations D-1 through D-4 become

$$\frac{\partial \theta}{\partial \tau} = \frac{\partial^2 \theta}{\partial r^2} + \frac{\dot{r}}{r_0} \frac{\partial \theta}{\partial r} + \bar{Z}_3 e^{-k_3/RT} \theta \quad (D-5)$$

at $\zeta = 0$

$$-\frac{\partial \theta}{\partial \zeta} = \frac{\eta}{\phi} + \bar{P} \exp \left[-E/RT_{\infty} \right] - \frac{E}{\phi} \quad (D-6)$$

$\zeta \rightarrow \quad \quad \quad \theta \rightarrow 1.0$

where

$$\bar{P} \equiv \frac{Z_1 P_o}{r_o T_{\infty} C_p}, \quad \bar{Z}_3 \equiv \frac{Z_3 r_o}{T_{\infty} r_o}$$

Because of the nonlinearity of these expressions, a finite difference algorithm was developed for digital computer solution. Equation D-5 in continuum form replaced the finite difference approximation, as shown by equation D-7, where the mesh points of the difference scheme are represented by i from $i = 1$ at the propellant surface to n at a point $n\Delta\zeta$ within the solid propellant.

Cas Phase

Solid Phase

1 + + + + . . . + . . +
 2 3 4 5 i n

For $i = 2, 3, 4, i, n$

$$\frac{\partial \theta_i}{\partial \tau} = \frac{\theta_{i+1} - 2\theta_i + \theta_{i-1}}{\Delta \zeta^2} + \frac{\dot{r}}{r_o} \frac{\theta_{i+1} - \theta_{i-1}}{2\Delta \zeta} + B e^{-E/RT} \theta_i \quad (D-7)$$

Writing the boundary condition equation at $\zeta = 0$ in finite difference form results in

$$-\frac{\partial \theta}{\partial \zeta} = \frac{\theta_3 - 4\theta_2 + 3\theta_1}{2\Delta \zeta} = \frac{\eta}{\phi} + \bar{P} e^{-E/RT} \theta - \frac{E}{\phi} \left(\frac{\dot{r}}{r_o} \right) \quad (D-8)$$

This equation may be differentiated with respect to the time variable, τ , to give

$$\left(\frac{\partial^3 \theta_3}{\partial \tau^3} - \frac{4 \partial^2 \theta_2}{\partial \tau^2} + 3 \frac{\partial \theta_1}{\partial \tau} \right) / 2\Delta z = \frac{\partial \eta / \phi}{\partial \tau} + \frac{\partial \bar{P}}{\partial \tau} e^{-E_2/RT} \theta_1$$

$$+ \bar{P} \frac{E_2}{\theta_1^2 RT} e^{-E_2/RT} \theta_1 \cdot \frac{\partial \theta_1}{\partial \tau} - \frac{\partial}{\partial \tau} \left(\frac{E_3}{RT \theta_1^2} \right) \theta_1 \left(\frac{\dot{\tau}}{\tau_0} \right) \quad (D-9)$$

Rearranging

$$\frac{\partial \theta_1}{\partial \tau} = \frac{4 \frac{\partial^2 \theta_2}{\partial \tau^2} - \frac{\partial^3 \theta_3}{\partial \tau^3} + 2\Delta z \frac{\partial \bar{P}}{\partial \tau} e^{-E_2/RT} \theta_1 + \frac{1}{\phi} \frac{\partial \eta}{\partial \tau}}{3 + 2\Delta z \bar{P} \frac{E_2}{RT \theta_1^2} e^{-E_2/RT} \theta_1 + 2\Delta z \frac{E_3}{\phi} \frac{\dot{\tau}}{\tau_0} \frac{1}{RT \theta_1^2}} \quad (D-10)$$

Thus, equation D-7 plus the n-1 equations of the form of equation D-4 provides a set of n simultaneous differential equations which can be solved with the aid of a digital computer. Various expressions can be used for P , $\partial P / \partial \tau$, and η / ϕ and the time differential form of the burning rate equation.

In these studies a method of solution has been used which is unique in solving the transient diffusion and chemical reaction equations. First, a system of ordinary differential equations is generated from the relevant partial differential equation by discretization in terms of the space variable; then the sequence of values of the dependent variables. This leads to a system of ordinary differential equations (in derivatives with respect to time). This means of solution of boundary value problems was extensively exploited for

some time in analogue computer work for solution of such problems as transient conduction of heat in solids. In analogue computer work, the limitation is usually the capacity of the computer. The relatively recent development of digital computer subroutines ("package solvers") "analogue discretization" methods have been used as a competitive means for solving certain types of partial differential equations.

The specific advantages of this approach to solution of boundary problems may be listed as follows:

- A. The programming time is reduced to a minimum as most of the difficult programming has been done in the development of the ordinary differential equations subroutine. Also, the computer running time for the differential equations approach seems to offer an advantage compared to problems involving differencing in both the space and time steps.
- B. Numerical convergence problems, i.e., convergence problems arising in numerical solution of the partial differential equations, are relegated to problems of convergence of solutions of systems of ordinary differential equations. Most subroutines for solution of ordinary differential equations have some means of assurance of numerical convergence of the solution.
- C. Conversion of a boundary value problem into a system of ordinary differential equations provides a means of handling nonlinear difficulties. This point is particularly important because many

of the equations involve an exponential Arrhenius term as well as reactant product terms.

- D. The capacity of the differential equation "package solvers" is sufficiently large to allow use of a fairly large number of mesh points in the discretization.

The study of the acoustic response requires that the oscillations occur about the steady state. Hence, the analysis must first predict the steady-state conditions for a given set of combustion parameters and then calculate the transient behavior. To do this, two approaches are possible. One approach is to assume some initial temperature distribution within the solid and let the transient equations relax to the appropriate steady state. The pressure oscillations are then started because the steady state is reacted.

The second approach is to neglect the transient terms and calculate the steady-state conditions by a trial-and-error process. In this process, the surface temperature is assumed, and the equations are solved using a forward differencing procedure for the temperature deep within the solid. The surface temperature is then adjusted until the desired temperature in the propellant is obtained. The resulting steady-state profile is then used in the transient model, and the oscillations are initiated immediately.

Of these two possible approaches, the second is preferred for economic reasons. The calculations using the forward difference approach can be done rapidly on the computer in comparison to the transient calculations. Hence, this is the approach used in these studies.

As mentioned in the main body of this report, even this approach did not prove to be economical. The difficulty arose when the steady-state profile was inserted into the transient equations. Even though close convergence was specified, the predicted steady state never matched the exact steady state. When such information is inserted in the transient equations, further relaxation to the true steady state occurs. This relaxation occurs during the initiation of the oscillations, and this compounding effect was found to require extremely small ratios of $\Delta t/\Delta \xi^2$ to maintain numerical stability. This, in turn, results in extremely long computer running time (i.e., 1/2 to 1 hr) before the steady oscillatory behavior is achieved. Many such calculations would be required to assess the effects desired; therefore, these studies were terminated because of the excessive cost.

APPENDIX E

PRESENTATIONS AND PUBLICATIONS

"Linear and Nonlinear Pressure Coupled Combustion Instability of Solid Rocket Propellants," Presented at 3rd ICRPG Conference, Atlantic City, New Jersey, June 4-6, 1968.

"Surface Reaction Effects on the Acoustic Response of Composite Solid Propellants." AIAA Journal. Vol. 6, No. 3, 1968.

"Effect of Surface Reactions on Acoustic Response of Solid Propellants." AIAA Journal. Vol. 5, No. 9, 1967.

"The Influence of Exothermic Surface Reactions on Pressure Coupled Combustion Instability of Composite Solid Propellants," Presented at 4th ICRPG Combustion Conference, Menlo Park, California, October 12-13, 1967.

"Acoustic Response of Composite Solid Propellants," Presented at 3rd ICRPG Combustion Conference, Cocoa Beach, Florida, October 17-21, 1966.

"Linear and Nonlinear Pressure Coupled Combustion Instability," Presented at 2nd ICRPG Combustion Conference, Los Angeles, California, November 1-5, 1965.

Unclassified

Security Classification

DOCUMENT CONTROL DATA - R & D

(Security classification of title, body of abstract and indexing annotation must be entered when the overall report is classified)

1. ORIGINATING ACTIVITY (Corporate author)		2a. REPORT SECURITY CLASSIFICATION	
United Technology Center Sunnyvale, California		Unclassified	
3. REPORT TITLE		2b. GROUP	
RESEARCH ON COMBUSTION OF SOLID PROPELLANTS			
4. DESCRIPTIVE NOTES (Type of report and inclusive dates)			
Final Report, 20 April 1965 to 31 Aug. 1968			
5. AUTHOR(S) (First name, middle initial, last name)			
Robert S. Brown and R y J. Muzzy			
6. REPORT DATE	7a. TOTAL NO. OF PAGES	7b. NO. OF REFS	
September 1968		35	
8a. CONTRACT OR GRANT NO.	8b. ORIGINATOR'S REPORT NUMBER(S)		
DA-04-200-AMC-968 (X)	UTC Report 2136 - FR		
b. PROJECT NO.	9b. OTHER REPORT NO(S) (Any other numbers that may be associated with this report)		
c.			
d.			
10. DISTRIBUTION STATEMENT			
This document has been approved for public release and sale; its distribution is unlimited.			
11. SUPPLEMENTARY NOTES		12. SPONSORING MILITARY ACTIVITY	
		USA Aberdeen Research & Development Center Aberdeen Proving Ground, Maryland 21005	

13. ABSTRACT

A study has been made to relate theoretically predicted and experimentally observed pressure-coupled combustion instability behavior of solid propellants. Using a generalized theoretical model which incorporates both surface and gas phase combustion effects, the linear and nonlinear (higher pressure amplitude) region has been characterized by a group of combustion parameters. Concurrent experimental studies have been directed toward investigating (1) the effects of coating the solid oxidizer crystals, (2) the chemical and physical nature of the propellant binder, catalysts, and cross-linking agents on the acoustic admittance, (3) nonlinear response properties, and (4) propellant burning rate. The data show that small changes in propellant formulation can have a significant effect on the derived parameters characterizing the surface and, therefore, on relative contributions of these reactions to the acoustical response properties.

Higher order effects show that, depending on the magnitude of the constants, both positive and negative values for the shift in the time average burning rate with acoustic pressure can be obtained. Additional studies show that the acoustic response function decreases with increasing acoustic pressure for reasonable second and third order coefficients. Hence, the combustion process itself can limit the acoustic pressure amplitude in the T-tuner. On the basis of these calculations, limiting amplitudes of 0.1 to 0.5 can be expected without consideration of acoustic losses. The combined linear and nonlinear results indicate that a homogeneous nonreacting solid characterizes the transient behavior of the solid phase with sufficient accuracy.

NO 11 1968

REPLACES GPO FC, 11/70, 1 JAN 63, WHICH IS OBSOLETE FOR ARMY USE.

Security Classification